Energy & Environmental Science

ROYAL SOCIETY OF CHEMISTRY

REVIEW

View Article Online
View Journal | View Issue

Cite this: *Energy Environ. Sci.*, 2025, **18**, 509

Suppressing non-radiative recombination for efficient and stable perovskite solar cells†

Jiahua Tao,[a] Chunhu Zhao,*[ab] Zhaojin Wang,[cd] You Chen,[cd] Lele Zang,[a] Guang Yang,[e] Yang Bai*[cd] and Junhao Chu[af]

Perovskite solar cells (PSCs) have emerged as prominent contenders in photovoltaic technologies, reaching a certified efficiency of 26.7%. Nevertheless, the current record efficiency is still far below the theoretical Shockley–Queisser (SQ) limit due to the presence of non-radiative recombination losses. Here, we provide a comprehensive review exploring the fundamental mechanisms driving non-radiative recombination and the intricate dynamics of photocurrent hysteresis. The interconnectedness between these issues and their collective impact on the operational stability of PSCs, which is essential for practical application, is emphasized. Notable advancements in understanding and mitigating performance losses caused by non-radiative recombination in PSCs are thoroughly overviewed, including advanced passivation techniques, sophisticated interface engineering, precise compositional tuning, development of novel materials, and state-of-the-art fabrication methods. These innovative approaches are making significant progress in minimizing efficiency losses and further improving device stability. Moreover, this review identifies the ongoing challenges and outlines a strategic research agenda aimed at harnessing the full potential of PSCs. To achieve the theoretical maximum efficiency defined by the SQ limit, this agenda sets a visionary goal for PSCs to transition from laboratory breakthroughs to widespread commercial reality. Such advancements could revolutionize the global energy landscape, underscoring the critical importance of continued innovation and development in this rapidly progressing field.

Received 3rd July 2024,
Accepted 25th November 2024

DOI: 10.1039/d4ee02917h

rsc.li/ees

Broader context

In the quest for efficient renewable energy solutions, perovskite solar cells (PSCs) have made significant strides in photovoltaic technologies, with power conversion efficiencies rising from an initial 3.8% to a certified 26.7%. Nevertheless, the current record efficiency is still far below the theoretical Shockley–Queisser limit due to the presence of non-radiative recombination losses. To address this issue, it is essential to explore the latest advancements in mitigating non-radiative recombination losses, which are crucial for enhancing the efficiency and stability of PSCs while providing future research directions. This review systematically examines novel materials and advanced fabrication methods, with an in-depth analysis of the fundamental mechanisms driving non-radiative recombination. By summarizing recent research findings, identifying current challenges, and proposing future research pathways, the work provides valuable insights into the mechanisms governing non-radiative recombination, device stability, and *J–V* hysteresis. These insights are crucial for advancing perovskite photovoltaic technology and enabling the transition of PSCs from laboratory research to scalable, commercially viable renewable energy solutions. This review serves as a significant contribution to the development of more efficient and stable photovoltaic technologies.

[a] *Engineering Research Center for Nanophotonics and Advanced Instrument, Key Laboratory of Polar Materials and Devices, Ministry of Education, School of Physics and Electronic Science, East China Normal University, Shanghai 200241, China*
[b] *Hunan Key Laboratory of Carbon Neutrality and Intelligent Energy, Research Institute of New Energy and Novel Energy Storage, School of Resource and Environment, Hunan University of Technology and Business, Changsha 410205, China. E-mail: chzhao@hutb.edu.cn*
[c] *Faculty of Materials Science and Energy Engineering, Shenzhen University of Advanced Technology, Shenzhen 518107, China*
[d] *Institute of Technology for Carbon Neutrality, Shenzhen Institute of Advanced Technology, Chinese Academy of Sciences, Shenzhen 518055, China. E-mail: y.bai@siat.ac.cn*
[e] *Department of Electrical and Electronic Engineering, Photonic Research Institute, Research Institute of Smart Energy, Research Institute for Advanced Manufacturing, The Hong Kong Polytechnic University, Hung Hom, Kowloon, Hong Kong 999077, China*
[f] *National Laboratory for Infrared Physics, Shanghai Institute of Technical Physics of the Chinese Academy of Science, Shanghai 200083, China*
† Electronic supplementary information (ESI) available. See DOI: https://doi.org/10.1039/d4ee02917h

1. Introduction

As the global community confronts the urgent challenges of climate change, the pursuit of efficient renewable energy solutions has become increasingly critical. Western countries aim to achieve carbon neutrality by 2050, while China has set its target for 2060, reflecting the global imperative for rapid innovation in sustainable energy technologies. In this context, perovskite-based photovoltaics have emerged as a transformative force in solar energy conversion. Their distinctive properties, from exceptional absorption coefficients to extended carrier diffusion lengths, have driven a paradigm shift in photovoltaic research. Over the past decade or so, the power conversion efficiency (PCE) of PSCs has surged from an initial 3.8%[1] to a certified 26.7%,[2] with tandem configurations further pushing the efficiency limit.[3,4] However, a significant gap remains between the current achievements and the theoretical SQ limits, which can be attributed to defects in the perovskite layer, interfaces, or contact materials.[5–8] Therefore, suppressing non-radiative recombination losses is crucial to realizing more efficient and stable PSCs.

Achieving this goal requires a comprehensive understanding of the intricate relationships between recombination mechanisms, device stability, and hysteresis effects in PSCs. Trap states in perovskite films predominantly act as non-radiative recombination sites, significantly influencing charge recombination dynamics.[9,10] Under illumination, this issue is exacerbated as ionic vacancies or interstitial defects become activated, leading to higher trap density.[11–14] Due to the photo-induced ion migration effect, the traps in the films are redistributed, leading to the increase of photoluminescence (PL) lifetime and total intensity. These changes correlate closely with the substantial reduction and stabilization of fast nonradiative decay pathways. Thus, both ion migration and electronic charge traps serve as recombination centers to achieve hysteresis in the modeled *J–V* characteristics.[15–17] Reducing trap density has been shown to mitigate hysteresis, thereby suppressing trap-mediated non-radiative recombination.[18,19] Another major obstacle to the commercialization of PSCs is the limited stability of perovskite absorbers. Stability issues in PSCs can be

Jiahua Tao

Jiahua Tao is an Associate Professor at the Engineering Research Center for Nanophotonics and Advanced Instrument, Ministry of Education, East China Normal University in Shanghai. He received his PhD in Microelectronics and Solid-State Electronics from the same university in 2016. From 2011 to 2013, he worked at Mengzi Mining and Metallurgy Co. Ltd in Yunnan. His current research primarily focuses on semiconductor materials and optoelectronic devices.

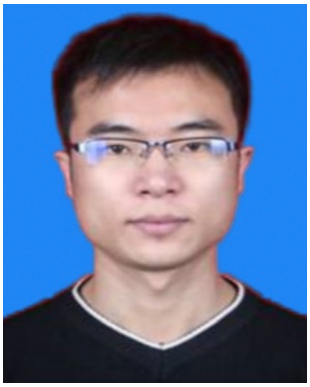

Chunhu Zhao

Chunhu Zhao received his bachelor's and master's degree from Central South University, and his PhD from South China University of Technology. He spent two years as a postdoctoral researcher at East China Normal University and then joined Hunan University of Technology and Business as an associate professor. His research focuses on semiconductor optoelectronic materials and devices.

Yang Bai

Yang Bai is currently a Professor affiliated with Shenzhen University of Advanced Technology (SUAT) and also Shenzhen Institute of Advanced Technology (SIAT), Chinese Academy of Sciences. Yang received his PhD in Chemical Engineering from The University of Queensland (UQ), Australia, in 2014, and then he moved to the United States to conduct a two-year postdoc training at the University of Nebraska-Lincoln. Before joining SUAT, he worked at UQ for four years. Yang's research focuses on hybrid semiconductor materials for new-generation thin film photovoltaics and optoelectronics.

Junhao Chu

Junhao Chu is an Academician of Chinese Academy of Sciences; Professor of Shanghai Institute of Technical Physics, Chinese Academy of Sciences; Director of Shanghai Center for Photovoltaics; and Dean of School of Information Science Technology, East China Normal University. He received his PhD degree from Shanghai Institute of Technical Physics, Chinese Academy of Sciences, in 1984. From 1986 to 1988 he was a Humboldt Fellow at Technical University of Munich, Germany. He is an expert in semiconductor physics and devices. He has made a systematic investigation on the opto-electronics of narrow gap semiconductors and low dimensional semiconductor systems.

dichotomized into extrinsic factors, which can be addressed through external encapsulation methodologies,[20–22] and intrinsic determinants, which mandate rigorous refinements in the crystalline integrity and compositional purity.[23] Defect states, particularly at grain boundaries and surfaces, create diverse pathways for ion migration, accelerating device degradation and compromising long-term performance stability. These defects also form deep-level traps that enhance non-radiative recombination, further reducing device efficiency and stability.

Despite several review articles on non-radiative recombination, the rapid advancements in PSC technology necessitate the need for a more up-to-date and comprehensive review. Recent research has introduced new insights and methodologies, such as the development of multifunctional materials,[24–26] improved fabrication methods,[27–29] and a deeper understanding of the fundamental processes governing non-radiative recombination.[30] However, these advancements have not been fully explored in existing reviews. Therefore, there is a pressing need to systematically summarize these latest developments, identify the remaining challenges, and propose future research directions. The review seeks to enhance the understanding of the fundamental mechanisms underlying non-radiative recombination and provide innovative strategies for reducing trap states, thereby improving the performance and stability of PSCs. By thoroughly examining the relationship between non-radiative recombination, stability, and hysteresis, we aim to offer valuable insights that contribute to the development of more efficient and stable solar energy solutions.

This comprehensive review elucidates key advancements in mitigating non-radiative recombination losses, underscoring their pivotal role in enhancing efficiency and ensuring operational longevity of PSCs. The analysis meticulously examines current device architectures and the intricacies of associated charge transport phenomena. The multifaceted origins of non-radiative losses are explored, with particular emphasis on defect-induced pathways, interfacial recombination dynamics, and other notable non-radiative mechanisms. These include the formation of deep-level defects, the influence of grain boundaries on charge carrier dynamics, and the impact of surface states on overall device performance. In parallel, the complex physics governing device stability and the intricacies of *J–V* hysteresis are explored in depth. The discussion subsequently transitions to a systematic exploration of strategies aimed at reducing non-radiative recombination and hysteresis, emphasizing innovations in crystallization processes and advanced interface engineering. Finally, the review concludes with an insightful evaluation of the prevailing challenges, offering a forward-looking perspective on the future trajectory of PSCs within the commercial landscape.

2. Device physics for high-performance PSCs

2.1 Device configuration and efficiency

The typical device architecture of PSCs comprises five interacting layers, including an intrinsic perovskite absorber, positive and negative charge transport layers (CTLs), and dual electrodes for charge collection. These configurations are primarily classified into three types: mesoporous n–i–p, planar n–i–p, and inverted p–i–n structures (Fig. 1a). Table S1 (ESI†) compares the photovoltaic parameters of single-junction PSCs across both n–i–p and p–i–n configurations. Notably, n–i–p PSCs have traditionally maintained the highest PCEs. Nevertheless, recent developments indicate that p–i–n PSCs have surpassed n–i–p configurations in certified efficiency. This significant shift highlights the latest advancements in PSC technology. In addition, p–i–n PSCs offer greater commercial viability due to their straightforward fabrication process, compatibility with flexible substrates, and potential for tandem cell integration (Fig. 1b and c). While n–i–p PSCs excel in PCEs, the commercial appeal of p–i–n configurations is undeniable, largely attributed to their ease of fabrication and adaptability. Furthermore, n–i–p PSCs face challenges with imbalanced charge transport at their interfaces,[31] an issue effectively mitigated in inverted p–i–n configurations through fullerene passivation. As shown in Table S2 (ESI†), significant progress has been made in the PCE of PSCs and perovskite–silicon tandem solar cells (TSCs), with TSCs reaching efficiency levels as high as 33.9%. This substantial improvement underscores the ongoing advancements in material design, interface engineering, and manufacturing processes, all of which are critical for enhancing the commercial viability of solar cell technologies.

In the rapidly evolving landscape of photovoltaic technologies, metal-halide perovskites have emerged as a focal point of research due to their direct bandgap crystalline nature, which imparts an absorption coefficient surpassing that of silicon by over an order of magnitude. This intrinsic property allows the use of a thin perovskite layer to achieve optimal light absorption, significantly enhancing the V_{OC}.[32,33] Beyond their intrinsic optical properties, the versatility of perovskites is further highlighted by the tunability of their bandgap, which can be adjusted between 1.2 eV and 3 eV depending on chemical composition or crystal dimension alterations (Fig. 2a). Notably, perovskites calibrated to a bandgap of approximately 1.7 eV demonstrate exceptional potential for tandem integration with silicon.[34] The performance of PSCs hinges on the properties of the perovskite layer, especially its crystallinity. High-crystallinity films are vital as they enable superior charge transport, enhance carrier mobility, reduce series resistance, and fine-tune the FF and photocurrent. The architecture and thickness of the perovskite layer are equally critical. While a uniform layer ensures consistent light absorption, precise control over its thickness is required to balance light capture and charge extraction effectively.[35] However, further optimization of PSCs faces significant challenges, such as achieving a seamless interface between the perovskite and CTLs to maximize charge extraction and minimize recombination losses.

Electron transport layers (ETLs) are critical components in the architecture of PSCs, profoundly affecting device performance. Among ETLs, prevalent choices encompass TiO_2, SnO_2, ZnO, Zn_2SnO_4, $BaSnO_3$, fullerene (C_{60}), and phenyl-C_{61}-butyric acid methyl ester (PCBM).[36] The primary function of the ETLs is to prevent hole migration towards the cathode and accelerate

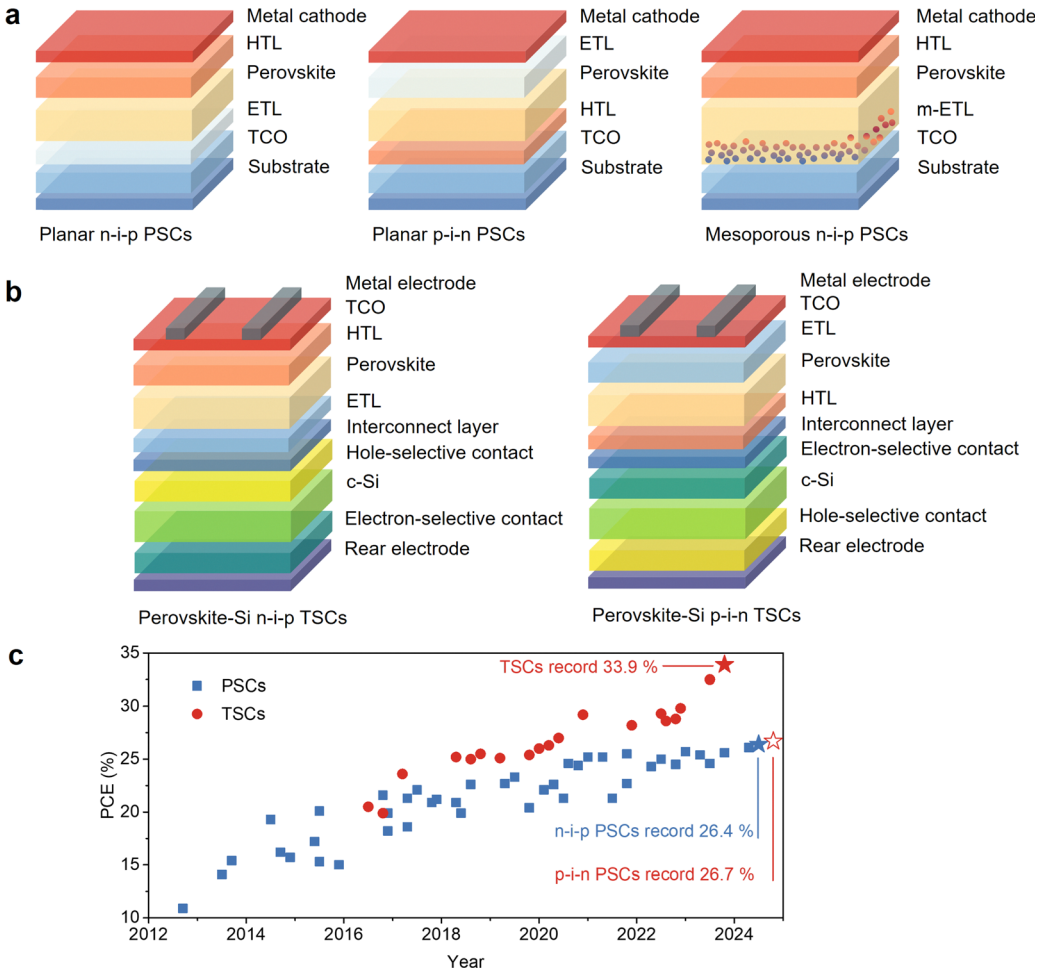

Fig. 1 Device configurations and progression of device efficiency. (a) PSCs with mesoporous n–i–p, planar n–i–p and inverted planar p–i–n configurations. (b) Perovskite–silicon tandem solar cells (TSCs) with n–i–p and inverted p–i–n architectures. (c) Major advancements in the PCEs of PSCs and TSCs.

the efficient transfer of electrons to the anode. Thus, ETLs with low electron affinity are preferred, as they facilitate electron reception and transport, create favorable band offsets, and facilitate efficient carrier collection.[37] Interestingly, while PSCs can operate without ETLs,[38–41] potentially lowering production costs, this typically compromises the efficiency and stability of the devices. In the domain of PSC research, hole transport layers (HTLs) are equally indispensable, with materials such as NiO_x, Cu_xO, CuSCN, 2,2′,7,7′-tetrakis-(*N*,*N*-di-*p*-methoxyphenylamine)-9,9′-spirobifluorene (spiro-OMeTAD), polytriarylamine (PTAA), poly(3,4-ethylenedioxythiophene)–poly(styrenesulfonate) (PEDOT:PSS), and poly(3-hexylthiophene-2,5-diyl) (P3HT) being integral to PSCs.[42] These materials are crucial for efficiently extracting and transporting holes from the perovskite active layer to the anode. The effectiveness of this process is significantly enhanced when HTLs exhibit a high hole mobility and appropriate energy level alignment with the perovskite layer.[43] Additionally, HTL-free architectures have also been explored, revealing superior photovoltaic performance compared to ETL-free designs due to the formation of a beneficial depletion region between the perovskite and ETL, which promotes efficient charge separation and reduces recombination losses.[44–46]

2.2 Charge dynamics in PSCs

Understanding the intricate mechanisms governing the operation of PSCs is pivotal for harnessing their full potential. Central to their operation is the process of charge dynamics, encompassing charge extraction, transport, and recombination. Upon illumination, the perovskite active layer absorbs photons, generating electron–hole pairs, termed excitons. These excitons diffuse, and due to the inherently low exciton binding energy of perovskite materials, readily dissociate into free electrons and holes. Propelled by the built-in electric field, electrons migrate toward the perovskite/ETL interface, and subsequently enter the lowest unoccupied molecular orbital (LUMO) of the ETLs.[47] Simultaneously, holes ascend to the highest occupied molecular orbital (HOMO) of the HTL. These mobilized electrons are collected at the front electrode and flow through the external circuit, generating electrical energy. According to the principle of charge conservation, an equivalent number of electrons return *via* the external circuit to the back electrode, diffuse to

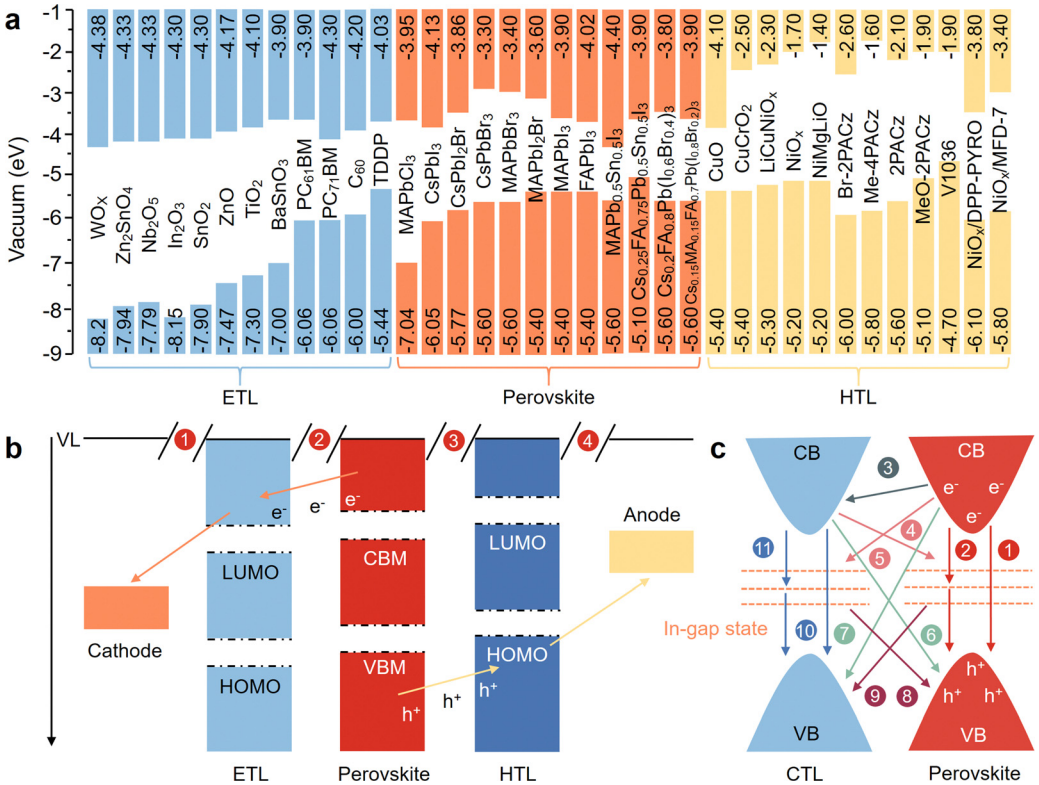

Fig. 2 Band alignment, charge transfer, and recombination process in PSCs. (a) Band alignment of various perovskite absorbers and charge transport layers. (b) Schematic of charge transport behaviors in PSCs. (c) Schematic illustration of carrier dynamic pathways at metal-oxide/perovskite (n-type) interfaces; CB denotes the conduction band and VB represents the valence band.

the perovskite/HTL interface, and recombine with holes, completing the carrier transport cycle and sustaining the device's operation. As illustrated in Fig. 2b, interfaces ① and ② manage electron transfer, facilitating electron movement from the perovskite's conduction band to the ETL's LUMO and onward to the cathode. Conversely, interfaces ③ and ④ handle hole transfer, guiding holes from the perovskite's valence band to the HTL's HOMO, culminating in their transfer to the anode.

The efficiency of PSCs hinges primarily on the charge extraction process, which is intricately linked to the precise energy level alignment at the interfaces. This alignment dictates the carrier transport from the valence and conduction bands of the perovskite to the CTLs.[48] Moreover, for efficient charge transport between the CTLs and their respective electrodes, the energy level alignment of CTLs must also resonate with both electrodes' work functions.[49,50] As a result, carefully designing and fine-tuning energy levels at these interfaces are crucial for achieving high-performance PSCs. Diving deeper into organic–inorganic hybrid perovskites, $FAPbI_3$ boasts the narrowest bandgap (E_g ~ 1.48 eV), while $CsPbI_3$, among inorganic perovskites, has a bandgap of approximately 1.73 eV. Striking a balance between an ideal bandgap and stability in pure perovskites poses a formidable challenge. Consequently, modulating the halide composition in pure perovskites has become a prevalent strategy to optimize the energy level alignment at the interfaces. It is worth noting that when different functional layers are integrated during device assembly, the standard vacuum level configuration might no longer apply. Various factors, including material properties, interlayer interactions, and dipole formation, can redefine the energy level alignment. Addressing the nuances of perovskite materials and CTLs involves two primary aspects: (1) minimizing defect ions, which can distort interfacial energy levels; and (2) developing more robust CTLs to mitigate photo-induced shifts at the CTL/perovskite interface, prevent photo-induced degradation of the perovskite layer, and bolster light absorption in the active layer.

Beyond energy level considerations, charge recombination is influenced by bulk and interface defects, charge mobility, and the diffusion length of charges within both the perovskite and CTLs. The lattice structure of the perovskite absorber, coupled with the varied lattice constants across the functional layers in PSCs, inevitably leads to defects and potential barriers at the interfaces. These imperfections can lead to charge accumulation and subsequent recombination. This defect density plays a pivotal role in determining the charge carrier diffusion lengths. For instance, perovskite single crystals with minimal trap densities (approximately 10^8–10^{10} cm^{-3}) have been shown to possess diffusion lengths exceeding 100 μm. In contrast, polycrystalline thin films, with trap densities ranging between 10^{16} and 10^{18} cm^{-3}, typically exhibit diffusion lengths less than 10 μm.[51,52] As is known, the gap between theoretical and practical PCE in PSCs is mainly ascribed to charge collection losses, electrical losses, non-radiative recombination losses, and interface recombination losses.[53–55] While the first two are contingent on the specific device designs, the latter two, particularly non-radiative

recombination, are perceived as the primary culprits for efficiency losses in PSCs (as depicted in Fig. 2c). The subsequent sections will present a more in-depth exploration of this topic.

3. Non-radiative recombination in PSCs

3.1 Defect-assisted recombination

Defects within the grain structure, at grain boundaries, and at interfaces of PSCs are widely recognized as the primary sources for non-radiative recombination losses, which significantly affect device efficiency. These defects emerge predominantly due to the volatilization of organic constituents during the annealing process.[56] Under open-circuit conditions, the role of these defects in mediating carrier recombination becomes paramount, directly influencing the efficiency of PSCs.[57] Intrinsically, these defects can either augment charge transport by increasing the population of free carriers *via* doping mechanisms or impede charge transport by functioning as carrier traps or scattering centers.[58] A comprehensive classification of these defects, as delineated in Fig. 3a and b, includes intrinsic point

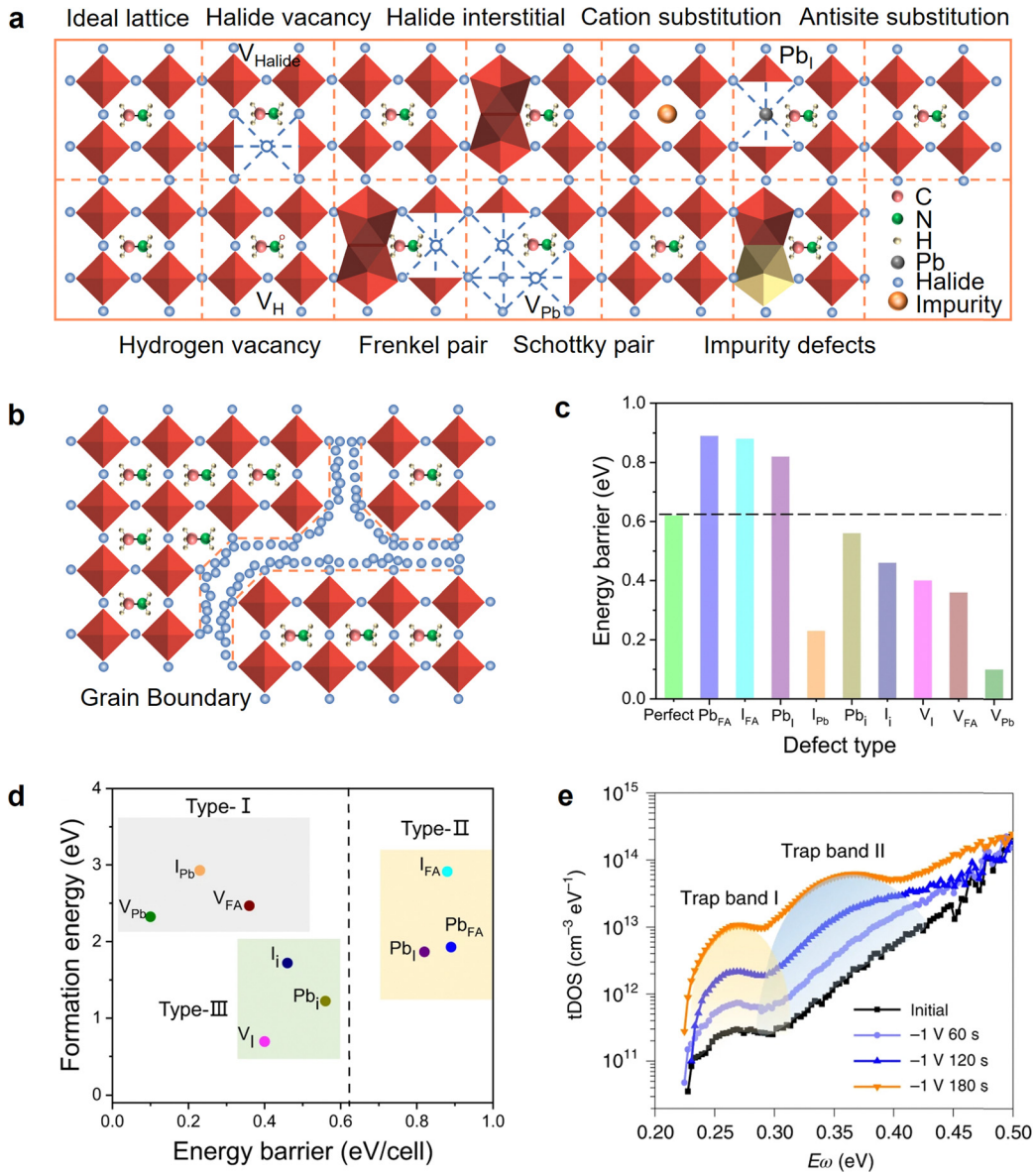

Fig. 3 Point defects, extended defects, and defect evolution in metal halide perovskites. (a) Schematic representation of point defects and combinations of point defects. (b) Illustration of grain boundaries. (c) The energy barrier of α-to-δ phase transition in $FAPbI_3$ based on various native point defects. The dashed line shows the energy barrier of the perfect crystal (0.62 eV). This figure has been reproduced from ref. 66 with permission from Springer Nature, Copyright 2023. (d) The defect formation energies of native point defects on a Pb-rich perovskite surface. The abscissa represents the energy barrier of the α-to-δ phase transition, and the ordinate is the formation energy of defects. This figure has been reproduced from ref. 66 with permission from Springer Nature, Copyright 2023. (e) Defect evolution depicted by tDOS spectra before and after applying a reverse bias of −1 V with different durations. This figure has been reproduced from ref. 67 with permission from Springer Nature, Copyright 2022.

defects,[59–61] metallic impurity sites,[62,63] two-dimensional (2D) extended defects, notably grain boundaries and surface irregularities, and three-dimensional (3D) conglomerate defects,[64] exemplified by lead clusters. From an energy perspective, these defects are bifurcated into shallow and deep defects. Shallow defects reside near the band edges, whereas deep defects are positioned at intermediary energy states within the bandgap.[65]

Taking $FAPbI_3$ as an example, deep defects, such as I_{FA}, Pb_I, Pb_{FA}, and Pb_i, which possess elevated formation energies (Fig. 3c–e), are identified as the primary sources of trap states.[66] In contrast, shallow defects, which have lower formation energies, exert a minimal influence on V_{OC} and non-radiative decay processes.[68] However, it is noteworthy that even shallow defects, when present in high densities, can induce detrimental effects, manifesting as hysteresis, phase segregation, and material degradation.[69] Grain boundaries, characterized by their heightened defect density and accelerated non-radiative decay rates,[70] negatively impact device performance by curtailing carrier diffusion and introducing sites conducive to non-radiative recombination.[71] Three-dimensional (3D) defects predominantly encompass structural anomalies within perovskite films, such as pinholes, fissures, and precipitates. Most of these are deep defects and require careful mitigation. Additionally, 3D defects compromise the interface between the perovskite absorber and the CTLs, increasing series resistance and consequently reducing both J_{SC} and FF.[72]

3.2 Interface-mediated recombination

Non-radiative recombination losses at the interfaces between the perovskite absorber and CTLs are critical factors affecting the performance of PSCs. Several mechanisms underpin interface-mediated recombination, including charge-carrier back transfer,[73] surface/interface defects,[74,75] energy level mismatch,[76–78] and field-effect recombination caused by surface potential inhomogeneity.[79,80] One prominent issue is the conduction band offset,[81] which induces the reverse flow of electrons from CTLs back to the perovskite absorbers, resulting in charge-carrier back-transfer recombination events. This offset at the interface is also implicated in the hysteresis observed in *J–V* curves.[82] Interfacial anomalies, such as unregulated intermediate phase formations, especially prevalent in all-inorganic perovskite films, compromise the interfacial integrity. Often, these irregularities result in the formation of dangling bonds at the interface, introducing electronic states within the bandgap.[83] To mitigate this issue, it is imperative to shift these electronic states outside the bandgap by forming new molecular orbitals at the interface.

Beyond the superficial anomalies of perovskites, achieving an optimal energy level alignment for efficient selective contacts remains a paramount challenge. Nonetheless, the ramifications of energy level alignment for PSC performance are a topic of ongoing debate, with the consensus leaning towards the notion that curtailing non-radiative recombination through charge-blocking at the interface is of more significant consequence than achieving pristine energy level alignment in the past.[84,85] However, recent research has indicated that energy level mismatch can significantly contribute to non-radiative recombination losses in PSCs,[86] underscoring the need for proper energy alignment to minimize recombination losses. Ideally, the heterointerface should manifest a pronounced Schottky barrier, adept at the selective extraction of majority carriers while concurrently impeding the transit of minority carriers. Therefore, developing strategies to ensure precise energy level alignment and reduce interface defects is crucial for advancing the performance and stability of PSCs.

3.3 Other non-radiative recombination

In contrast to defect-assisted and interface-mediated recombination losses, Auger recombination and band-tail recombination are less important and not universal across all types of PSCs. Auger recombination is a thermal dissipation process in which the excess energy from the electron–hole recombination is transferred to electrons or holes, exciting them to higher energy states within the same band rather than emitting photons.[87] It has been demonstrated that Auger recombination becomes dominant (Fig. 4a) when the carrier concentrations in perovskite absorbers exceed 10^{17} cm^{-3}.[88] However, under AM 1.5G illumination (carrier concentrations $<10^{15}$ cm^{-3}), the effect of Auger recombination on PSC performance is negligible.[70,89] Band-tail recombination involves charge-carrier relaxation from the energy-band edges into the band-tail states by emitting photons. When the photon energy decreases to below the bandgap, an exponential decrease known as the Urbach tail appears due to band tailing in the valence and conduction bands,[90] as shown in Fig. 4b. The band-tail region can be clearly observed in the external quantum efficiency (EQE) spectrum (Fig. 4c–e). The band-tail states have been attributed to various types of lattice disorder in the perovskite,[91–93] contributing to the V_{OC} losses. These states, often classified as shallow trap states, can be mitigated by enhancing the crystallinity of the perovskite and reducing the degree of energetic disorder.[94,95]

3.4 Non-radiative recombination on PSC efficiency and stability

To date, state-of-the-art PSCs have struggled to achieve the theoretical PCE limits predicted by the SQ model. This limitation is primarily attributed to non-radiative recombination losses, which substantially reduce V_{OC} and FF.[96,97] V_{OC} can also be expressed by the relation[14]

$$V_{OC} = V_{OC}^{rad} - \Delta V_{OC}^{non\text{-}rad}$$

where V_{OC}^{rad} is the open-circuit voltage in the radiative limit where all recombination is radiative and $\Delta V_{OC}^{non\text{-}rad}$ is the loss in V_{OC} due to non-radiative recombination. Recently, a many-diode model was applied to quantify the non-radiative voltage losses,[98] as shown in Fig. 5a–c. In addition to V_{OC}, non-radiative recombination also has a pronounced effect on the FF of PSC devices. The maximum FF (FF_{max}) can be calculated using the equation[53]

$$FF_{max} = \frac{v_{OC} - \ln(v_{OC} + 0.72)}{v_{OC} + 1}$$

where v_{OC} is proportional to V_{OC}. Within the framework of SQ theory, V_{OC} is often equated with the quasi-Fermi level splitting (QFLS). However, in suboptimal PSCs, a discrepancy exists

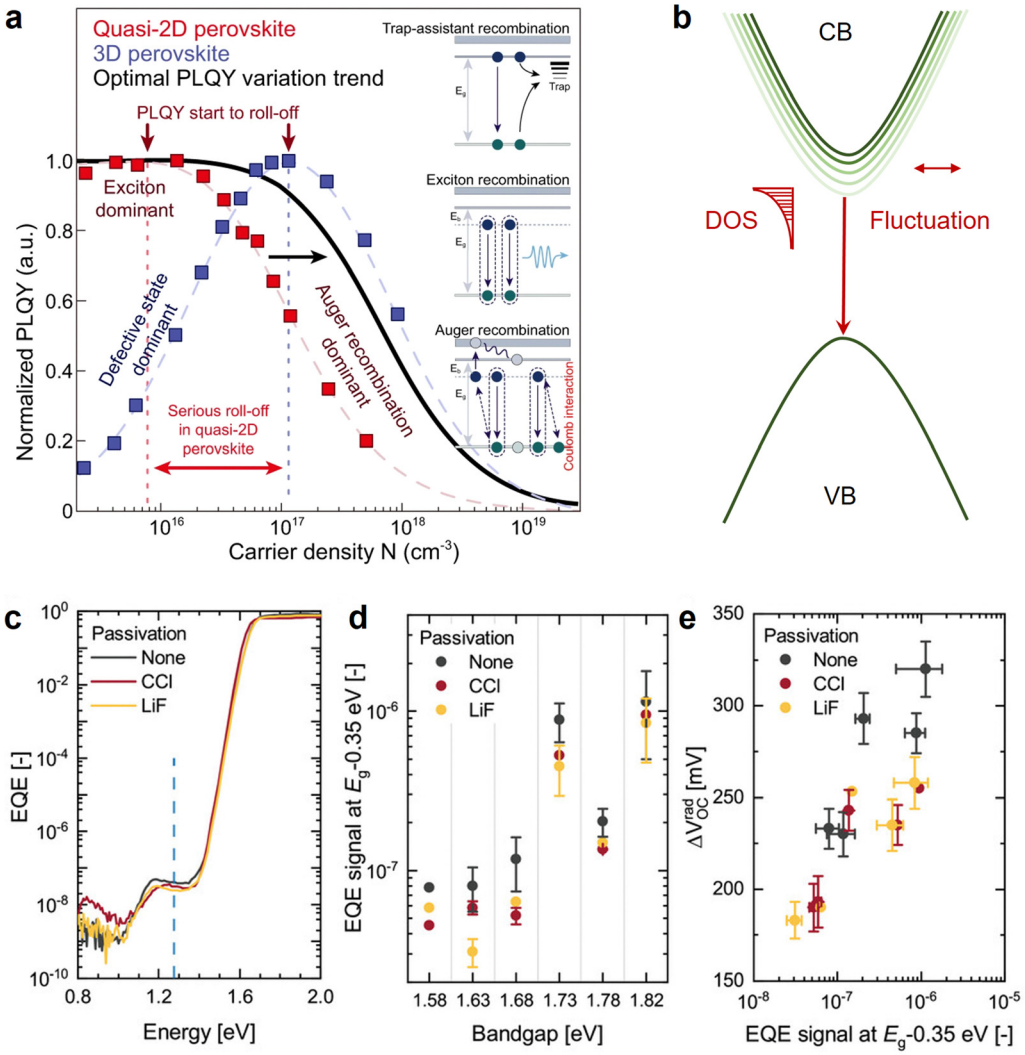

Fig. 4 Auger recombination and band-tail recombination. (a) Photoluminescence quantum yields (PLQYs) of quasi-2D perovskite and 3D perovskite films as a function of carrier density; the curves indicate that serious Auger recombination occurs in the quasi-2D case compared to the 3D one; the black curve illustrates an ideal PLQY evolution trend for the optimal perovskite emitter. This figure has been reproduced from ref. 88 with permission from Springer Nature, Copyright 2021. (b) Schematics of the formation of the Urbach tail states. (c) Semilogarithmic plot of the sensitive external quantum efficiency (EQE) spectra of PSCs without passivation and with two different passivation strategies. This figure has been reproduced from ref. 90 with permission from Wiley, Copyright 2024. (d) Semilogarithmic plot of the sensitive EQE response spaced 0.35 eV from the bandgap for various bandgaps without passivation and with two different passivation strategies. This figure has been reproduced from ref. 90 with permission from Wiley, Copyright 2024. (e) The voltage loss as a function of the EQE response spaced 0.35 eV from the bandgap for all PSCs with and without passivation. This figure has been reproduced from ref. 90 with permission from Wiley, Copyright 2024.

between the external V_{OC} and the intrinsic QFLS (Fig. 5d and e),[100,101] named ΔQFLS:[96]

$$\Delta\mathrm{QFLS} = -\frac{kT}{q} \times \ln(\mathrm{PLQY})$$

where k is Boltzmann's constant, T is the temperature, q is the elemental charge and PLQY is the photoluminescence quantum yield. The PLQY value can be expressed in terms of the radiative (R_{rad}) and non-radiative ($R_{non\text{-}rad}$) recombination rates:

$$\mathrm{PLQY} = \frac{R_{rad}}{R_{rad} + R_{non\text{-}rad}}$$

Hence, this discrepancy is primarily due to non-radiative recombination losses, which curtail the QFLS, thereby reducing V_{OC}.

For planar p–i–n structured PSCs, the non-radiative energy losses of devices with different interlayers have been systematically investigated,[99] as shown in Fig. 5f. The analysis revealed that these devices suffer from a QFLS-V_{OC} mismatch of almost 100 meV (Fig. 5g). Notably, wide bandgap perovskites with an E_g exceeding 1.7 eV, pivotal for perovskite/silicon tandem solar cell applications, exhibit pronounced V_{OC} deficits. These losses were primarily ascribed to imperfections within the perovskite material and at the perovskite/CTL interface rather than to halide segregation.[102] Non-radiative recombination mediated by these imperfections was pinpointed as the predominant

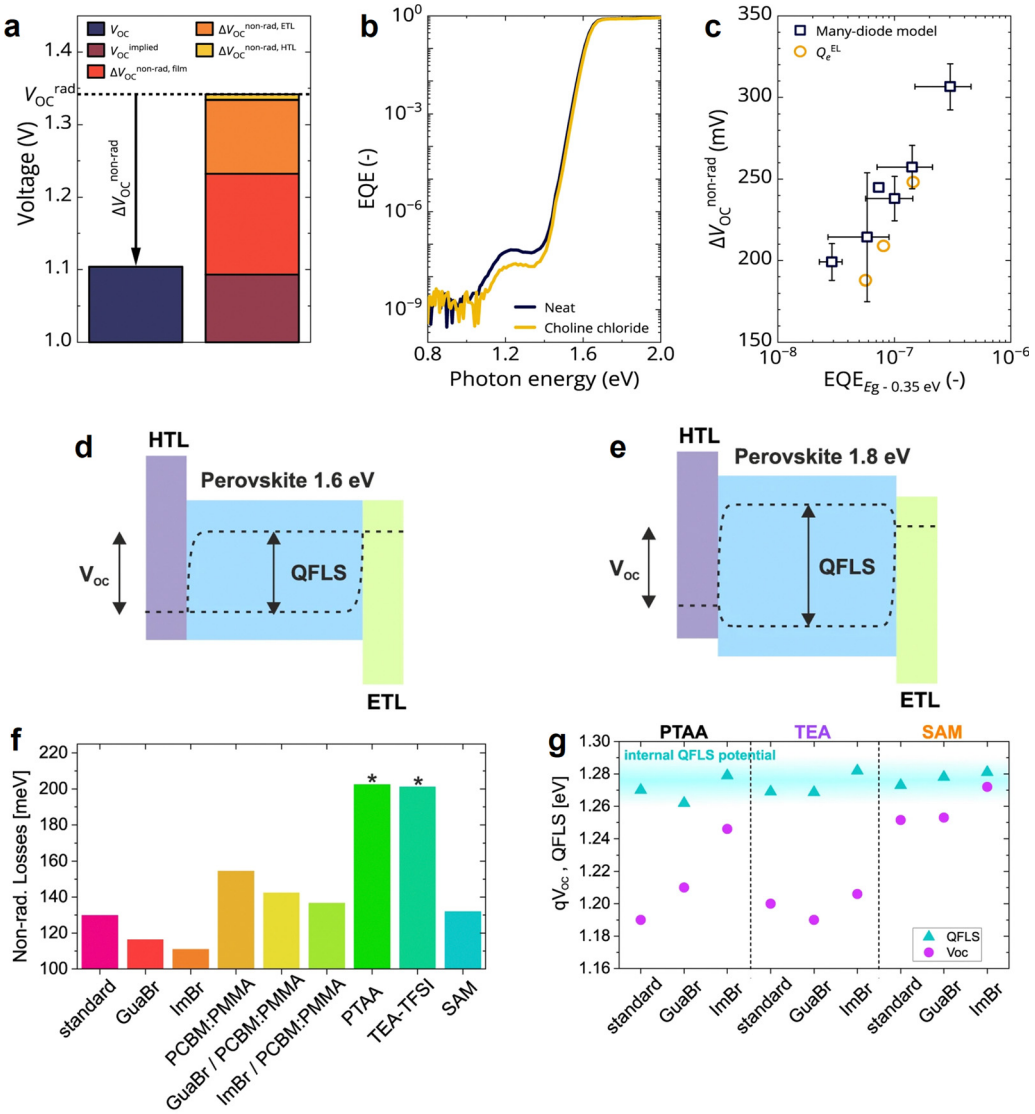

Fig. 5 Assessment of the nonradiative voltage losses in the perovskites. (a) Disentanglement of voltage losses in PSCs. This figure has been reproduced from ref. 98 with permission from Springer Nature, Copyright 2024. (b) Semilogarithmic plot of the sensitive EQE spectrum of solar cell without (dark blue) and with choline chloride passivation (yellow). This figure has been reproduced from ref. 98 with permission from Springer Nature, Copyright 2024. (c) Semilogarithmic plot of the average total nonradiative voltage losses *vs.* the average EQE signal at energies 0.35 eV below the bandgap ($E = E_g - 0.35$ eV) for several PSCs. This figure has been reproduced from ref. 98 with permission from Springer Nature, Copyright 2024. (d) and (e) Schematic diagrams illustrating the relationship between the internal QFLS and external V_{OC} for PSCs with bandgaps of 1.6 eV (d) and 1.8 eV (e). These figures have been reproduced from ref. 99 with permission from Springer Nature, Copyright 2023. (f) Non-radiative recombination losses relative to the radiative thermodynamic limit of the perovskite absorber. This figure has been reproduced from ref. 99 with permission from Springer Nature, Copyright 2023. (g) Comparison of QFLS-V_{OC} in full devices. This figure has been reproduced from ref. 99 with permission from Springer Nature, Copyright 2023.

channel for V_{OC} losses. Further studies discerned that the non-radiative recombination losses in wide bandgap perovskites predominantly occur at the interface with the HTL.[103] In contrast, for p–i–n structured triple-cation perovskite cells (with an E_g of approximately 1.6 eV), non-radiative recombination typically occurs at the interface with the ETL.[104] Hence, a nuanced understanding of the non-radiative recombination mechanisms in PSCs is essential for further advancing the device efficiency.

A high density of non-radiative recombination centers exacerbates the degradation susceptibility of the PSCs.[105] Even under a vacuum or nitrogen atmosphere, the degradation of MAFA-based PSCs has been observed due to the migration of excess PbI_2 phases to the perovskite/HTL interface.[106] For Sn-based PSCs, the oxygen-induced degradation leads to the formation of SnI_4, which quickly evolves into iodine, further oxidizing the perovskite to more SnI_4, establishing a cyclic degradation mechanism.[107] Additionally, recent studies have identified the formation of δ-phases on the (100) facet as non-radiative recombination centers in $FAPbI_3$ thin films (Fig. 6a–c), which adversely affect the optoelectronic properties and accelerate degradation.[108] In comparison to standard PSCs, inverted structures typically manifest a reduced V_{OC}, indicative of

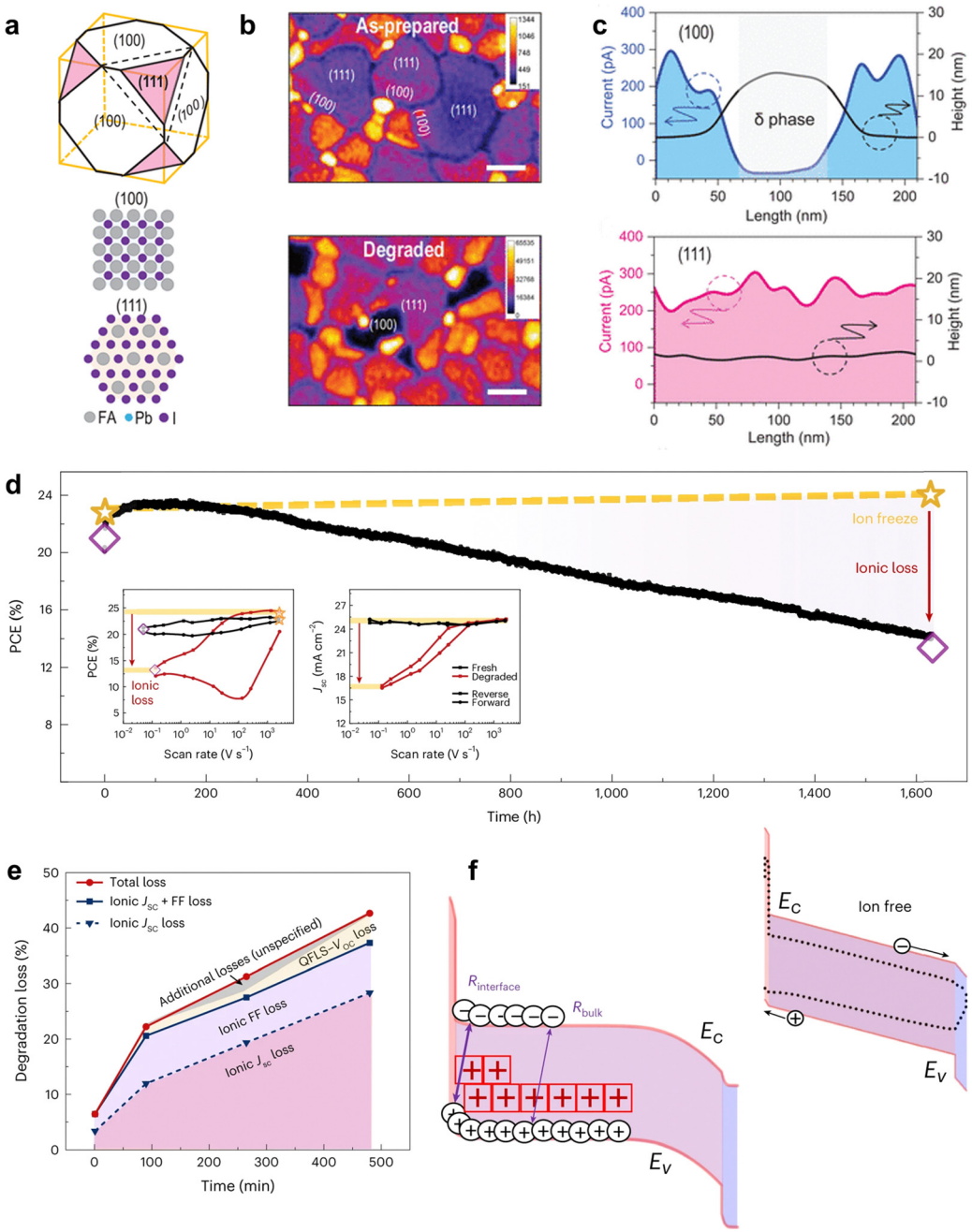

Fig. 6 Degradation mechanisms of the perovskite absorbers. (a) Schematic model of the (100) and (111) facets on a perovskite cubic crystal (top) and the atomic arrangements on the (100) and (111) facets (down). This figure has been reproduced from ref. 108 with permission from AAAS, Copyright 2023. (b) Confocal PL mapping of the as-prepared and degraded samples, with the inset legend indicating PL intensity. This figure has been reproduced from ref. 108 with permission from AAAS, Copyright 2023. (c) Current and height profiles extracted from the degraded (100) and (111) facets, respectively. This figure has been reproduced from ref. 108 with permission from AAAS, Copyright 2023. (d) Ionic losses under operational conditions. This figure has been reproduced from ref. 109 with permission from Springer Nature, Copyright 2024. (e) A breakdown of the loss processes: mobile ion-induced J_{SC} and FF losses, QFLS and V_{OC} mismatch, attributed to the accumulation of ions at the interfaces, and other losses. This figure has been reproduced from ref. 109 with permission from Springer Nature, Copyright 2024. (f) A schematic band diagram of the HTL (red)/perovskite (purple)/ETL (blue) stacks under short-circuit conditions. This figure has been reproduced from ref. 109 with permission from Springer Nature, Copyright 2024.

heightened non-radiative recombination losses. In inverted PSCs, defects have been found to detrimentally influence performance, particularly under illumination or reverse bias conditions. The genesis of iodide interstitials at the interface has been pinpointed as a primary factor for this degradation.[67] In the case of commonly used triple-cation inverted PSCs, the role of ionic losses in intrinsic PSC degradation was revealed,[109] as shown in Fig. 6d. It was found that the ionic losses in J_{SC} and FF can be attributed to the field screening effect caused by the movement of mobile ions (Fig. 6e and f).

3.5 Non-radiative recombination on PSC hysteresis

Hysteresis in the *J–V* characteristics of PSCs, initially identified in dye-sensitized, organic, and silicon solar cells,[110–112] presents a significant challenge in accurately measuring photovoltaic device performance. The hysteresis leads to an underestimation of the real *J–V* curve during the forward scan (from J_{SC} to V_{OC}) and an overestimation in the reverse scan (from V_{OC} to J_{SC}), thus skewing the efficiency measurements.[113] To correct this discrepancy, methods such as averaging forward and reverse scans or stabilizing the device at its maximum power point (MPP) to achieve steady-state output are commonly employed.[114] The hysteresis phenomenon in PSCs encompasses a spectrum of behaviors, including capacitive hysteresis, noncapacitive hysteresis, normal hysteresis, and inverted hysteresis. Capacitive hysteresis is predominantly observed in conventional PSCs employing TiO_2 as CTLs, while noncapacitive hysteresis emerges across various architectures at sufficiently slow scan rates.[115] The emergence of inverted hysteresis, which results in diminished performance during the reverse scan compared to the forward scan, adds complexity to the PSC hysteresis behavior.[116–118] Consequently, scan parameters, such as scan speed, scan range, scan direction, and pre-biasing, must be carefully considered, as they directly influence the type and degree of hysteresis. A thorough understanding of the factors contributing to hysteresis is imperative, and we will explore these determinants in the following discussion.

In PSCs, hysteresis is closely associated with the device architecture, the perovskite absorber, and the interface between the perovskite and CTLs. The device configuration notably influences the extent of hysteresis; planar n–i–p PSCs typically exhibit more pronounced hysteresis compared to mesoporous structures,[119] whereas inverted p–i–n configurations generally show milder hysteresis.[120] This behavior is primarily attributed to the passivating effects of fullerene-based CTLs on the perovskite surface, which penetrate the grain boundaries to enhance electron extraction and transport, thereby reducing hysteresis and stabilizing power output. The intrinsic characteristics of the perovskite absorber, such as the ferroelectric effect[121] and ion migration,[122] have also been linked to hysteresis in PSCs. The ferroelectric effect is often invoked to explain charge carrier dynamics, including non-radiative recombination and hysteresis. Ferroelectric domains within PSCs are thought to enhance charge extraction and influence recombination processes.[121] For example, in p–i–n structured devices, polarization effects during scanning can modify the built-in potential and depletion region width, leading to altered charge separation and performance.[123] The direction of the electric field poling can either impair or improve device performance, depending on its polarity. However, this poling effect is sensitive to temperature,[124] and its interplay with ion migration complicates the overall understanding. Evidence suggests that while ferroelectric properties have been observed in $MAPbI_3$ films, ion migration is widely regarded as the dominant contributor to the macroscopic photocurrent hysteresis observed in PSCs.[125] Ion migration, initially proposed as an explanation for the field-switchable photovoltaic effect and hysteresis,[126,127] involves ions or vacancies moving towards the electrodes under an electric field, potentially leading to a reversed p–i–n structure post-poling. To deepen our comprehension of ion migration and its role in PSC hysteresis, we delve into the nuances of mobile species, their migration pathways, and their impact on charge extraction.

First-principles calculations of activation energies for ionic vacancy migration reveal that halide anions and organic cations, such as MA^+ or FA^+, possess lower diffusion barriers than Pb^{2+} vacancies.[128] Notably, the migration of MA^+ or FA^+ is linked to the observed slow response in PSCs.[129] Halide ions have been identified as the primary contributors to ion migration, moving over distances of hundreds of micrometers near the surface and within the bulk of the perovskites, with vertical migration of lead ions also observed (Fig. 7a and b).[130] Ion migration occurs *via* two concurrent pathways: slower diffusion within crystalline grains and faster diffusion along grain boundaries,[131] where photogenerated carriers can become trapped, generating an internal field within the perovskite layer (Fig. 7c and d). Moreover, ionic polarization also plays a crucial role during voltage scans, as the expansion or charging of the space charge region changes with ionic polarization, effectively creating a variable capacitance during forward and reverse bias scans.[132–134] This capacitance stems from charge accumulation within the perovskite films.[135] Studies indicate that hysteresis in PSCs manifests as sensitivity in the photogenerated charge collection efficiency to the modified electric fields within the devices.[136–138]

Ion migration, facilitated by inherent defects within the perovskite absorber, has been implicated as a primary contributor to the hysteresis observed in the *J–V* characteristics of PSCs (Fig. 7e–h). Nonetheless, this mechanism does not act in isolation; the distribution of defects, especially at the perovskite/CTL interface, also significantly influences hysteresis. Research indicates that negatively charged defects near the CTLs can modify the electronic states of the perovskite, impeding efficient interface charge extraction.[139] Moreover, the impact of interface recombination on PSC performance has been the focus of numerous studies.[140–142] This type of recombination, exacerbated by defects that trap carriers at the interface, is now recognized as a more critical factor than recombination within the grains or along grain boundaries, leading to faster carrier recombination and additional energy losses. Defects and trap states at the perovskite/CTL interfaces have been directly linked to the hysteresis phenomenon.[143] Furthermore, the latest research demonstrated that a negative work function change, which is equivalently described as a negative vacuum-level change at the heterointerface, can accumulate charges in a potential well, lowering ion migration activation energy to aggravate the PSC hysteresis.[144] The localized interface charges at the electron-selective contact can modify the electric field, thereby influencing charge extraction in PSCs. The interplay of these ionic interface charges, rather than the ionic transport rate, determines the hysteresis time scales in PSCs.[145] These insights underscore the necessity of considering both the perovskite's intrinsic properties and the interface behaviors to fully comprehend the origin of PSC hysteresis.

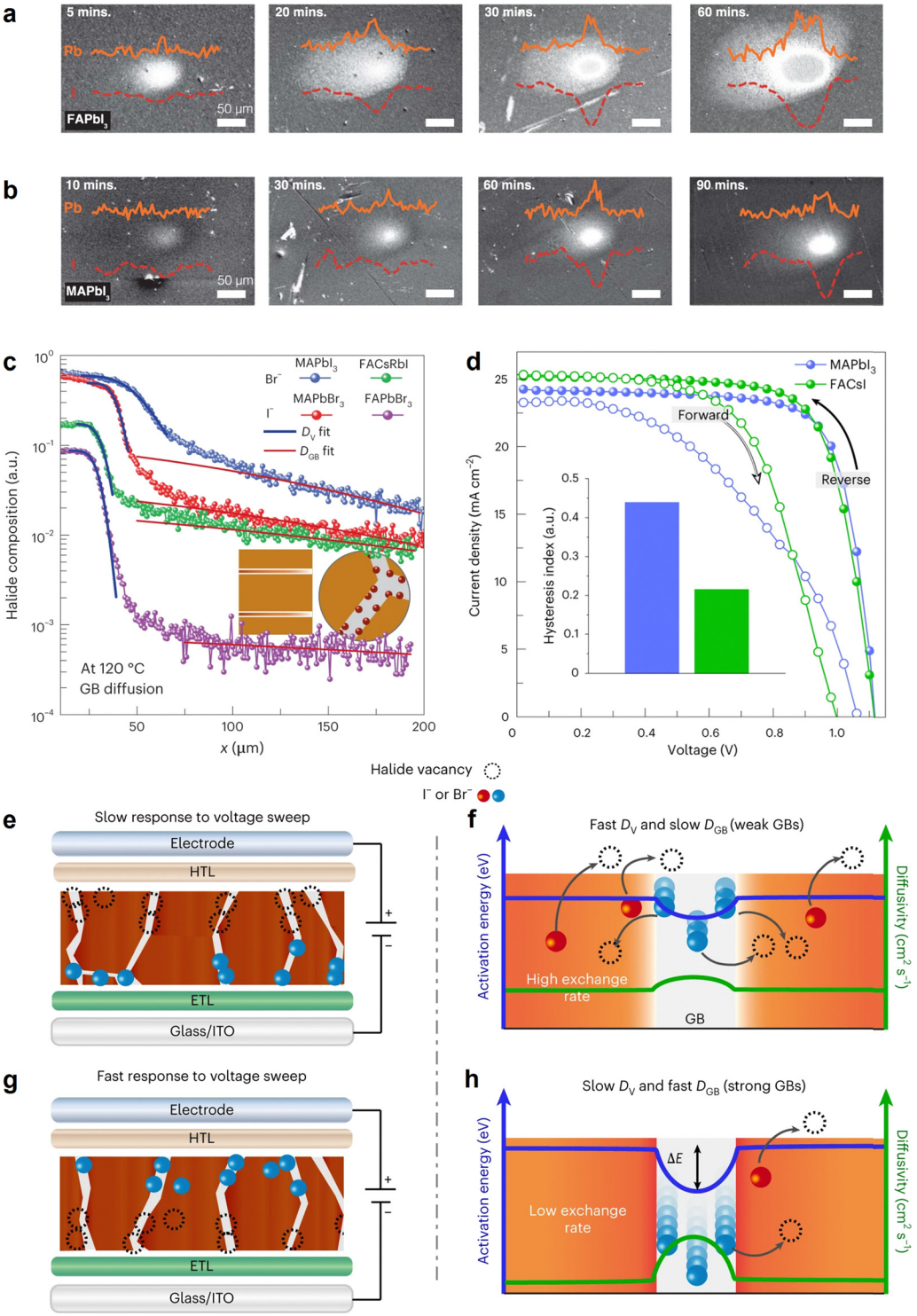

Fig. 7 Ion diffusion–stability–hysteresis mechanism in metal halide perovskites. (a) and (b) Secondary electron images of $FAPbI_3$ after laser illumination for 5–60 min (a) and $MAPbI_3$ after laser illumination for 10–90 min (b). This figure has been reproduced from ref. 130 with permission from Springer Nature, Copyright 2023. (c) GB diffusion as a function of temperature, halide type, and composition function. The inset shows the schematic of GB diffusion. This figure has been reproduced from ref. 131 with permission from Springer Nature, Copyright 2023. (d) *J*–*V* curves of $MAPbI_3$ and FACsI perovskite devices under both forward and reverse voltage scans. The inset shows the hysteresis indexes extracted from the forward and reverse scans. These figures have been reproduced from ref. 131 with permission from Springer Nature, Copyright 2023. (e) and (f) Schematics of halide diffusion along GBs and the D_{GB} relationship with *J*–*V* hysteresis (e) and halide exchange (f) in an MHP system with a fast D_V and slow D_{GB}. (g) and (h) Schematic of halide diffusion along GBs and the D_{GB} relationship with *J*–*V* hysteresis (g) and halide exchange (h) in an MHP system with a slow D_V and fast D_{GB}. These figures have been reproduced from ref. 131 with permission from Springer Nature, Copyright 2023.

4. Strategies to suppress non-radiative recombination

4.1 Crystallization regulation

Achieving high-efficiency PSCs is contingent upon the quality of perovskite films, where enhanced surface coverage and minimized defect density are crucial for reducing non-radiative recombination losses and bolstering device stability. Precise control over the perovskite crystallization process is central to attaining these qualities, encompassing nucleation, intermediate phase formation, and crystal growth. Recent advancements have led to the development of diverse processing techniques designed to fine-tune this process, such as anti-solvent treatment,[146–148] gas-assisted spin-coating,[149–151] vacuum flash-assisted solution processing,[152,153] solvent additive engineering,[154–158] and solvent annealing.[159,160] The fundamental principle underlying these methods is to induce rapid nucleation, followed by controlled crystal growth.[161] Optimal nucleation and growth dynamics involve quickly achieving supersaturation in the perovskite precursor solutions to initiate a high nucleation rate while concurrently moderating the crystal growth rate. The following discussion delves into the strategies that govern the nucleation–growth process of perovskite films.

Anti-solvent treatment is pivotal for synthesizing high-quality perovskite films. Commonly utilized anti-solvents include chlorobenzene (CB), trifluorotoluene (TFT), dichloromethane (DCM), chloroform (CF), toluene, *etc.* Considering environmental impact, green anti-solvents such as ethyl acetate (EA), methyl acetate (MA), diethyl ether (DE), diisopropyl ether (DIE), dibutyl ether (DBE), and anisole[162–164] have also been developed. Owing to better miscibility, higher boiling points and dielectric constants, anti-solvents can quickly extract the host solvents, such as dimethylsulfoxide (DMSO), *N*-methyl-2-pyrrolidone (NMP), *N*,*N*-dimethylformamide (DMF), dimethylacetamide (DMAC), and γ-butyrolactone (GBL), thereby triggering homogeneous nucleation.[165] Noteworthily, the anti-solvent dripping process requires precise control to avoid induction of heterogeneous nucleation, which can arise due to the creation of oversaturation gradients in the precursor solution.[166] Moreover, the strong coordination between polar aprotic solvents and perovskite precursors frequently results in intermediate phase formation before the final film crystallization.[167] Anti-solvents play a critical role in suppressing the growth of these intermediate phases, particularly along the (020) plane, thus averting the formation of needle-like perovskite structures riddled with pinholes.[168] The polarity of the chosen anti-solvent influences the purity of these intermediate phases, which in turn determines the crystallinity and morphology of the resulting perovskite films.

Solvent additive engineering has emerged as a potent strategy to synthesize pure-phase perovskite films by adjusting crystal growth dynamics and facilitating the formation of new intermediate phases. For example, $FAPbI_3$ is favored as an absorber material due to its optimal bandgap range of 1.45–1.51 eV for single-junction photovoltaics.[169] However, its tendency to transition from the desired black α-phase to the non-photoactive yellow δ-phase under ambient conditions poses a challenge. This issue can be addressed by adding I_2 into the $FAPbI_3$ precursor solution containing methylammonium chloride (MACl) additives, which suppresses the MA-FA side reaction and promotes the formation of the α-$FAPbI_3$ phase.[170] To avoid the additive volatilization during annealing, 4-guanidinobenzoic acid hydrochloride (GBAC) has been used to modulate the crystallization kinetics by forming tight packs at the grain boundaries,[171] significantly reducing non-radiative recombination. Despite these advancements, the thermal stability of α-$FAPbI_3$ with MA^+ incorporation remains a concern. To enhance stability without relying on MA^+, researchers have explored surface functionalization with aromatic or aliphatic ammonium cations,[172–175] as well as compositional engineering with alternative cations like Rb^+ and Cs^+.[176–178] Notably, 3-fluoro-4-methoxy-4′,4″-bis((4-vinyl benzyl ether) methyl) triphenylamine (FTPA)[167] or pentanamidine hydrochloride (PAD)[179] can be employed to restrain the intermediate phases (Fig. 8a and b) and induce orientated crystallization of α-$FAPbI_3$ (Fig. 8c and d). In addition, 1-ethyl-3-methylimidazolium hydrogen sulfate ($EMIMHSO_4$) has been predicted to prevent the formation of δ-$FAPbI_3$ during crystallization.[180] Although these approaches yield stable α-$FAPbI_3$ phases, the PCEs of the resulting PSCs have not surpassed those of MA-based PSCs. A breakthrough was achieved by adding DMAcPA into the grain boundaries of FA-based perovskites, achieving a certified PCE of 25.39%.[181] More recently, incorporating alkylammonium chlorides (RACl) into the precursors has effectively controlled the crystallization of the α-$FAPbI_3$ phase.[182] The final α-$FAPbI_3$ films have high crystallinity, preferred orientation, and superior surface morphology, enabling a certified PCE of 25.73%.

Addressing the evaporation of residual solvents is crucial for maintaining the balance between nucleation and crystal growth rates in perovskite film formation. Excessive dimethyl sulfoxide (DMSO) has been shown to form adducts with metal halides, and upon evaporation of DMSO, this can promote undesirable downward crystal growth[183] leading to the formation of pinholes at the buried interface, which adversely impacts PSC performance.[184,185] To mitigate these issues, a novel close-space annealing technique has been developed, precisely regulating the amounts of residual solvents in the intermediate-phase perovskites.[186] In this method, the film is positioned face-down towards an underlying cover, which decelerates the DMSO evaporation, causing slower and more controlled crystal growth. Applying this technique has led to improvements in grain size, crystallinity, and carrier lifetime, thus enhancing the efficiency of both narrow and wide bandgap perovskite absorbers in single-junction PSCs. Moreover, the aqueous synthesis method has emerged as an effective solution to the residual solvent evaporation challenge. Recently, the use of HI aqueous solution as a solvent has been introduced to synthesize α-$FAPbI_3$ perovskite films, free from the intermediate phase.[187] The resulting PSCs demonstrate excellent charge transport properties, achieving a certified PCE of 25.3%.

Controlling the residual PbI_2 content is of great importance, as it can have positive or negative effects on the PSC performance. A slight excess of PbI_2 in the perovskite precursors can

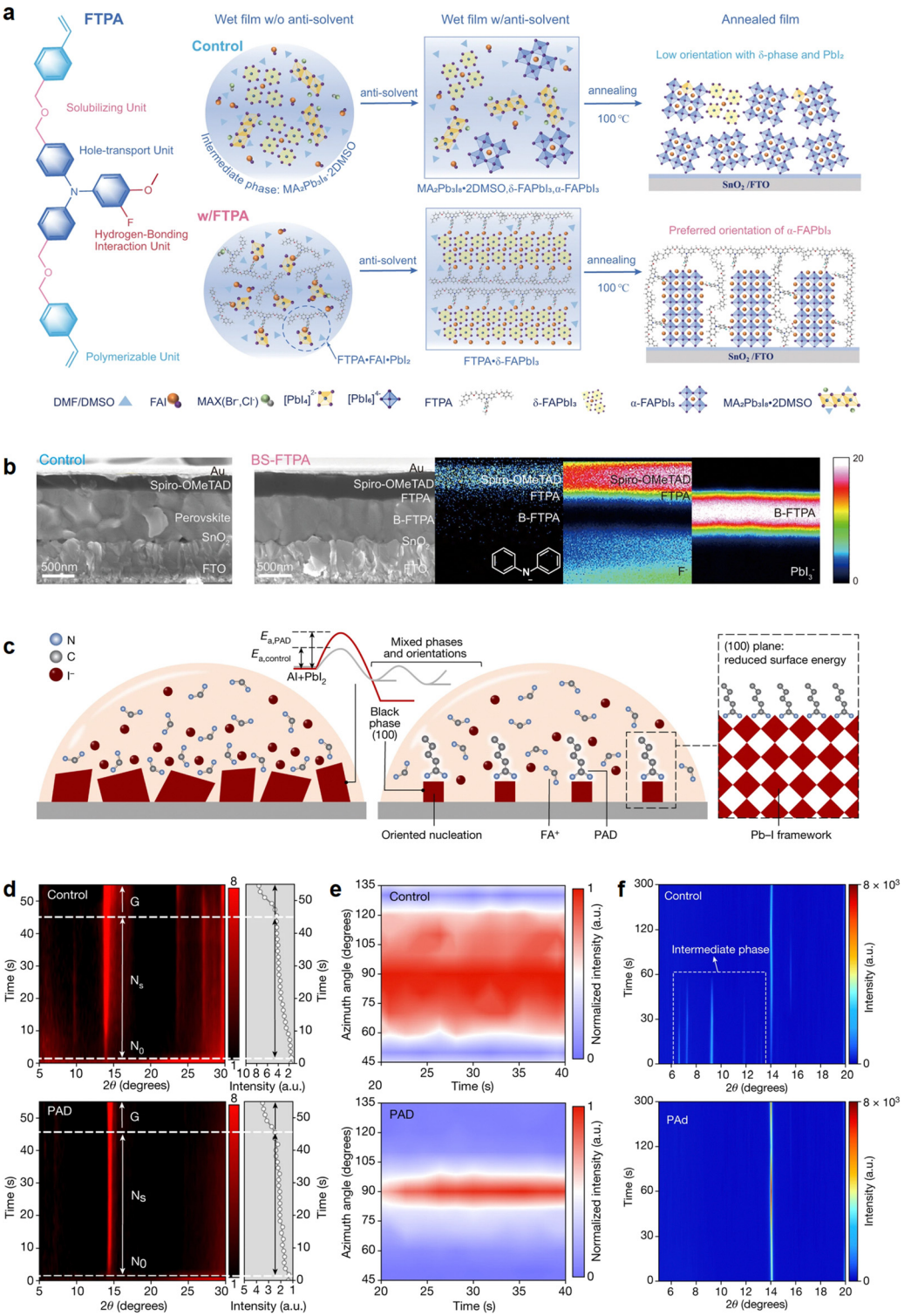

Fig. 8 Crystallization regulation of black-phase $FAPbI_3$. (a) Molecular structure design of FTPA and a schematic diagram illustrating the possible phase evolution of the nucleation and crystallization of FA-based mixed anion perovskites during the film-forming process with (w) or without (w/o) FTPA. This figure has been reproduced from ref. 167 with permission from Springer Nature, Copyright 2023. (b) Cross-sectional SEM images showing the device architectures; ToF-SIMS cross-section images presenting the elemental distribution of $C_{12}H_{10}N^-$, F^-, and PbI_3^- signals in BS-FTPA. This figure has been reproduced from ref. 167 with permission from Springer Nature, Copyright 2023. (c) Schematic illustration of the thermodynamic driving force and the kinetics of the oriented nucleation of perovskite films, where *E* represents the change in energy and a.u. stands for arbitrary units. This figure has been reproduced from ref. 179 with permission from Springer Nature, Copyright 2023. (d) *In situ* GIXRD measurements of perovskite films fabricated without PAD (top) and with PAD (bottom), where N_0 denotes the start of the nucleation, N_s denotes the nucleation stage, and *G* denotes the growth stage. The black–red color scale is the intensity in arbitrary units. This figure has been reproduced from ref. 179 with permission from Springer Nature, Copyright 2023. (e) The evolution of the azimuth angle during the nucleation stage of perovskite films without PAD (top) and with PAD (bottom). This figure has been reproduced from ref. 179 with permission from Springer Nature, Copyright 2023. (f) *In situ* XRD measurements of perovskite films, showing that the control sample contains a mixture of intermediate phases during the annealing process. This figure has been reproduced from ref. 179 with permission from Springer Nature, Copyright 2023.

prevent the formation of organic-rich surfaces, thus reducing defect states and enhancing carrier extraction.[188] However, the excess PbI_2 is prone to decompose into Pb^0 by releasing I_2 (Fig. 9a) due to its photolysis nature.[23] These species generate non-radiative recombination centers and accelerate ion migration, resulting in the degradation and hysteresis of the PSCs.[189–191] Furthermore, the excess PbI_2 at the buried interface (Fig. 9b) leads to the mismatched interfacial energy levels, further hindering charge transfer and increasing V_{OC} loss.[192] To counteract these detrimental effects, 1-butyl-1-methylpiperidinium tetrafluoroborate ($[BMP]^+[BF4]^-$) has been employed to reduce residual PbI_2 levels, thereby preventing the growth of impurity phases and the formation of pinholes.[193] Additionally, RbCl doping has been utilized to convert excess PbI_2 into the more stable compound $(PbI_2)_2RbCl$.[194] This stabilization approach has yielded PSCs with enhanced thermal stability and a certified PCE of 25.6%, free from hysteresis. To further eliminate unstable residual PbI_2 at the buried interface of the PSCs, a pre-embedded mixed A-cation halide strategy was adapted to balance the lattice strain in the $FAPbI_3$ perovskites,[195] which suppresses the

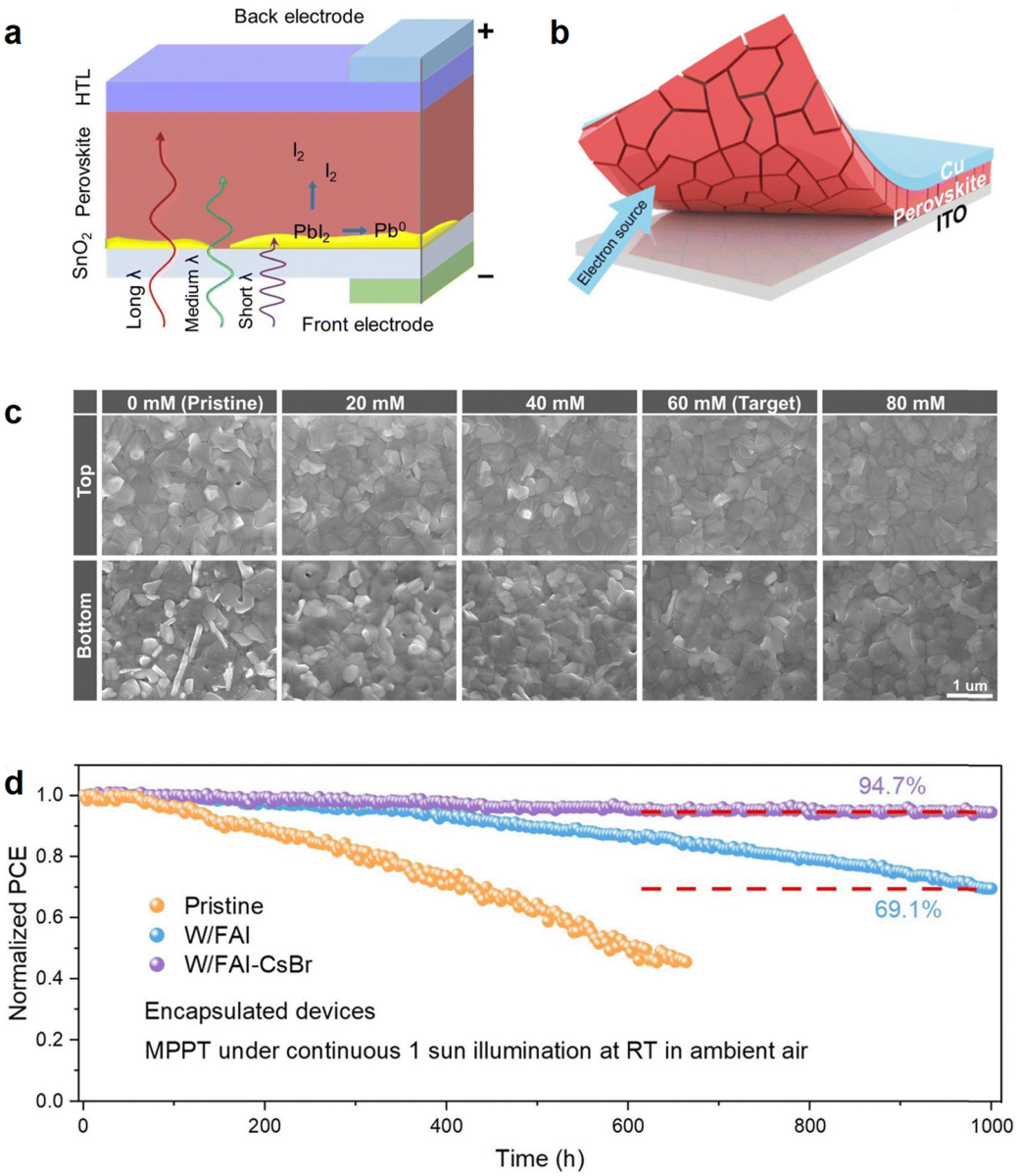

Fig. 9 Elimination of residual PbI_2 at the buried interface. (a) Schematic of the PSCs illuminated by light with different wavelengths. This figure has been reproduced from ref. 195 with permission from Royal Society of Chemistry, Copyright 2023. (b) Lift-off process used to characterize the bottom interface of pristine and pre-embedded A-cation halide-based samples. This figure has been reproduced from ref. 195 with permission from Royal Society of Chemistry, Copyright 2023. (c) SEM images of the top and bottom interfaces of the pristine perovskite films and the perovskite films with different pre-embedded A-cation halide concentrations. This figure has been reproduced from ref. 195 with permission from Royal Society of Chemistry, Copyright 2023. (d) Long-term stability performance of the encapsulated PSCs with the continuous maximum power point tracking under one sun illumination. This figure has been reproduced from ref. 195 with permission from Royal Society of Chemistry, Copyright 2023.

detrimental α to δ phase transition and improves the device stability (Fig. 9c and d).

4.2 Defect passivation

Defect passivation strategies are critical for enhancing the PCE of PSCs by reducing non-radiative recombination losses and improving steady-state device stability. A variety of materials, including organic molecules, polymers, and organic and inorganic salts (Fig. 10–13), have been employed to passivate defects in PSCs.[64] Among these, Lewis base molecules are particularly promising due to their ability to form coordination bonds with uncoordinated metal cations, which are prevalent at grain boundaries and interfaces, thus facilitating more efficient charge transport.[196–198] Nitrogen (N)-containing Lewis base molecules have shown substantial passivation effects.[199–208] These molecules interact with surface cations or the Pb–I lattice, effectively passivating the non-radiative trapping centers in the perovskite layer.[209] Conjugated molecules, in particular, have been shown to chemically passivate a broad range of defect states, spanning shallow to deep levels.[210] However, achieving complete defect site coverage remains challenging, as passivation agents may not fully penetrate all defective regions.[211]

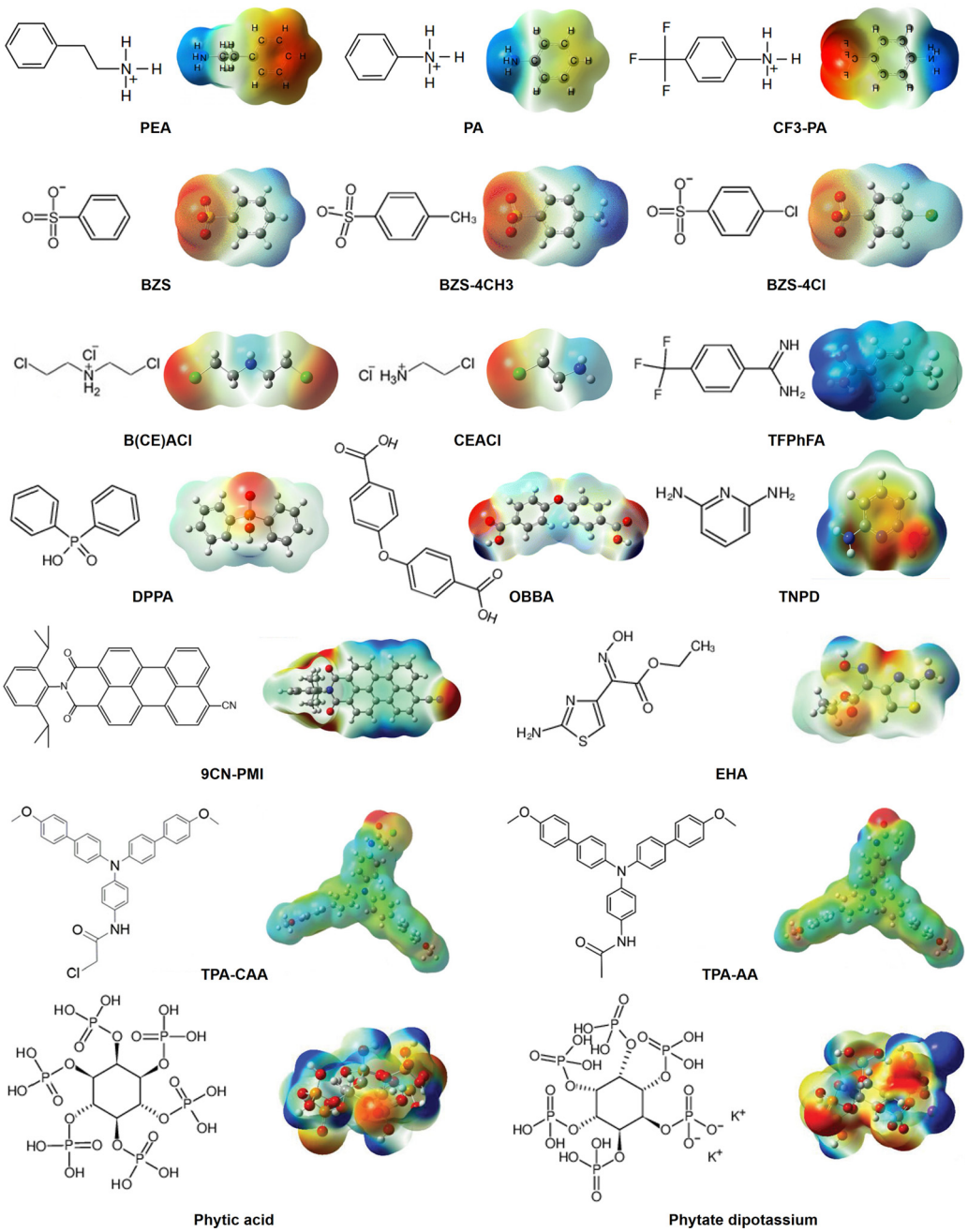

Fig. 10 Molecular structures and electrostatic potential maps of representative passivators. The passivators shown include PEA, PA, CF3-PA, BZS, BZS-4CH3, BZS-4Cl, B(CE)ACl, CEACl, TFPhFA, DPPA, OBBA, TNPD, 9CN-PMI, EHA, TPA-CAA, TPA-AA, phytic acid, and phytate dipotassium.

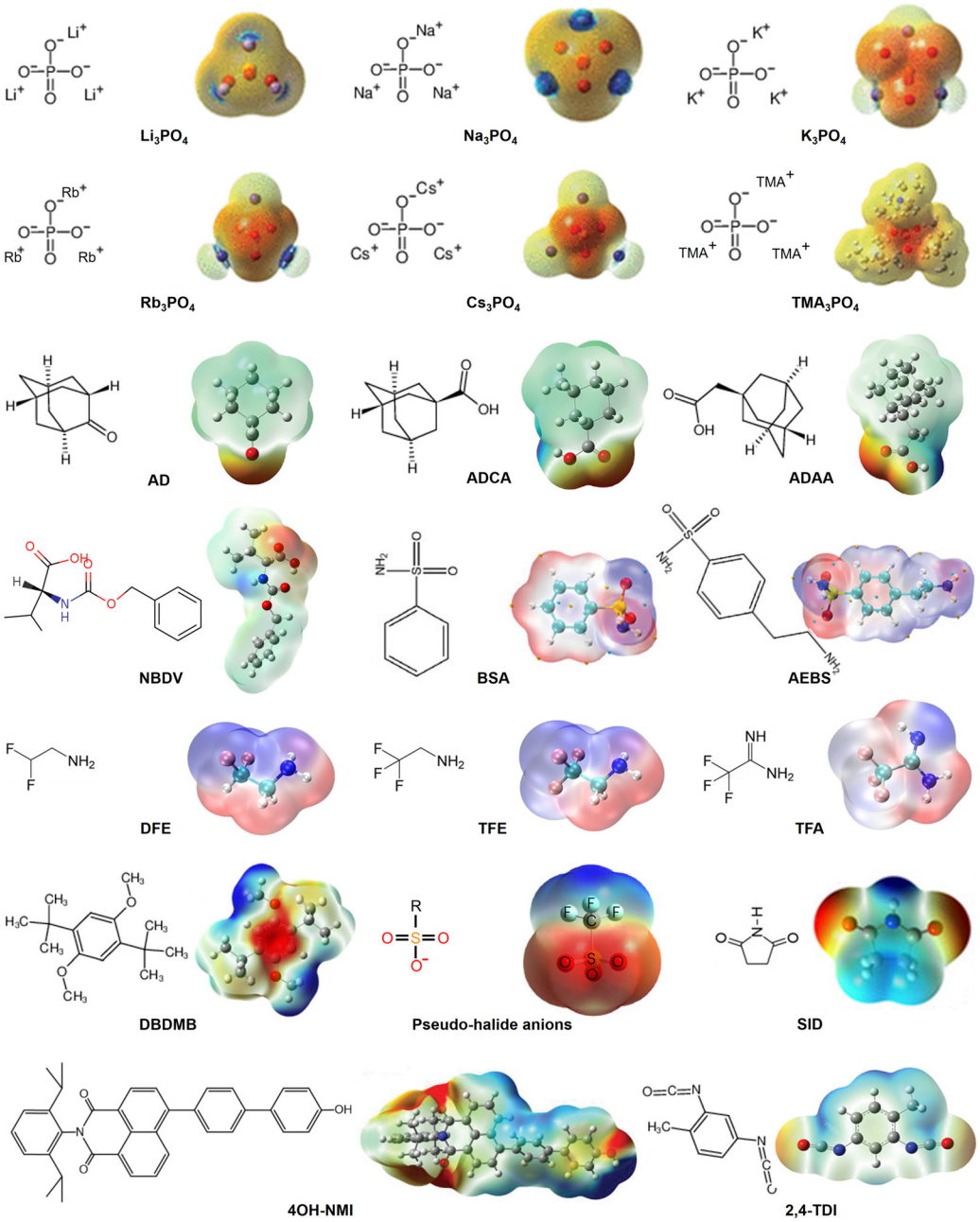

Fig. 11 Molecular structures and electrostatic potential maps of representative passivators. The passivators shown include Li_3PO_4, Na_3PO_4, K_3PO_4, Rb_3PO_4, Cs_3PO_4, TMA_3PO_4, AD, ADCA, ADAA, NBDV, BSA, AEBS, DFE, TFE, TFA, DBDMB, pseudo-halide anions, SID, 4OH-NMI, and 2,4-TDI.

Furthermore, non-radiative recombination at the buried bottom perovskite/CTL interface, particularly in Pb–Sn mixed PSCs, continues to be a limiting factor.[67] To address this issue, sodium 2-cyanoacetate (SZC) was used at the perovskite/SnO_2 interface to simultaneously achieve *in situ* passivation of interfacial defects and bottom-up crystallization modulation.[212–214] This approach effectively reduces non-radiative recombination losses and promotes more efficient charge extraction.

To address the incomplete coverage of defect sites in perovskite films, ammonium cations have been introduced to enhance surface passivation (Fig. 14a). Notably, CF_3-PA has been found to interact more effectively with the perovskite surface than two other passivators (Fig. 14b), leading to increased carrier diffusion lengths and improved efficiency in Pb–Sn PSCs.[215] Furthermore, butylammonium (BA), octylammonium (OA), and symmetrical bis(2-chloroethyl)ammonium ($B(CE)A^+$) have been shown to produce a homogeneous surface potential, which promotes hole carrier extraction and reduces non-radiative recombination.[216,217] Recently, it was reported that treatment with hexylammonium bromide (HABr) can lead to the simultaneous formation of an iodide-rich 2D layer along with a Br halide gradient that extends from defective surfaces and grain boundaries into the bulk 3D layer, extending the charge carrier lifetime and reducing interfacial recombination

velocities.[218] Moreover, printable mesoscopic PSCs designed with mesoporous layers of semiconducting TiO_2, insulating ZrO_2, and conducting carbon infiltrated with perovskite (Fig. 14c and d) showed reduced non-radiative recombination losses when ammonium phosphate was used to modify the bulk TiO_2/perovskite interface. As a result, the charge transport lifetime was shortened, and the charge recombination lifetime was extended (Fig. 14e and f), indicating enhanced charge transfer and suppressed charge recombination in the device.[57]

Sulfur (S)-containing Lewis base molecules, such as 1-butanethiol, have also been anchored onto the perovskite surface to extend carrier diffusion lengths and further suppress phase segregation.[219] Similarly, the functional groups of 2,5-thiophenedicarboxylic acid (TDCA) can bind to the perovskite surface *via* coordination and hydrogen bonding, reducing halide vacancy defects and suppressing interface recombination.[220,221] Another effective Lewis base additive, dibutyl sulfoxide, has been demonstrated to improve perovskite crystallinity, reduce defect density, and release internal residual stress in the bulk.[222] Phosphorus (P)-containing Lewis base molecules, like 1,3-bis(diphenylphosphino)propane (DPPP), possess two phosphorus atoms with sp^3 hybridization in tetrahedral coordination, forming the P–Pb

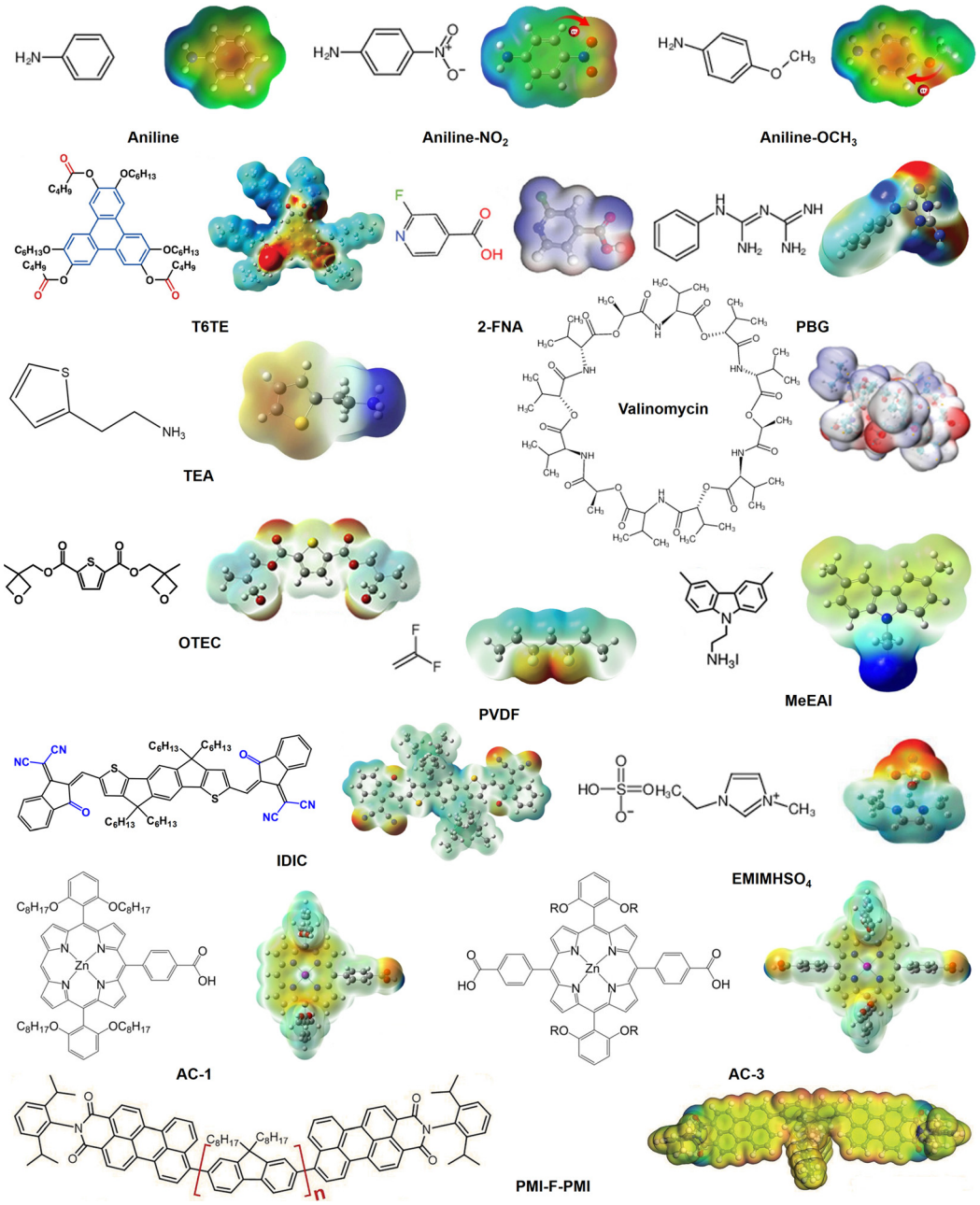

Fig. 12 Molecular structures and electrostatic potential maps of representative passivators. The passivators shown include aniline, aniline-NO_2, aniline-OCH_3, T6TE, 2-FNA, PBG, TEA, valinomycin, OETC, PVDF, MeEAI, IDIC, $EMIMHSO_4$, AC-1, AC-3, and PMI-F-PMI.

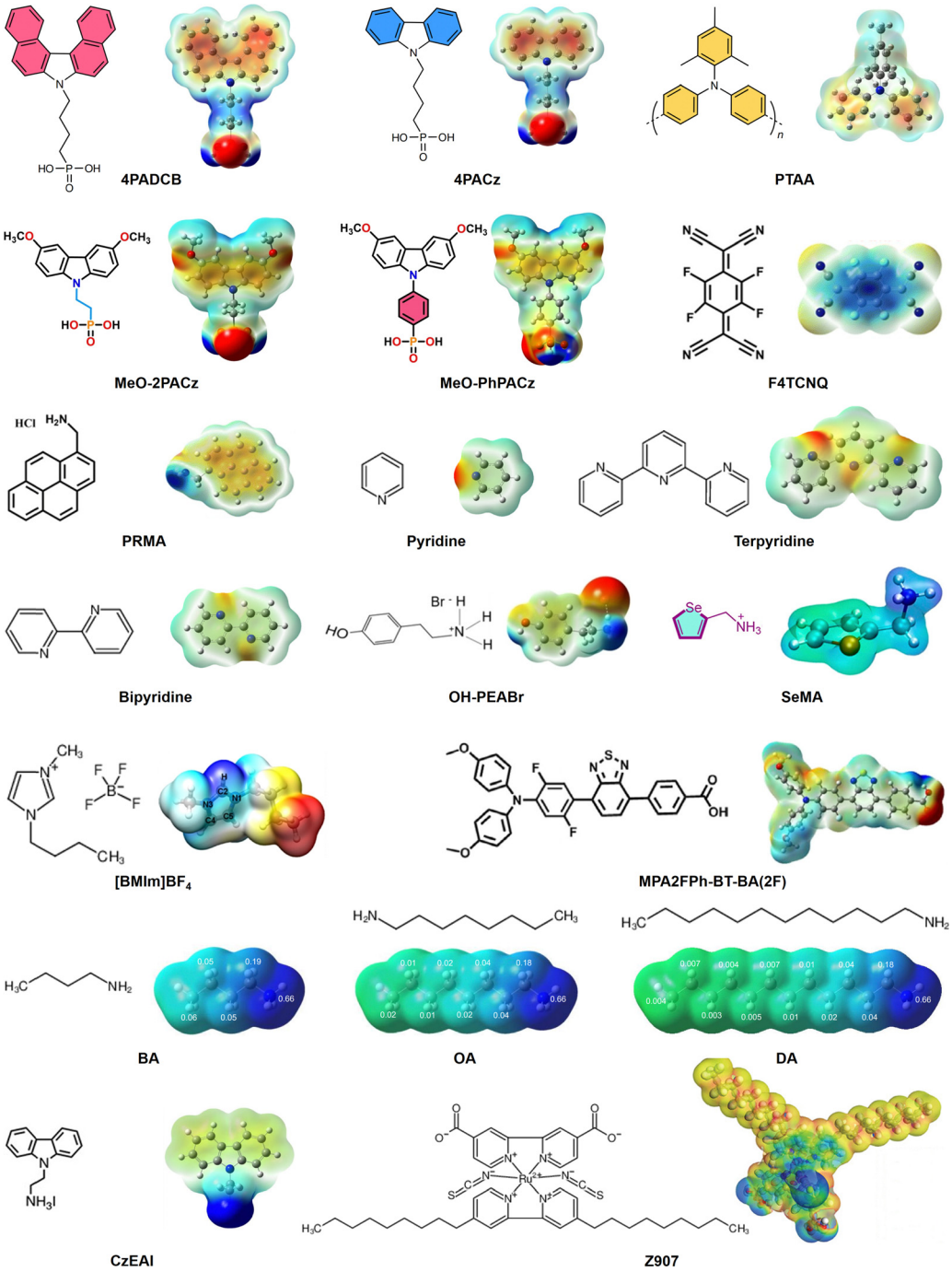

Fig. 13 Molecular structures and electrostatic potential maps of representative passivators. The passivators shown include 4PADCB, 4PACz, PTAA, MeO-2PACz, MeO-PhPACz, F4TCNQ, PRMA, pyridine, terpyridine, bipyridine, OH-PEABr, SeMA, [BMIm]BF_4, MPA2FPh-BT-BA(2F), BA, OA, DA, CzEAI, and Z907.

bond with PbI_2,[223] significantly suppressing non-radiative recombination at interfaces and grain boundaries. Ethane-1,2-diylbis-(diphenylphosphine oxide) (DPPO) also coordinates with PbI_2, but the strong binding of the DPPO molecule to PbI_2 is through the O atom in the P=O bond.[224]

In addition to Lewis base molecules, the functionalization of organic molecule passivation has garnered significant attention due to the coexistence of multiple defect types in perovskites. For instance, D-4-*tert*-butylphenylalanine (D4TBP), containing carboxyl, amine, and aromatic functional groups, is designed to heal charged defects, neutral iodine-related defects, and grain boundary defects.[225] Combinations of EDA and acetylacetone (ACAC) have been selected to regulate the energy level, reduce defect density, and increase grain size.[226] Furthermore, ethyl 2-(2-aminothiazole-4-yl)-2-hydroxyiminoacetate (EHA) with multi-coordination sites is incorporated into the PbI_2 precursor

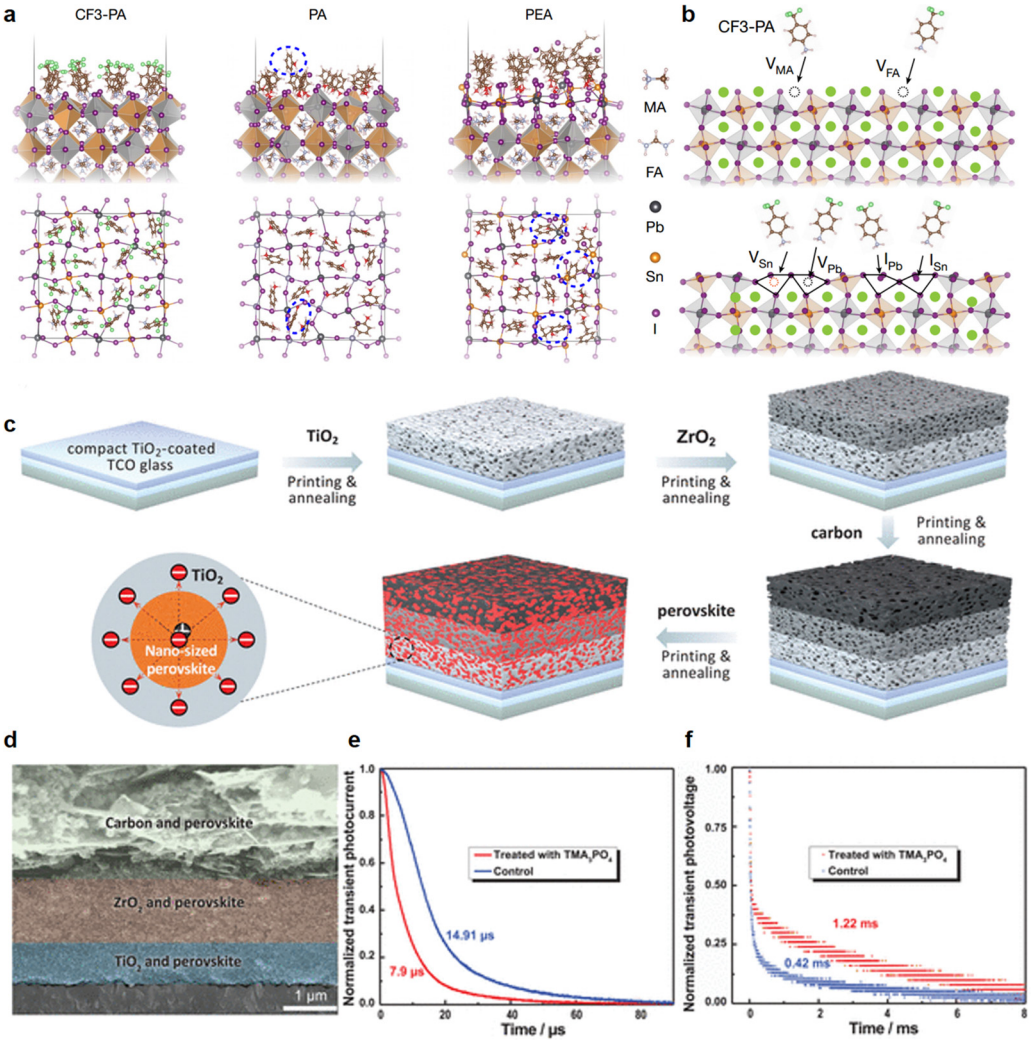

Fig. 14 Ammonium cations for defect passivation of the PSCs. (a) *Ab initio* molecular dynamics snapshots and top views of the CF_3-PA, PA and PEA adsorbed perovskite surfaces at a temperature of 400 K. This figure has been reproduced from ref. 215 with permission from Springer Nature, Copyright 2022. (b) Schematic diagram of the interaction of the ammonium cations with the acceptor-like defects. This figure has been reproduced from ref. 215 with permission from Springer Nature, Copyright 2022. (c) Schematics of the fully wet-processed fabrication process of p-MPSCs and the charge separation process in the printed triple-layer mesoscopic structure. This figure has been reproduced from ref. 57 with permission from AAAS, Copyright 2024. (d) Cross-sectional SEM image of a p-MPSC. This figure has been reproduced from ref. 57 with permission from AAAS, Copyright 2024. (e) and (f) Transient photocurrent (e) and transient photovoltage (f) curves for the control and target p-MPSC. These figures have been reproduced from ref. 57 with permission from AAAS, Copyright 2024.

solution to control crystal growth and passivate defects, connecting grains and filling grain boundaries *via* a multidimensional coordination effect.[227] The amidine group of trifluoroacetamidine (TFA) also strongly chelates onto the perovskite surface to suppress the iodide vacancy, strengthened by additional hydrogen bonds.[228] More recently, bifunctional pseudohalide anions, such as sodium thioglycolate,[229] amylamine hydroiodide (AAI), and 3-(methylthio)propylamine hydroiodide (3MTPAI),[230] have been employed to passivate both positively charged and negatively charged defects on the perovskite surface or interface, effectively reducing non-radiative recombination losses.

Another efficient class of defect passivators is polymers, which are widely used to reduce the risk of producing unwanted defects. For instance, an n-type polymeric small molecule, PY-IT, was utilized to passivate defects and facilitate electron transfer. Due to its strong planarity and rotatable linkers, this polymer can effectively optimize perovskite grain growth orientation and charge transport channels.[231,232] To cap significant grain boundaries, linear polymers are also reported.[233–235] These linear polymers increase the growth activation energy, enable slow crystal growth, and provide efficient defect passivation, which reduces non-radiative recombination. However, these polymers can interact intensely with PbI_2, leading to their precipitation in the precursor solution. Therefore, a cross-linking strategy was developed to passivate the surface and grain boundary of the perovskites (Fig. 15a and b) or the interface of 2D/3D heterostructures (Fig. 15c). The cross-linked

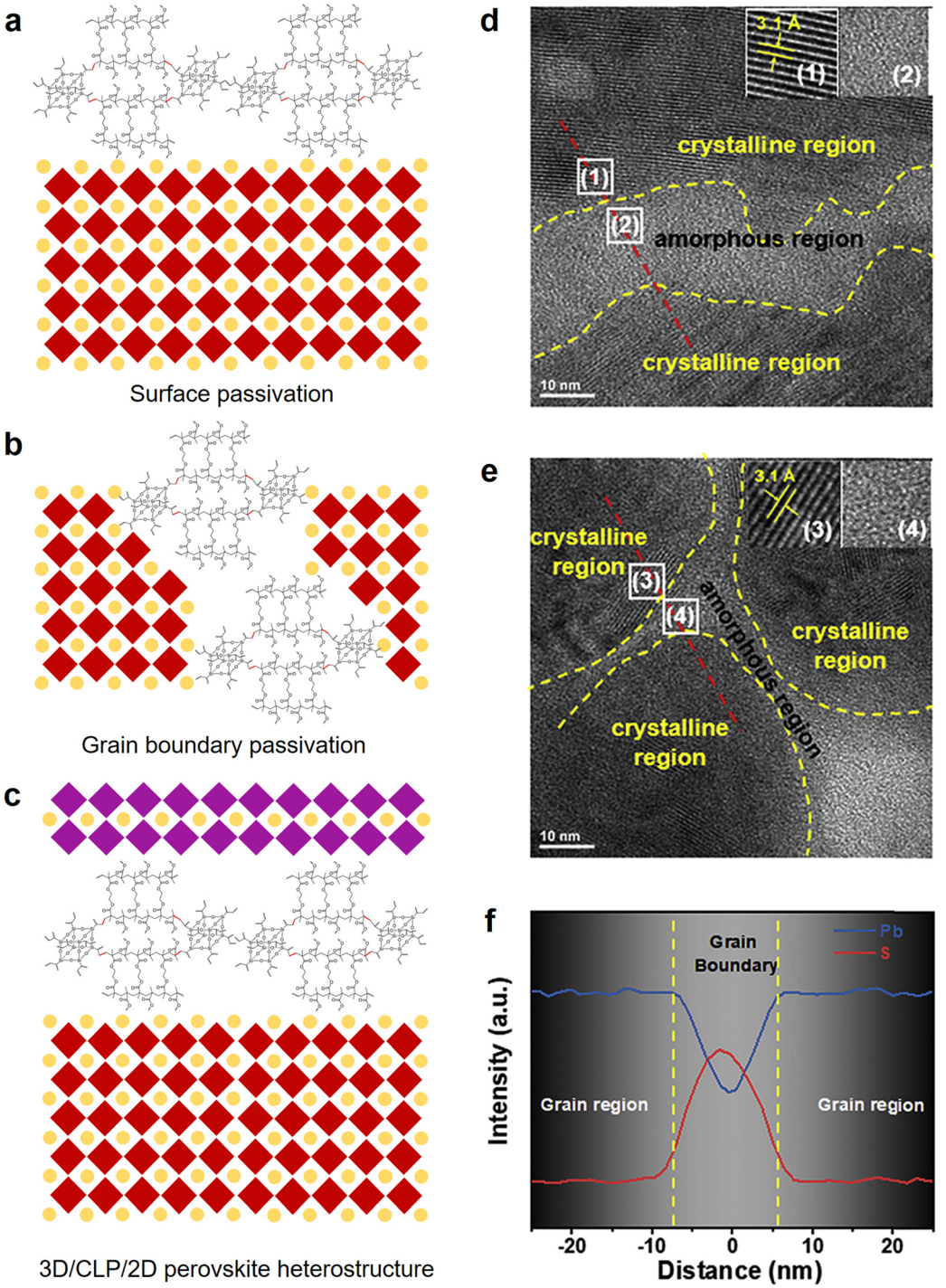

Fig. 15 Cross-linking passivation (CLP) strategy. (a) Schematic illustration of the surface passivation. (b) Grain boundary passivation. (c) Cross-linked polymer used as the interlayer of 2D/3D perovskite heterostructures. (d) Magnified HR-TEM images of the pero-pristine; inset: highlighted regions 1 and 2. This figure has been reproduced from ref. 237 with permission from Elsevier, Copyright 2023. (e) Magnified HR-TEM images of the pero-COETC; inset: highlighted regions 3 and 4. This figure has been reproduced from ref. 237 with permission from Elsevier, Copyright 2023. (f) EDS elemental line scan profiles for the red line shown in Fig. 3e. This figure has been reproduced from ref. 237 with permission from Elsevier, Copyright 2023.

polymer layer not only largely inhibits ion diffusion between the stacked perovskite layers but also effectively stabilizes the phase states of the 3D and 2D perovskites under thermal stress.[236] Additionally, *in situ* crosslinking of bis((3-methyloxetan-3-yl)-methyl)thiophene-2,5-dicarboxylate (OETC), which accumulates at the grain boundaries (Fig. 15d–f), has been explored to release mechanical stress, making it ideal for flexible PSC applications.[237] Other materials such as acrylamide monomers,[238] poly(propylene carbonate) (PPC),[239] PPP polymer,[240] PECL polymer[241] and Rb-functionalized PAA polymer[242] have also

been predicted to enable the cross-linking of perovskite grains, thus inhibiting non-radiative recombination losses. Due to the strong interaction between C═O bonds and Pb^{2+}, the non-radiative recombination is suppressed effectively, improving the PSC performance.

Inorganic compounds offer stronger chemical bonds and greater stability than organic molecules. A CS_2 vapor-assisted passivation strategy has been proposed to manage surface defects and regulate interfacial energy alignment. Through *in situ* reaction, the uncoordinated Pb^{2+} and unanchored I^- on the perovskite surface were passivated by the CS_2, impeding the degradation and reducing trap-state density at the grain boundaries and interfaces.[243] The role of inorganic compounds as extrinsic dopants or passivators significantly impacts the PSC performance. Extrinsic doping typically leads to lattice microstrain side effects, especially when involving cations of inappropriate sizes. To overcome this, cadmium acetate ($CdAc_2$) was introduced into the perovskite precursor solution, where Cd^{2+} incorporates into the PbI_2 lattice to substitute Pb^{2+}, while Ac^- binds at the surfaces of PbI_2 to replace I^-, contributing to an increase in the distance between the PbI_2 layers.[244] Recently, A–B mixed doping has emerged as a synergistic strategy to stabilize α-$FAPbI_3$. Compared to the Cs-doped counterpart, Cs–Eu-doped $FAPbI_3$ exhibits higher optoelectronic characteristics and better phase stability.[245,246] Potassium formate can also reduce the defect density within the perovskite film by modulating perovskite growth and passivating electronic defects, significantly prolonging the carrier lifetime and reducing the *J–V* hysteresis.[247] In addition, the neodymium cation (Nd^{3+}) has recently been employed to mitigate the ion migration in the perovskite lattice, showing enhanced performance compared to monovalent cation dopants.[248] These interstitial cations strongly interact with the charged defects,[249] beneficially mitigating defect trapping and restricting ion migration.

4.3 Contact interface engineering

To mitigate the detrimental effects of non-radiative recombination at the interfaces, several optimization strategies have been explored, such as doping, passivation interlayers, graded junctions, and interfacial dipole engineering. The essence of contact interface engineering is to achieve proficient charge extraction coupled with a significant reduction in non-radiative recombination. Within the framework of p–i–n PSCs, introducing a selenophene-based n-type spacer onto PCBM ETLs has significantly reduced interfacial charge recombination losses.[250] Concurrently, a concerted focus has shifted to doping HTLs with p-type materials for improving hole transport.[251] These p-type dopants elevate the Fermi level, facilitating an optimal energy level alignment at the perovskite/HTL interface and enhancing the HTLs' conductivity, thereby improving the FF. However, in p–i–n PSCs, excessive doping concentration in PEDOT:PSS has been identified as a contributor to pronounced recombination losses at the interface. To address this, a strategic dedoping of PEDOT:PSS with aqueous NaOH has refined the HTLs, optimizing them for enhanced hole extraction and diminished interfacial charge carrier recombination.[252] This intricate interplay of interfacial chemistry and engineering underscores the necessity for precision in PSC design, aiming to propel PSC performance to new heights.

For n–i–p PSCs, the strategic incorporation of chloride ions into CTLs has proven particularly productive.[253–257] This strategy finely adjusts the energy level alignment and effectively passivates defects, substantially bolstering electron extraction and curbing interfacial charge recombination. To modify the TiO_2 surface and interface, ammonium sulfamate with desired NH_4^+ and S═O functional groups was designed to improve the PCE of PSCs.[258] For spiro-OMeTAD HTLs, introducing additives like polyoxyethylene with 2,2,6,6-tetramethylpiperidin-1-yl)oxyl (PPO-TEMPO),[152] 1-dodecanethiol (DDT),[259] or 2,7-bis(bis(4-methoxyphenyl)amino)-9*H*-fluoren-9-one (TPA-O)[260] at the perovskite/HTL interface prevented ion diffusion and facilitated carrier transport. Moreover, the performance enhancement of inverted PSCs using NiO_x HTLs has been limited by impurity ions (such as NO_3^-). Incorporating the ionic liquid (IL) 1-butyl-3-methylimidazolium tetrafluoroborate ([BMIm]BF_4) into the $Ni(NO_3)_2$ precursor before its reaction with NaOH improves the performance of NiO_x-IL-based devices by increasing V_{OC}, which is attributed to reduced interfacial recombination and better energy level alignment.[261] Lead chelation molecules, which strongly interact with Pb^{2+} ions, were added into PTAA HTLs (Fig. 16a), resulting in a reduced amorphous region in perovskites near HTLs, resulting in a passivated perovskite bottom surface.[262]

Inserting a passivation interlayer between the perovskite and CTLs has become an important strategy for suppressing non-radiative recombination losses in the PSCs. To reduce non-radiative recombination at the perovskite/C_{60} interface (Fig. 16b), passivators like *ortho*-carborane,[263] 2-thiopheneethylammonium chloride (TEACl),[265] and A–D–A type perylene monoimide (PMI) derivatives[266] were designed to attenuate the interface energy loss and enhance the interfacial stability. Moreover, another report reported that AlO_x interlayers could be incorporated between the perovskite and C_{60} ETL *via* the atomic layer deposition method. Such interlayers can modify energy levels and suppress the generation of metallic Pb^0, improving the efficiency and stability of PSCs.[267] However, the challenges with the passivating interlayer strategy include a trade-off between V_{OC} and FF, as well as difficulties in uniformly covering a rough large-area surface with an ultrathin passivation layer. To overcome this problem, a porous insulator contact (Al_2O_3) with random nanoscale openings was introduced between the perovskite and HTLs (Fig. 16c and d). The incorporation of Al_2O_3 has been shown to dramatically reduce the surface recombination velocity, as demonstrated by the decrease from 64.2 cm s^{-1} to 9.2 cm s^{-1} (Fig. 16e). This reduction directly correlates with fewer non-radiative recombination events at the interface, greatly reducing non-radiative recombination[264] (Fig. 16f and g) and allowing for more efficient charge transfer and extraction. The porous nature of the Al_2O_3 layer allows for selective charge transport, particularly facilitating hole extraction while preventing undesired recombination. The random nanoscale openings within the Al_2O_3 structure provide channels for efficient charge extraction, enhancing the overall charge collection efficiency of the device.

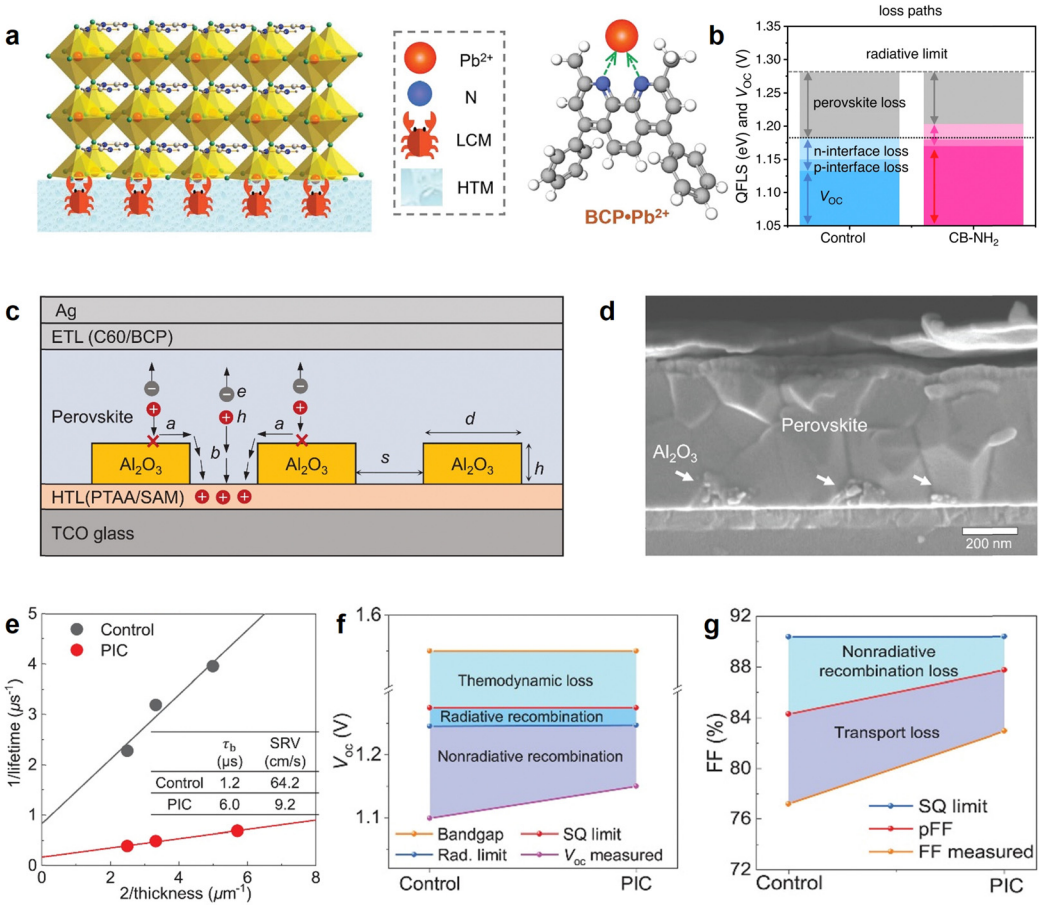

Fig. 16 Interface modification strategy to reduce nonradiative recombination. (a) Illustration depicting the chelation mechanism of lead chelation molecules (LCMs) with Pb^{2+} ions at the bottom side of the perovskite films. This figure has been reproduced from ref. 262 with permission from AAAS, Copyright 2023. (b) Voltage loss mechanism for the control and CB-NH_2-based samples. This figure has been reproduced from ref. 263 with permission from Springer Nature, Copyright 2022. (c) Schematic description of the porous insulator contact (PIC) device structure. This figure has been reproduced from ref. 264 with permission from AAAS, Copyright 2023. (d) Cross-sectional SEM image of the PIC device. This figure has been reproduced from ref. 264 with permission from AAAS, Copyright 2023. (e) Significant improvement in perovskite bulk lifetime and reduction in surface recombination velocity (SRV) observed in the PIC sample relative to the control revealed by fitting the TRPL transients of varied thickness through a double-sided heterostructure model. This figure has been reproduced from ref. 264 with permission from AAAS, Copyright 2023. (f) and (g) Detailed V_{OC} loss analysis (f) and FF loss analysis (g) of the control and PIC devices. These figures have been reproduced from ref. 264 with permission from AAAS, Copyright 2023.

In recent advancements, self-assembled monolayers (SAMs) have been recognized as highly effective in enhancing contact interfaces in PSCs. Fullerene-based SAMs and their derivatives have been particularly noted for their ability to passivate CTL surface defects and minimize interfacial non-radiative recombination.[268–270] This has led to notable improvements in the device performance and consistency of n–i–p PSCs, which is ascribed to the formation of robust interfacial chemical bonds, reducing surface defects and increasing electron mobility. Additionally, non-fullerene-based SAMs have also been employed for CTL defect passivation or as ETLs,[271–273] although they require electrons to tunnel through their insulating layers.[274] Moreover, iodine-terminated SAMs (I-SAMs) have been applied to reinforce the fragile perovskite/SnO_2 interface,[275] enhancing electron extraction, increasing V_{OC}, and mitigating charge accumulation, thus reducing hysteresis. In the context of inverted p–i–n PSCs, various SAMs have been explored as substitutes for conventional HTLs (Fig. 17a). These SAMs have demonstrated superior adhesion to perovskite surfaces,[276–288] increased hole selectivity, and expedited charge extraction while reducing non-radiative recombination losses (Fig. 17b and c). Devices incorporating these SAMs exhibit high FF, enhanced V_{OC}, and improved long-term stability. Carbazole derivative-based SAMs have also been widely used in perovskite tandem solar cells as hole selective layers.[289–293] Combining perovskite with piperazinium iodide interfacial modification (Fig. 17d), the perovskite–silicon tandem solar cells exhibit improved band alignment, reduced non-radiative recombination losses, and enhanced charge extraction at the electron-selective contact, achieving a PCE of up to 32.5% (Fig. 17e).[291]

Due to the inherent roughness of substrates and film deposition conditions, defects are often unavoidable in the SAMs, leading to leakage current at the interface and damaging the PSC performance and stability.[294] To resolve this problem, co-assembled monolayers (co-SAMs) have been innovatively designed as HTLs.[294–298] These co-SAMs feature a lower HOMO

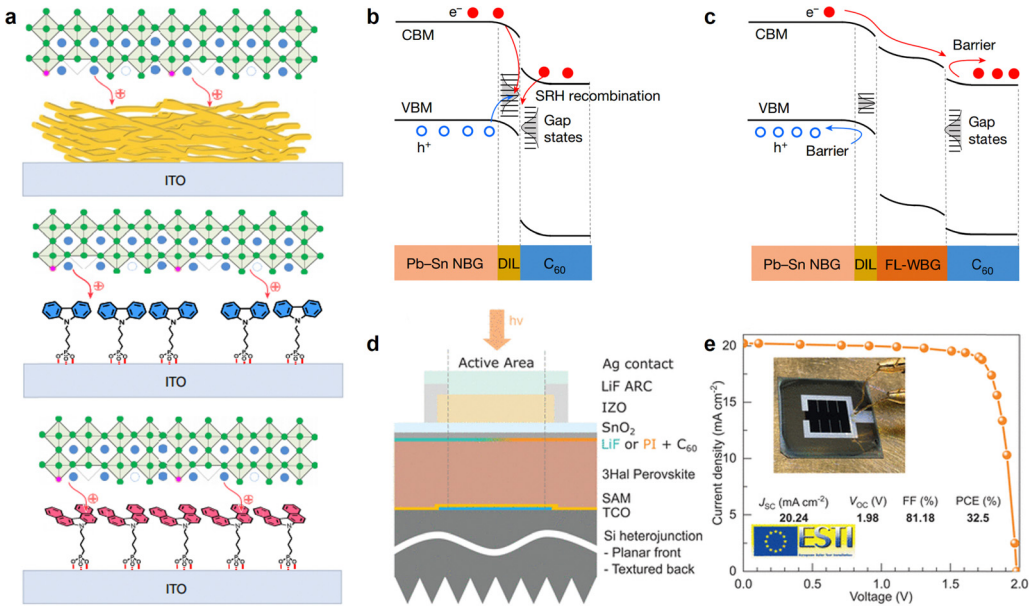

Fig. 17 SAMs as hole selective layers in tandem solar cells. (a) Schematic of the interconnection between ITO, HTL and perovskite for PTAA (top), 4PACz (middle) and 4PADCB (bottom). This figure has been reproduced from ref. 289 with permission from Springer Nature, Copyright 2023. (b) and (c) Energy diagram for the control and PHJ Pb–Sn PSCs. The PHJ structure enables holes to be driven away (blue lines) and accelerates the drift of electrons (red lines) into the C_{60} transport layer, effectively reducing the non-radiative recombination at the defective interface layer. This figure has been reproduced from ref. 290 with permission from Springer Nature, Copyright 2023. (d) Sketch of the perovskite–silicon tandem device. This figure has been reproduced from ref. 291 with permission from AAAS, Copyright 2023. (e) Certified (quasi-) steady-state *J*–*V* measurement conducted at JRC-ESTI, including the performance parameters and a photograph of the tandem cell. This figure has been reproduced from ref. 291 with permission from AAAS, Copyright 2023.

energy level and a large molecular dipole, aligning closely with the energy levels of perovskites and lowering the hole injection barrier. However, ultrathin SAMs can be thermally unstable. To address this limitation, surface-anchored (4-(3,11-dimethoxy-7*H*-dibenzo[*c*,*g*]carbazol-7-yl)butyl)phosphonic acid (MeO-4PADBC) was explored to stabilize the NiO_x/perovskite interface. The energetic alignment and favorable contact and binding between NiO_x/MeO-4PADBC and perovskite reduced the voltage deficit of PSCs and provided strong interface toughening effects under thermal stress, achieving a certified PCE of 25.6%.[299] Improving contact passivation between perovskites and NiO_x is a big challenge due to hindered buried interfaces. To address this issue, a potassium fluoride (KF) ultra-thin buffer layer between 2PACz SAMs and perovskites was used, which effectively prevented direct contact and reduced non-radiative recombination losses.[300] These advancements in SAM technology underscore a significant development in optimizing PSCs, with potential ramifications for sustainable energy solutions.

Forming graded junctions has been recognized as an effective strategy to accelerate charge transport and minimize interfacial non-radiative recombination. Recent developments have focused on the growth of low-dimensional (LD) perovskite modification layers on top of 3D perovskites, which serve to reduce interfacial non-radiative recombination by passivating surface defects[301–303] or by forming LD/3D heterojunctions with graded energy funnels.[304–306] These graded interface designs are advantageous for creating appropriate energy level alignment at the interface, thereby improving charge transport properties and reducing V_{OC} losses.[307,308] Additionally, using zero-dimensional (0D) PEA_2ZnX_4 (Fig. 18a and b) as a capping layer has also shown promise, leading to enhanced surface passivation and forming strong n-N isotype heterojunctions.[309] As a result, the p–i–n PSCs demonstrated significant suppression of charge recombination and a notable enhancement of the built-in potential (Fig. 18c). However, the confinement in the LD perovskite layers often causes electron blocking at the LD/3D interface, and the conventional solution post-treatment strategy is suboptimal.[310,311] To address this, both physical post-treatment and chemical solvent treatment have shown promising results, but their effectiveness varies depending on the specific interface properties and device architecture. For the physical post-treatment method, strong aromatic conjunction molecules were incorporated onto the perovskite surface, effectively modulating the surface electrical properties.[312,313] Physical post-treatment is particularly advantageous when precise control over the surface passivation is required, especially for minimizing electron blocking at the interface. This approach improves surface passivation without introducing additional chemical residues that might interfere with the interface. Besides physical post-treatment methods, chemical solvent treatment like chlorine-based additives can induce secondary growth of bulk grains and form high-quality heterojunctions.[314,315] This method is particularly effective in promoting the growth of a uniform 2D/3D interface, ensuring better energy level alignment and reducing recombination losses. For systems where grain size and crystallinity are critical, chemical solvent treatment is often preferred as

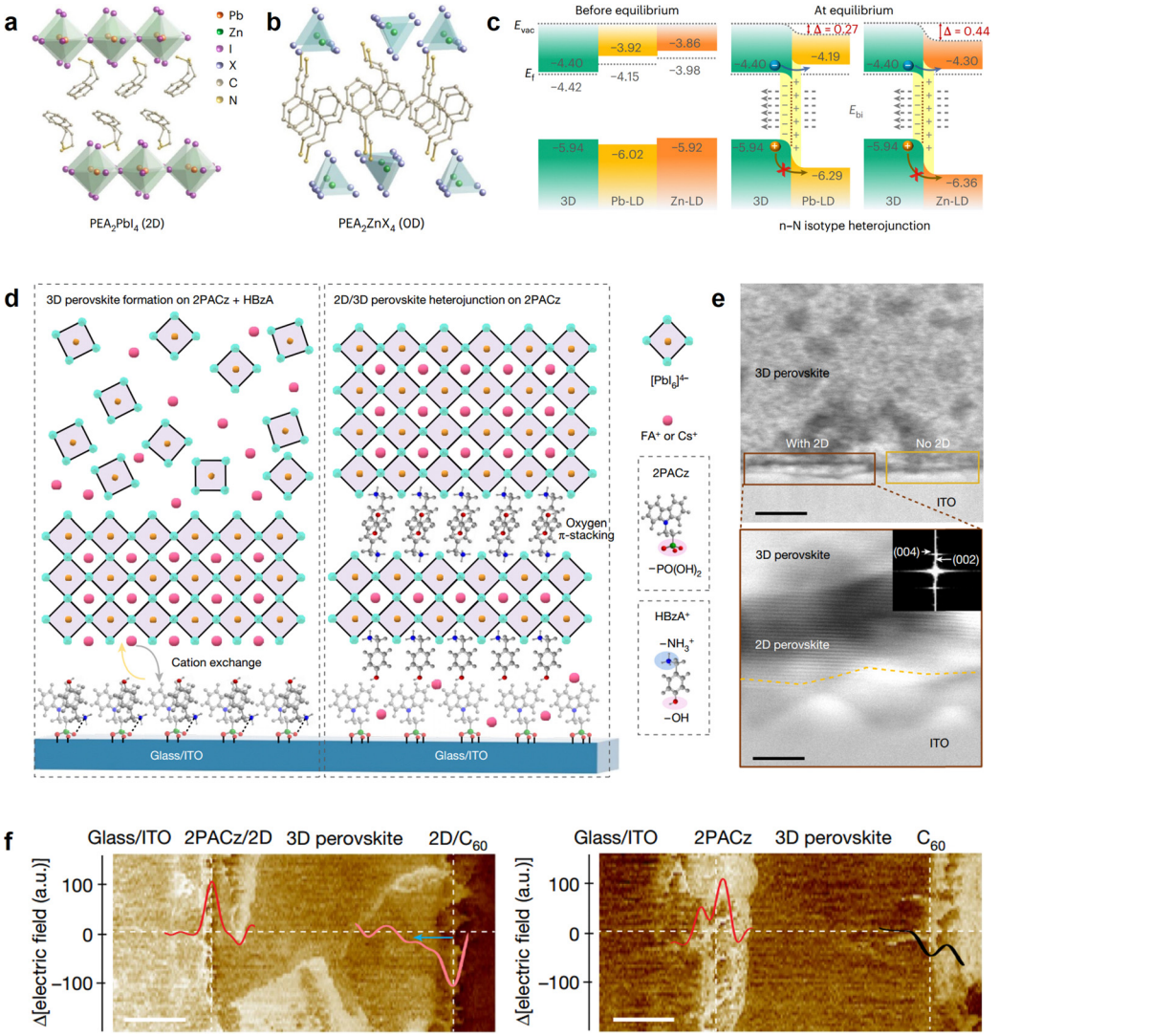

Fig. 18 Graded LD/3D perovskite heterojunctions for energy level alignment or electric-field regulation. (a) and (b) Crystal structures of 2D PEA_2PbI_4 (a) and 0D PEA_2ZnX_4 (b), X = Cl/I. These figures have been reproduced from ref. 309 with permission from Springer Nature, Copyright 2023. (c) Schematic illustration of the formation of the n-N isotype heterojunction. This figure has been reproduced from ref. 309 with permission from Springer Nature, Copyright 2023. (d) The mechanism of 3D perovskite formation on ITO/(2PACz + HBzA) with cation exchange occurring at the bottom interface (left); a 2D/3D heterojunction formed on the ITO/2PACz bottom contact (right). This figure has been reproduced from ref. 316 with permission from Springer Nature, Copyright 2024. (e) Cross-sectional STEM image of the near-bottom HTL contact, with a zoom-in of the area showing the parallel 2D perovskite layers. This figure has been reproduced from ref. 316 with permission from Springer Nature, Copyright 2024. (f) Electric field distribution through both interfaces from the C_{60} ETL to the glass/ITO side acquired through Kelvin probe force microscopy cross-sectional scans. This figure has been reproduced from ref. 316 with permission from Springer Nature, Copyright 2024.

it helps achieve more uniform layer formation. For instance, to resolve the challenge of 2D/3D heterojunction formation at the bottom of the perovskite film (Fig. 18d and e), the 4-hydroxybenzylamine (HBzA) ligand was mixed into the 2PACz SAM solution.[316] These long alkyl amine ligands can generate near-phase-pure 2D perovskites at the top and bottom 3D perovskite interfaces, effectively resolving issues related to charge recombination, ion migration and electric field inhomogeneity (Fig. 18f).

Additional interface modulators have been investigated to facilitate barrier-free hole extraction to the electrode. For instance, a graded HTL incorporating tetracene and Spiro-OMeTAD has been developed.[317] This design leverages the close match between the HOMO level of tetracene and the valence band of the perovskites, resulting in a significant decrease in non-radiative recombination losses at the interface. Other studies have shown that π-conjugated organic cations can effectively modulate the surface band edges and carrier dynamics,[318] or refine interfacial energy level alignment.[319] The carrier collection in these PSCs has been substantially improved owing to the enhanced hole mobility, increasing both J_{SC} and FF. In most cases, the HTL lowers the radiative efficiency of the perovskite absorber layer and increases the overall non-radiative recombination losses.[320] Therefore, HTLs that can support high-quality perovskite deposition at the buried interfaces are crucial

for enhancing hole extraction and reducing interface recombination.[321–324] In addition, employing dipole materials represents a pivotal approach in contact interface engineering within PSCs. The interfacial dipole effect can effectively upshift the Fermi level of n-type metal oxides, thereby reducing their effective work function.[325] For instance, the dipolar chemical bridge can form a beneficial interfacial dipole between the perovskite and CTLs, passivating the surface defects and lowering interfacial energy losses.[326,327] Moreover, applying a dipole layer with a π-conjugated backbone has demonstrated potential in passivating trap states and enhancing charge transfer.[328–334] These dipole interlayers create dipole moments and modulate the energy level at the perovskite/HTL interface, thus enhancing the device's overall performance and stability.

5. Conclusions and perspectives

The development of high-efficiency PSCs is critically dependent on mitigating non-radiative recombination losses and eliminating hysteresis, both of which are essential for enhancing device stability and efficiency. A comprehensive understanding of these detrimental effects is essential for devising strategies that push PCEs closer to their theoretical limits. This review identifies several key obstacles to optimization of PSCs, including energy level misalignment across functional layers, defect capture, and ion migration. These factors significantly contribute to non-radiative recombination and *J*–*V* hysteresis, with deep-level defects impacting V_{OC} and non-radiative decay pathways. Although shallow-level defects are more abundant, they lead to issues such as hysteresis, phase segregation, and overall device degradation. Recent scientific efforts to address these losses focus on innovative approaches in interface optimization. Techniques such as refined doping to reduce trap-assisted recombination, strategic insertion of passivation interlayers, graded junctions to minimize energy barriers, and the engineering of interfacial dipole moments have shown promise. These advancements have been instrumental in suppressing non-radiative recombination, driving PSCs towards achieving and even surpassing current performance benchmarks. Identifying and addressing the challenges that impede reaching the SQ limit is paramount. This review outlines several promising future research directions:

(1) Addressing energy level alignment at interfaces: achieving proper energy level alignment at the perovskite/CTL interface is critical for efficient charge transfer. Misalignment can increase non-radiative recombination, reducing V_{OC} and PCE. Future research should focus on understanding the complex relationship between interfacial defect states and energy alignment. Techniques like X-ray photoelectron spectroscopy, ultraviolet photoelectron spectroscopy, and Kelvin probe force microscopy can provide valuable insights. Additionally, theoretical modeling and simulations offer deeper understanding of the electronic structure and potential misalignments at the interface. Developing interfacial layers or treatments to better align energy levels will facilitate more efficient charge extraction and transport, ultimately enhancing PSC performance and stability.

(2) In-depth study of defect-assisted recombination processes: the field currently lacks a comprehensive quantitative approach to assess defect capture cross-sections. Future research should focus on integrating a deeper understanding of defect density, defect energy levels, and carriers' drift velocity to better quantify defect capture cross-sections. Parallel to this, the ongoing development of passivation molecules necessitates an expanded investigation into their mechanisms, particularly concerning their interactions with various defect types. Addressing these issues can significantly reduce defect-induced recombination, thereby enhancing the overall efficiency of PSCs.

(3) Developing graded junctions: reducing charge recombination rates at the heterojunction interface through implementing graded junctions remains an area ripe for exploration. However, detailed energy level offsets between the uppermost surface regions and the interfaces at the bottom of the PSC structure remain poorly understood. Addressing this knowledge gap requires the development of new materials capable of providing both stability and improved performance. Establishing stable graded junctions promises to enhance current PSC technologies and push the field into new areas of physics and chemistry. These advancements could pave the way for PSCs to achieve and potentially surpass the PCEs of traditional crystalline silicon solar cells.

(4) Advancing passivation techniques: effective passivation techniques are crucial for mitigating defect-induced recombination, thereby enhancing the overall efficiency of PSCs. Future research should delve deeper into the interactions between passivation molecules and various defect types. This involves both experimental studies and theoretical simulations. Techniques like scanning tunneling microscopy and density functional theory simulations can provide insights into atomic-level interactions. Developing multifunctional passivation molecules capable of addressing multiple defect types simultaneously is a promising direction. By improving passivation techniques, higher PCEs and better long-term stability for PSCs can be achieved.

(5) Enhancing long-term stability: long-term stability is a prerequisite for the practical application of PSCs. Organic semiconductors and perovskite materials are particularly vulnerable to degradation from oxygen and moisture under illumination. Addressing this degradation is crucial for commercialization. Special attention should be given to optimizing the mixed microstructure of organic films, the composition of perovskite materials, and the synergistic optimization of device interfaces. Developing reliable encapsulation methods, such as atomic layer deposition and advanced barrier coatings, will be key to extending the operational lifespan of PSCs. Understanding degradation mechanisms at the molecular level through advanced techniques like *in situ* X-ray diffraction and environmental transmission electron microscopy is essential.

(6) Achieving high-performance transparent electrodes: transparent electrodes significantly impact the performance of semi-transparent PSCs (ST-PSCs). Future research should focus on developing highly transparent and conductive materials for

transparent electrodes to meet the size requirements for window integration with minimal performance loss. Low-cost fabrication methods for transparent conductive oxides and thin metal films should also be explored to facilitate large-scale production of ST-PSCs. Promising materials include indium tin oxide, fluorine-doped tin oxide, and graphene. Additionally, developing new materials with better transparency and conductivity, such as metal nanowires and conductive polymers, can further enhance the performance of ST-PSCs. Integrating these transparent electrodes with efficient light management techniques, such as anti-reflective coatings and light-trapping structures, will also be crucial.

In summary, addressing these challenges will enable PSCs to set new benchmarks in solar energy conversion, marking a significant shift in the photovoltaic technology landscape. Continued research and innovation in these areas are essential to unlock the full potential of PSCs, leading to more efficient, stable, and cost-effective solar energy solutions for the future. The ongoing collaboration between materials scientists, chemists, and engineers will be crucial in realizing these advancements, ensuring PSC technology can meet the growing global demand for renewable energy.

Data availability

The data presented in this study are available and may be obtained by contacting the corresponding author.

Conflicts of interest

The authors declare no competing interests.

Acknowledgements

The authors gratefully acknowledge the National Natural Science Foundation of China (No. 61704057, 52302333), Natural Science Foundation of Shanghai (grant no. 20ZR1417400), Natural Science Foundation of Chongqing (No. cstc2021jcyj-msxmX0786), Shenzhen Science and Technology Program (No. KQTD20221101093647058, KJZD20231025152759001), Guangdong Basic and Applied Basic Research Foundation (No. 2023A1515012788), the PolyU Start-up Fund (No. 1-BEBB), the Photonics Research Institute Strategic Grant (No. 1-CDJ7), Hunan Provincial Natural Science Foundation of China (No. 2023JJ30198), Excellent Youth Funding of Hunan Provincial Education Department (No. 22B0624), and National Key Research and Development Program of China (No. 2019YFB1503402).

References

1 A. Kojima, K. Teshima, Y. Shirai and T. Miyasaka, *J. Am. Chem. Soc.*, 2009, **131**, 6050–6051.
2 The National Renewable Energy Laboratory (NREL), Solar Cell Efficiency Chart **https://www.nrel.gov/pv/assets/pdfs/best-research-cell-efficiencies.pdf** (accessed: August 2024).
3 E. Aydin, E. Ugur, B. K. Yildirim, T. G. Allen, P. Dally, A. Razzaq, F. Cao, L. Xu, B. Vishal, A. Yazmaciyan, A. A. Said, S. Zhumagali, R. Azmi, M. Babics, A. Fell, C. Xiao and S. De Wolf, *Nature*, 2023, **623**, 732–738.
4 S. Liu, Y. Lu, C. Yu, J. Li, R. Luo, R. Guo, H. Liang, X. Jia, X. Guo, Y.-D. Wang, Q. Zhou, X. Wang, S. Yang, M. Sui, P. Müller-Buschbaum and Y. Hou, *Nature*, 2024, **628**, 306–312.
5 Y. Yang, C. Liu, Y. Ding, B. Ding, J. Xu, A. Liu, J. Yu, L. Grater, H. Zhu, S. S. Hadke, V. K. Sangwan, A. S. R. Bati, X. Hu, J. Li, S. M. Park, M. C. Hersam, B. Chen, M. K. Nazeeruddin, M. G. Kanatzidis and E. H. Sargent, *Nat. Energy*, 2024, **9**, 316–323.
6 J. Li, H. Liang, C. Xiao, X. Jia, R. Guo, J. Chen, X. Guo, R. Luo, X. Wang, M. Li, M. Rossier, A. Hauser, F. Linardi, E. Alvianto, S. Liu, J. Feng and Y. Hou, *Nat. Energy*, 2024, **9**, 308–315.
7 J. Chen, J. Luo, E. Hou, P. Song, Y. Li, C. Sun, W. Feng, S. Cheng, H. Zhang, L. Xie, C. Tian and Z. Wei, *Nat. Photonics*, 2024, **18**, 464–470.
8 J. Luo, B. Liu, H. Yin, X. Zhou, M. Wu, H. Shi, J. Zhang, J. Elia, K. Zhang, J. Wu, Z. Xie, C. Liu, J. Yuan, Z. Wan, T. Heumueller, L. Lüer, E. Spiecker, N. Li, C. Jia, C. J. Brabec and Y. Zhao, *Nat. Commun.*, 2024, **15**, 2002.
9 X. Chu, Q. Ye, Z. Wang, C. Zhang, F. Ma, Z. Qu, Y. Zhao, Z. Yin, H.-X. Deng, X. Zhang and J. You, *Nat. Energy*, 2023, **8**, 372–380.
10 Y. Yang, S. Cheng, X. Zhu, S. Li, Z. Zheng, K. Zhao, L. Ji, R. Li, Y. Liu, C. Liu, Q. Lin, N. Yan and Z. Wang, *Nat. Energy*, 2024, **9**, 37–46.
11 S. Reichert, Q. An, Y.-W. Woo, A. Walsh, Y. Vaynzof and C. Deibel, *Nat. Commun.*, 2020, **11**, 6098.
12 X. Ren, J. Wang, Y. Lin, Y. Wang, H. Xie, H. Huang, B. Yang, Y. Yan, Y. Gao, J. He, J. Huang and Y. Yuan, *Nat. Mater.*, 2024, **23**, 810–817.
13 M. A. Uddin, P. J. S. Rana, Z. Ni, G. Yang, M. Li, M. Wang, H. Gu, H. Zhang, B. D. Dou and J. Huang, *Nat. Commun.*, 2024, **15**, 1355.
14 J. Min, Y. Choi, D. Kim and T. Park, *Adv. Energy Mater.*, 2024, **14**, 2302659.
15 Y. Zhong, J. Yang, X. Wang, Y. Liu, Q. Cai, L. Tan and Y. Chen, *Adv. Mater.*, 2023, **35**, 2302552.
16 Z. Shen, Q. Han, X. Luo, Y. Shen, Y. Wang, Y. Yuan, Y. Zhang, Y. Yang and L. Han, *Nat. Photonics*, 2024, **18**, 450–457.
17 J.-W. Lee, S.-G. Kim, S.-H. Bae, D.-K. Lee, O. Lin, Y. Yang and N.-G. Park, *Nano Lett.*, 2017, **17**, 4270–4276.
18 B. Ding, Y. Ding, J. Peng, J. Romano-deGea, L. E. K. Frederiksen, H. Kanda, O. A. Syzgantseva, M. A. Syzgantseva, J.-N. Audinot, J. Bour, S. Zhang, T. Wirtz, Z. Fei, P. Dörflinger, N. Shibayama, Y. Niu, S. Hu, S. Zhang, F. F. Tirani, Y. Liu, G.-J. Yang, K. Brooks, L. Hu, S. Kinge, V. Dyakonov, X. Zhang, S. Dai, P. J. Dyson and M. K. Nazeeruddin, *Nature*, 2024, **628**, 299–305.
19 S. Cai, Z. Li, Y. Zhang, T. Liu, P. Wang, M.-G. Ju, S. Pang, S. P. Lau, X. C. Zeng and Y. Zhou, *Nat. Commun.*, 2024, **15**, 2329.
20 L. Shi, M. P. Bucknall, T. L. Young, M. Zhang, L. Hu, J. Bing, D. S. Lee, J. Kim, T. Wu, N. Takamure, D. R. McKenzie,

S. Huang, M. A. Green and A. W. Y. Ho-Baillie, *Science*, 2020, **368**, eaba2412.
21 T. Wang, J. Yang, Q. Cao, X. Pu, Y. Li, H. Chen, J. Zhao, Y. Zhang, X. Chen and X. Li, *Nat. Commun.*, 2023, **14**, 1342.
22 P. Mariani, M. Á. Molina-García, J. Barichello, M. I. Zappia, E. Magliano, L. A. Castriotta, L. Gabatel, S. B. Thorat, A. E. D. R. Castillo, F. Drago, E. Leonardi, S. Pescetelli, L. Vesce, F. Di Giacomo, F. Matteocci, A. Agresti, N. De Giorgi, S. Bellani, A. Di Carlo and F. Bonaccorso, *Nat. Commun.*, 2024, **15**, 4552.
23 J. Liang, X. Hu, C. Wang, C. Liang, C. Chen, M. Xiao, J. Li, C. Tao, G. Xing, R. Yu, W. Ke and G. Fang, *Joule*, 2022, **6**, 816–833.
24 P. Chen, Y. Xiao, J. Hu, S. Li, D. Luo, R. Su, P. Caprioglio, P. Kaienburg, X. Jia, N. Chen, J. Wu, Y. Sui, P. Tang, H. Yan, T. Huang, M. Yu, Q. Li, L. Zhao, C.-H. Hou, Y.-W. You, J.-J. Shyue, D. Wang, X. Li, Q. Zhao, Q. Gong, Z.-H. Lu, H. J. Snaith and R. Zhu, *Nature*, 2024, **625**, 516–522.
25 W. Xu, B. Chen, Z. Zhang, Y. Liu, Y. Xian, X. Wang, Z. Shi, H. Gu, C. Fei, N. Li, M. A. Uddin, H. Zhang, L. Dou, Y. Yan and J. Huang, *Nat. Photonics*, 2024, **18**, 379–387.
26 D. Yu, M. Pan, G. Liu, X. Jiang, X. Wen, W. Li, S. Chen, W. Zhou, H. Wang, Y. Lu, M. Ma, Z. Zang, P. Cheng, Q. Ji, F. Zheng and Z. Ning, *Nat. Energy*, 2024, **9**, 298–307.
27 H. Aqoma, S.-H. Lee, I. F. Imran, H.-H. Hwang, S.-H. Lee and S.-Y. Jang, *Nat. Energy*, 2024, **9**, 324–332.
28 H. C. Weerasinghe, N. Macadam, J.-E. Kim, L. J. Sutherland, D. Angmo, L. W. T. Ng, A. D. Scully, F. Glenn, R. Chantler, N. L. Chang, M. Dehghanimadvar, L. Shi, A. W. Y. Ho-Baillie, R. Egan, A. S. R. Chesman, M. Gao, J. J. Jasieniak, T. Hasan and D. Vak, *Nat. Commun.*, 2024, **15**, 1656.
29 X. Zheng, W. Kong, J. Wen, J. Hong, H. Luo, R. Xia, Z. Huang, X. Luo, Z. Liu, H. Li, H. Sun, Y. Wang, C. Liu, P. Wu, H. Gao, M. Li, A. D. Bui, Y. Mo, X. Zhang, G. Yang, Y. Chen, Z. Feng, H. T. Nguyen, R. Lin, L. Li, J. Gao and H. Tan, *Nat. Commun.*, 2024, **15**, 4907.
30 J. Wang, L. Zeng, D. Zhang, A. Maxwell, H. Chen, K. Datta, A. Caiazzo, W. H. M. Remmerswaal, N. R. M. Schipper, Z. Chen, K. Ho, A. Dasgupta, G. Kusch, R. Ollearo, L. Bellini, S. Hu, Z. Wang, C. Li, S. Teale, L. Grater, B. Chen, M. M. Wienk, R. A. Oliver, H. J. Snaith, R. A. J. Janssen and E. H. Sargent, *Nat. Energy*, 2024, **9**, 70–80.
31 F. Ali, C. Roldán-Carmona, M. Sohail and M. K. Nazeeruddin, *Adv. Energy Mater.*, 2020, **10**, 2002989.
32 K. Deng, Q. Chen and L. Li, *Adv. Funct. Mater.*, 2020, **30**, 2004209.
33 J. Huang, Y. Yuan, Y. Shao and Y. Yan, *Nat. Rev. Mater.*, 2017, **2**, 17042.
34 G. E. Eperon, M. T. Hörantner and H. J. Snaith, *Nat. Rev. Chem.*, 2017, **1**, 0095.
35 L. M. Pazos-Outón, M. Szumilo, R. Lamboll, J. M. Richter, M. Crespo-Quesada, M. Abdi-Jalebi, H. J. Beeson, M. Vrućinić, M. Alsari, H. J. Snaith, B. Ehrler, R. H. Friend and F. Deschler, *Science*, 2016, **351**, 1430–1433.
36 S. Y. Park and K. Zhu, *Adv. Mater.*, 2022, **34**, 2110438.
37 A. Ho-Baillie, M. Zhang, C. F. J. Lau, F.-J. Ma and S. Huang, *Joule*, 2019, **3**, 938–955.
38 L. Zang, C. Zhao, X. Hu, J. Tao, S. Chen and J. Chu, *Small*, 2024, **20**, 2400807.
39 W. Hui, X. Kang, B. Wang, D. Li, Z. Su, Y. Bao, L. Gu, B. Zhang, X. Gao, L. Song and W. Huang, *Nano Lett.*, 2023, **23**, 2195–2202.
40 F. Gao, C. Luo, X. Wang, C. Zhan, Y. Li, Y. Li, Q. Meng, M. Yang, K. Su, D. Yuan, R. Zhu and Q. Zhao, *Adv. Funct. Mater.*, 2023, **33**, 2211900.
41 T. Liu, R. Chao, X. Wang, B. Wang, L. Wu, R. Zhu, J. Zhou and Y. Wang, *Chem. Eng. J.*, 2024, **484**, 149466.
42 B. Roose, Q. Wang and A. Abate, *Adv. Energy Mater.*, 2019, **9**, 1803140.
43 P. Ru, E. Bi, Y. Zhang, Y. Wang, W. Kong, Y. Sha, W. Tang, P. Zhang, Y. Wu, W. Chen, X. Yang, H. Chen and L. Han, *Adv. Energy Mater.*, 2020, **10**, 1903487.
44 J.-F. Liao, W.-Q. Wu, Y. Jiang, J.-X. Zhong, L. Wang and D.-B. Kuang, *Chem. Soc. Rev.*, 2020, **49**, 354–381.
45 Y. Huang, T. Liu, C. Liang, J. Xia, D. Li, H. Zhang, A. Amini, G. Xing and C. Cheng, *Adv. Funct. Mater.*, 2020, **30**, 2000863.
46 T. Ye, Y. Hou, A. Nozariasbmarz, D. Yang, J. Yoon, L. Zheng, K. Wang, K. Wang, S. Ramakrishna and S. Priya, *ACS Energy Lett.*, 2021, **6**, 3044–3052.
47 W. Zhang, X. Guo, Z. Cui, H. Yuan, Y. Li, W. Li, X. Li and J. Fang, *Adv. Mater.*, 2024, 2311025.
48 S. S. Shin, J. H. Suk, B. J. Kang, W. Yin, S. J. Lee, J. H. Noh, T. K. Ahn, F. Rotermund, I. S. Cho and S. I. Seok, *Energy Environ. Sci.*, 2019, **12**, 958–964.
49 Z. Wu, Z. Liu, Z. Hu, Z. Hawash, L. Qiu, Y. Jiang, L. K. Ono and Y. Qi, *Adv. Mater.*, 2019, **31**, 1804284.
50 C. Zhang, S. Liang, W. Liu, F. T. Eickemeyer, X. Cai, K. Zhou, J. Bian, H. Zhu, C. Zhu, N. Wang, Z. Wang, J. Zhang, Y. Wang, J. Hu, H. Ma, C. Xin, S. M. Zakeeruddin, M. Grätzel and Y. Shi, *Nat. Energy*, 2021, **6**, 1154–1163.
51 F. De Angelis and A. Petrozza, *Nat. Mater.*, 2018, **17**, 383–384.
52 T.-H. Han, S. Tan, J. Xue, L. Meng, J.-W. Lee and Y. Yang, *Adv. Mater.*, 2019, **31**, 1803515.
53 J. Chen and N.-G. Park, *Adv. Mater.*, 2019, **31**, 1803019.
54 P. Dörflinger, Y. Ding, V. Schmid, M. Armer, R. C. Turnell-Ritson, B. Ding, P. J. Dyson, M. K. Nazeeruddin and V. Dyakonov, *Adv. Sci.*, 2023, **10**, 2304502.
55 X. Sun, C. Zhang, D. Gao, S. Zhang, B. Li, J. Gong, S. Li, S. Xiao, Z. Zhu and Z. Li, *Adv. Funct. Mater.*, 2024, 2315157.
56 C. Shen, T. Ye, P. Yang and G. Chen, *Adv. Mater.*, 2024, 2401498.
57 J. Liu, X. Chen, K. Chen, W. Tian, Y. Sheng, B. She, Y. Jiang, D. Zhang, Y. Liu, J. Qi, K. Chen, Y. Ma, Z. Qiu, C. Wang, Y. Yin, S. Zhao, J. Leng, S. Jin, W. Zhao, Y. Qin, Y. Su, X. Li, X. Li, Y. Zhou, Y. Zhou, F. Ling, A. Mei and H. Han, *Science*, 2024, **383**, 1198–1204.
58 A. Walsh and A. Zunger, *Nat. Mater.*, 2017, **16**, 964–967.
59 S. Tan, I. Yavuz, M. H. Weber, T. Huang, C.-H. Chen, R. Wang, H.-C. Wang, J. H. Ko, S. Nuryyeva, J. Xue, Y. Zhao, K.-H. Wei, J.-W. Lee and Y. Yang, *Joule*, 2020, **4**, 2426–2442.

60 L. Qiao, W.-H. Fang, R. Long and O. V. Prezhdo, *ACS Energy Lett.*, 2020, **5**, 3813–3820.
61 D. J. Keeble, J. Wiktor, S. K. Pathak, L. J. Phillips, M. Dickmann, K. Durose, H. J. Snaith and W. Egger, *Nat. Commun.*, 2021, **12**, 5566.
62 J. Li, Q. Dong, N. Li and L. Wang, *Adv. Energy Mater.*, 2017, **7**, 1602922.
63 W. Ming, D. Yang, T. Li, L. Zhang and M.-H. Du, *Adv. Sci.*, 2018, **5**, 1700662.
64 H. Zhang, L. Pfeifer, S. M. Zakeeruddin, J. Chu and M. Grätzel, *Nat. Rev. Chem.*, 2023, **7**, 632–652.
65 L. K. Ono, S. Liu and Y. Qi, *Angew. Chem., Int. Ed.*, 2020, **59**, 6676–6698.
66 T. Chen, J. Xie, B. Wen, Q. Yin, R. Lin, S. Zhu and P. Gao, *Nat. Commun.*, 2023, **14**, 6125.
67 Z. Ni, H. Jiao, C. Fei, H. Gu, S. Xu, Z. Yu, G. Yang, Y. Deng, Q. Jiang, Y. Liu, Y. Yan and J. Huang, *Nat. Energy*, 2022, **7**, 65–73.
68 X. Zheng, B. Chen, J. Dai, Y. Fang, Y. Bai, Y. Lin, H. Wei, X. C. Zeng and J. Huang, *Nat. Energy*, 2017, **2**, 17102.
69 D. D. Girolamo, N. Phung, F. U. Kosasih, F. Di Giacomo, F. Matteocci, J. A. Smith, M. A. Flatken, H. Köbler, S. H. Turren Cruz, A. Mattoni, L. Cinà, B. Rech, A. Latini, G. Divitini, C. Ducati, A. Di Carlo, D. Dini and A. Abate, *Adv. Energy Mater.*, 2020, **10**, 2000310.
70 D. W. deQuilettes, S. M. Vorpahl, S. D. Stranks, H. Nagaoka, G. E. Eperon, M. E. Ziffer, H. J. Snaith and D. S. Ginger, *Science*, 2015, **348**, 683–686.
71 W. Li, S. K. Yadavalli, D. Lizarazo-Ferro, M. Chen, Y. Zhou, N. P. Padture and R. Zia, *ACS Energy Lett.*, 2018, **3**, 2669–2670.
72 L. Fu, H. Li, L. Wang, R. Yin, B. Li and L. Yin, *Energy Environ. Sci.*, 2020, **13**, 4017–4056.
73 H. Hu, S. Moghadamzadeh, R. Azmi, Y. Li, M. Kaiser, J. C. Fischer, Q. Jin, J. Maibach, I. M. Hossain, U. W. Paetzold and B. A. Nejand, *Adv. Funct. Mater.*, 2022, **32**, 2107650.
74 D. Glowienka, D. Zhang, F. Di Giacomo, M. Najafi, S. Veenstra, J. Szmytkowski and Y. Galagan, *Nano Energy*, 2020, **67**, 104186.
75 B. T. van Gorkom, T. P. A. van der Pol, K. Datta, M. M. Wienk and R. A. J. Janssen, *Nat. Commun.*, 2022, **13**, 349.
76 W. Xu, F. He, M. Zhang, P. Nie, S. Zhang, C. Zhao, R. Luo, J. Li, X. Zhang, S. Zhao, W.-D. Li, F. Kang, C.-W. Nan and G. Wei, *ACS Energy Lett.*, 2019, **4**, 2491–2499.
77 L. Canil, T. Cramer, B. Fraboni, D. Ricciarelli, D. Meggiolaro, A. Singh, M. Liu, M. Rusu, C. M. Wolff, N. Phung, Q. Wang, D. Neher, T. Unold, P. Vivo, A. Gagliardi, F. De Angelis and A. Abate, *Energy Environ. Sci.*, 2021, **14**, 1429–1438.
78 J. Fu, J. Zhang, T. Zhang, L. Yuan, Z. Zhang, Z. Jiang, Z. Huang, T. Wu, K. Yan, L. Zhang, A. Wang, W. Ji, Y. Zhou and B. Song, *ACS Nano*, 2023, **17**, 2802–2812.
79 H. Chen, A. Maxwell, C. Li, S. Teale, B. Chen, T. Zhu, E. Ugur, G. Harrison, L. Grater, J. Wang, Z. Wang, L. Zeng, S. M. Park, L. Chen, P. Serles, R. A. Awni, B. Subedi, X. Zheng, C. Xiao, N. J. Podraza, T. Filleter, C. Liu, Y. Yang, J. M. Luther, S. De Wolf, M. G. Kanatzidis, Y. Yan and E. H. Sargent, *Nature*, 2023, **613**, 676–681.
80 J. Nie, Y. Zhang, J. Wang, L. Li and Y. Zhang, *ACS Energy Lett.*, 2024, **9**, 1674–1681.
81 C. Ding, Y. Zhang, F. Liu, Y. Kitabatake, S. Hayase, T. Toyoda, K. Yoshino, T. Minemoto, K. Katayama and Q. Shen, *Nano Energy*, 2018, **53**, 17–26.
82 D. Luo, X. Li, A. Dumont, H. Yu and Z.-H. Lu, *Adv. Mater.*, 2021, **33**, 2006004.
83 T. Kirchartz, J. A. Márquez, M. Stolterfoht and T. Unold, *Adv. Energy Mater.*, 2020, **10**, 1904134.
84 C. M. Wolff, F. Zu, A. Paulke, L. P. Toro, N. Koch and D. Neher, *Adv. Mater.*, 2017, **29**, 1700159.
85 W. Tress, M. Yavari, K. Domanski, P. Yadav, B. Niesen, J. P. Correa Baena, A. Hagfeldt and M. Grätzel, *Energy Environ. Sci.*, 2018, **11**, 151–165.
86 J. E. Lee, S. G. Motti, R. D. J. Oliver, S. Yan, H. J. Snaith, M. B. Johnston and L. M. Herz, *Adv. Funct. Mater.*, 2024, 2401052.
87 Z. Guo, A. K. Jena, G. M. Kim and T. Miyasaka, *Energy Environ. Sci.*, 2022, **15**, 3171–3222.
88 Y. Jiang, M. Cui, S. Li, C. Sun, Y. Huang, J. Wei, L. Zhang, M. Lv, C. Qin, Y. Liu and M. Yuan, *Nat. Commun.*, 2021, **12**, 336.
89 L. M. Pazos-Outón, T. P. Xiao and E. Yablonovitch, *J. Phys. Chem. Lett.*, 2018, **9**, 1703–1711.
90 W. H. M. Remmerswaal, B. T. van Gorkom, D. Zhang, M. M. Wienk and R. A. J. Janssen, *Adv. Energy Mater.*, 2024, **14**, 2303664.
91 A. D. Wright, R. L. Milot, G. E. Eperon, H. J. Snaith, M. B. Johnston and L. M. Herz, *Adv. Funct. Mater.*, 2017, **27**, 1700860.
92 B. Wu, H. Yuan, Q. Xu, J. A. Steele, D. Giovanni, P. Puech, J. Fu, Y. F. Ng, N. F. Jamaludin, A. Solanki, S. Mhaisalkar, N. Mathews, M. B. J. Roeffaers, M. Grätzel, J. Hofkens and T. C. Sum, *Nat. Commun.*, 2019, **10**, 484.
93 V. M. Caselli, Z. Wei, M. M. Ackermans, E. M. Hutter, B. Ehrler and T. J. Savenije, *ACS Energy Lett.*, 2020, **5**, 3821–3827.
94 D. Jia, J. Chen, R. Zhuang, Y. Hua and X. Zhang, *Adv. Mater.*, 2023, **35**, 2212160.
95 B. Nath, S. K. Behera, J. Kumar, A. Hemmerle, P. Fontaine, P. C. Ramamurthy, D. R. Mahapatra and G. Hegde, *Adv. Mater.*, 2024, **36**, 2307547.
96 C. Xu, S. Zhang, W. Fan, F. Cheng, H. Sun, Z. Kang and Y. Zhang, *Adv. Mater.*, 2023, **35**, 2207172.
97 J. Li, L. Xie, G. Liu, Z. Pu, X. Tong, S. Yang, M. Yang, J. Liu, J. Chen, Y. Meng, Y. Wang, T. Wang and Z. Ge, *Angew. Chem., Int. Ed.*, 2024, **63**, e202316898.
98 G. J. W. Aalbers, T. P. A. van der Pol, K. Datta, W. H. M. Remmerswaal, M. M. Wienk and R. A. J. Janssen, *Nat. Commun.*, 2024, **15**, 1276.
99 P. Caprioglio, J. A. Smith, R. D. J. Oliver, A. Dasgupta, S. Choudhary, M. D. Farrar, A. J. Ramadan, Y.-H. Lin, M. G. Christoforo, J. M. Ball, J. Diekmann, J. Thiesbrummel, K.-A. Zaininger, X. Shen, M. B. Johnston, D. Neher, M. Stolterfoht and H. J. Snaith, *Nat. Commun.*, 2023, **14**, 932.

100 M. Stolterfoht, P. Caprioglio, C. M. Wolff, J. A. Márquez, J. Nordmann, S. Zhang, D. Rothhardt, U. Hörmann, Y. Amir, A. Redinger, L. Kegelmann, F. Zu, S. Albrecht, N. Koch, T. Kirchartz, M. Saliba, T. Unold and D. Neher, *Energy Environ. Sci.*, 2019, **12**, 2778–2788.
101 S. Cacovich, G. Vidon, M. Degani, M. Legrand, L. Gouda, J.-B. Puel, Y. Vaynzof, J.-F. Guillemoles, D. Ory and G. Grancini, *Nat. Commun.*, 2022, **13**, 2868.
102 S. Mahesh, J. M. Ball, R. D. J. Oliver, D. P. McMeekin, P. K. Nayak, M. B. Johnston and H. J. Snaith, *Energy Environ. Sci.*, 2020, **13**, 258–267.
103 R. D. J. Oliver, P. Caprioglio, F. Peña-Camargo, L. R. V. Buizza, F. Zu, A. J. Ramadan, S. G. Motti, S. Mahesh, M. M. McCarthy, J. H. Warby, Y.-H. Lin, N. Koch, S. Albrecht, L. M. Herz, M. B. Johnson, D. Neher, M. Stolterfoht and H. J. Snaith, *Energy Environ. Sci.*, 2022, **15**, 714–726.
104 M. Stolterfoht, C. M. Wolff, J. A. Márquez, S. Zhang, C. J. Hages, D. Rothhardt, S. Albrecht, P. L. Burn, P. Meredith, T. Unold and D. Neher, *Nat. Energy*, 2018, **3**, 847–854.
105 N. Li, S. Pratap, V. Körstgens, S. Vema, L. Song, S. Liang, A. Davydok, C. Krywka and P. Müller-Buschbaum, *Nat. Commun.*, 2022, **13**, 6701.
106 R. Guo, D. Han, W. Chen, L. Dai, K. Ji, Q. Xiong, S. Li, L. K. Reb, M. A. Scheel, S. Pratap, N. Li, S. Yin, T. Xiao, S. Liang, A. L. Oechsle, C. L. Weindl, M. Schwartzkopf, H. Ebert, P. Gao, K. Wang, M. Yuan, N. C. Greenham, S. D. Stranks, S. V. Roth, R. H. Friend and P. Müller-Buschbaum, *Nat. Energy*, 2021, **6**, 977–986.
107 L. Lanzetta, T. Webb, N. Zibouche, X. Liang, D. Ding, G. Min, R. J. E. Westbrook, B. Gaggio, T. J. Macdonald, M. S. Islam and S. A. Haque, *Nat. Commun.*, 2021, **12**, 2853.
108 C. Ma, F. T. Eickemeyer, S.-H. Lee, D.-H. Kang, S. J. Kwon, M. Grätzel and N.-G. Park, *Science*, 2023, **379**, 173–178.
109 J. Thiesbrummel, S. Shah, E. Gutierrez-Partida, F. Zu, F. Peña-Camargo, S. Zeiske, J. Diekmann, F. Ye, K. P. Peters, K. O. Brinkmann, P. Caprioglio, A. Dasgupta, S. Seo, F. A. Adeleye, J. Warby, Q. Jeangros, F. Lang, S. Zhang, S. Albrecht, T. Riedl, A. Armin, D. Neher, N. Koch, Y. Wu, V. M. Le Corre, H. Snaith and M. Stolterfoht, *Nat. Energy*, 2024, **9**, 664–676.
110 L. Yang, B. Xu, D. Bi, H. Tian, G. Boschloo, L. Sun, A. Hagfeldt and E. M. J. Johansson, *J. Am. Chem. Soc.*, 2013, **135**, 7378–7385.
111 U. Würfel, D. Neher, A. Spies and S. Albrecht, *Nat. Commun.*, 2015, **6**, 6951.
112 T. G. Allen, J. Bullock, X. Yang, A. Javey and S. D. Wolf, *Nat. Energy*, 2019, **4**, 914–928.
113 E. H. Balaguera and J. Bisquert, *ACS Energy Lett.*, 2024, **9**, 478–486.
114 J. Jeong, M. Kim, J. Seo, H. Lu, P. Ahlawat, A. Mishra, Y. Yang, M. A. Hope, F. T. Eickemeyer, M. Kim, Y. J. Yoon, I. W. Choi, B. P. Darwich, S. J. Choi, Y. Jo, J. H. Lee, B. Walker, S. M. Zakeeruddin, L. Emsley, U. Rothlisberger, A. Hagfeldt, D. S. Kim, M. Grätzel and J. Y. Kim, *Nature*, 2021, **592**, 381–385.
115 O. Almora, C. Aranda, I. Zarazua, A. Guerrero and G. Garcia-Belmonte, *ACS Energy Lett.*, 2016, **1**, 209–215.
116 H. Shen, D. Jacobs, Y. Wu, T. Duong, J. Peng, X. Wen, X. Fu, S. K. Karuturi, T. P. White, K. Weber and K. R. Catchpole, *J. Phys. Chem. Lett.*, 2017, **8**, 2672–2680.
117 F. Wu, R. Pathak, K. Chen, G. Wang, B. Bahrami, W.-H. Zhang and Q. Qiao, *ACS Energy Lett.*, 2018, **3**, 2457–2460.
118 P. Liu, W. Wang, S. Liu, H. Yang and Z. Shao, *Adv. Energy Mater.*, 2019, **9**, 1803017.
119 M. Grätzel, *Nat. Mater.*, 2014, **13**, 838–842.
120 Q. Jiang, J. Tong, Y. Xian, R. A. Kerner, S. P. Dunfield, C. Xiao, R. A. Scheidt, D. Kuciauskas, X. Wang, M. P. Hautzinger, R. Tirawat, M. C. Beard, D. P. Fenning, J. J. Berry, B. W. Larson, Y. Yan and K. Zhu, *Nature*, 2022, **611**, 278–283.
121 H. Röhm, T. Leonhard, M. J. Hoffmann and A. Colsmann, *Adv. Funct. Mater.*, 2020, **30**, 1908657.
122 Y. Chen, W. Zhou, X. Chen, X. Zhang, H. Gao, N. A. N. Ouedraogo, Z. Zheng, C. B. Han, Y. Zhang and H. Yan, *Adv. Funct. Mater.*, 2022, **32**, 2108417.
123 H.-S. Kim, S. K. Kim, B. J. Kim, K.-S. Shin, M. K. Gupta, H. S. Jung, S.-W. Kim and N.-G. Park, *J. Phys. Chem. Lett.*, 2015, **6**, 1729–1735.
124 C. Zhang, D. Sun, X. Liu, C.-X. Sheng and Z. V. Vardeny, *J. Phys. Chem. Lett.*, 2017, **8**, 1429–1435.
125 D. Seol, A. Jeong, M. H. Han, S. Seo, T. S. Yoo, W. S. Choi, H. S. Jung, H. Shin and Y. Kim, *Adv. Funct. Mater.*, 2017, **27**, 1701924.
126 Z. Xiao, Y. Yuan, Y. Shao, Q. Wang, Q. Dong, C. Bi, P. Sharma, A. Gruverman and J. Huang, *Nat. Mater.*, 2015, **14**, 193–198.
127 D. Li, Y. Wang, T. Niu, L. Chao and Y. Chen, *J. Phys. Chem. C*, 2022, **126**, 6892–6903.
128 J. Haruyama, K. Sodeyama, L. Han and Y. Tateyama, *J. Am. Chem. Soc.*, 2015, **137**, 10048–10051.
129 J. M. Azpiroz, E. Mosconi, J. Bisquert and F. De Angelis, *Energy Environ. Sci.*, 2015, **8**, 2118–2127.
130 T. Kim, S. Park, V. Iyer, B. Shaheen, U. Choudhry, Q. Jiang, G. Eichman, R. Gnabasik, K. Kelley, B. Lawrie, K. Zhu and B. Liao, *Nat. Commun.*, 2023, **14**, 1846.
131 M. Ghasemi, B. Guo, K. Darabi, T. Wang, K. Wang, C.-W. Huang, B. M. Lefler, L. Taussig, M. Chauhan, G. Baucom, T. Kim, E. D. Gomez, J. M. Atkin, S. Priya and A. Amassian, *Nat. Mater.*, 2023, **22**, 329–337.
132 W. Tress, N. Marinova, T. Moehl, S. M. Zakeeruddin, M. K. Nazeeruddin and M. Grätzel, *Energy Environ. Sci.*, 2015, **8**, 995–1004.
133 O. Almora, I. Zarazua, E. Mas-Marza, I. Mora-Sero, J. Bisquert and G. Garcia-Belmonte, *J. Phys. Chem. Lett.*, 2015, **6**, 1645–1652.
134 S. Meloni, T. Moehl, W. Tress, M. Franckevičius, M. Saliba, Y. H. Lee, P. Gao, M. K. Nazeeruddin, S. M. Zakeeruddin, U. Rothlisberger and M. Grätzel, *Nat. Commun.*, 2016, **7**, 10334.
135 H.-S. Kim, I. Mora-Sero, V. Gonzalez-Pedro, F. Fabregat-Santiago, E. J. Juarez-Perez, N.-G. Park and J. Bisquert, *Nat. Commun.*, 2013, **4**, 2242.

136 G. Richardson, S. E. J. O'Kane, R. G. Niemann, T. A. Peltola, J. M. Foster, P. J. Cameron and A. B. Walker, *Energy Environ. Sci.*, 2016, **9**, 1476–1485.
137 W. Tress, *J. Phys. Chem. Lett.*, 2017, **8**, 3106–3114.
138 F. Ebadi, N. Taghavinia, R. Mohammadpour, A. Hagfeldt and W. Tress, *Nat. Commun.*, 2019, **10**, 1574.
139 T. Leijtens, G. E. Eperon, A. J. Barker, G. Grancini, W. Zhang, J. M. Ball, A. R. S. Kandada, H. J. Snaith and A. Petrozza, *Energy Environ. Sci.*, 2016, **9**, 3472–3481.
140 T. S. Sherkar, C. Momblona, L. Gil-Escrig, J. Ávila, M. Sessolo, H. J. Bolink and L. J. A. Koster, *ACS Energy Lett.*, 2017, **2**, 1214–1222.
141 C. M. Wolff, P. Caprioglio, M. Stolterfoht and D. Neher, *Adv. Mater.*, 2019, **31**, 1902762.
142 D. Luo, R. Su, W. Zhang, Q. Gong and R. Zhu, *Nat. Rev. Mater.*, 2020, **5**, 44–60.
143 J. Peng, Y. Wu, W. Ye, D. A. Jacobs, H. Shen, X. Fu, Y. Wan, T. Duong, N. Wu, C. Barugkin, H. T. Nguyen, D. Zhong, J. Li, T. Lu, Y. Liu, M. N. Lockrey, K. J. Weber, K. R. Catchpole and T. P. White, *Energy Environ. Sci.*, 2017, **10**, 1792–1800.
144 S. Tan, T. Huang, I. Yavuz, R. Wang, T. W. Yoon, M. Xu, Q. Xing, K. Park, D.-K. Lee, C.-H. Chen, R. Zheng, T. Yoon, Y. Zhao, H.-C. Wang, D. Meng, J. Xue, Y. J. Song, X. Pan, N.-G. Park, J.-W. Lee and Y. Yang, *Nature*, 2022, **605**, 268–273.
145 S. A. L. Weber, I. M. Hermes, S.-H. Turren-Cruz, C. Gort, V. W. Bergmann, L. Gilson, A. Hagfeldt, M. Grätzel, W. Tress and R. Berger, *Energy Environ. Sci.*, 2018, **11**, 2404–2413.
146 A. D. Taylor, Q. Sun, K. P. Goetz, Q. An, T. Schramm, Y. Hofstetter, M. Litterst, F. Paulus and Y. Vaynzof, *Nat. Commun.*, 2021, **12**, 1878.
147 Y. Su, J. Yang, H. Rao, Y. Zhong, W. Sheng, L. Tan and Y. Chen, *Energy Environ. Sci.*, 2023, **16**, 2177–2186.
148 X. Huang, F. Cao, S. Zhan, Q. Feng, M. Zhu, Z. Su, X. Gao, J. Yin, J. Li, N. Zheng and B. Wu, *Joule*, 2023, **7**, 1556–1573.
149 W. Li, M. U. Rothmann, Y. Zhu, W. Chen, C. Yang, Y. Yuan, Y. Y. Choo, X. Wen, Y.-B. Cheng, U. Bach and J. Etheridge, *Nat. Energy*, 2021, **6**, 624–632.
150 T. Bu, L. K. Ono, J. Li, J. Su, G. Tong, W. Zhang, Y. Liu, J. Zhang, J. Chang, S. Kazaoui, F. Huang, Y.-B. Cheng and Y. Qi, *Nat. Energy*, 2022, **7**, 528–536.
151 C. Ge, B. Jiang, J. Zhu, P. Zhang, R. Ma, S. Yan, Z. Liu, A. Shaker, M. S. Salem, J. Luo, L. Xu, J. Yang, Z. Li, H. Song, C. Chen and J. Tang, *Adv. Funct. Mater.*, 2024, 2400075.
152 S. You, H. Zeng, Y. Liu, B. Han, M. Li, L. Li, X. Zheng, R. Guo, L. Luo, Z. Li, C. Zhang, R. Liu, Y. Zhao, S. Zhang, Q. Peng, T. Wang, Q. Chen, F. T. Eickemeyer, B. Carlsen, S. M. Zakeeruddin, L. Mai, Y. Rong, M. Grätzel and X. Li, *Science*, 2023, **379**, 288–294.
153 D. Gao, R. Li, X. Chen, C. Chen, C. Wang, B. Zhang, M. Li, X. Shang, X. Yu, S. Gong, T. Pauporté, H. Yang, L. Ding, J. Tang and J. Chen, *Adv. Mater.*, 2023, **35**, 2301028.
154 K. Xiao, R. Lin, Q. Han, Y. Hou, Z. Qin, H. T. Nguyen, J. Wen, M. Wei, V. Yeddu, M. I. Saidaminov, Y. Gao, X. Luo, Y. Wang, H. Gao, C. Zhang, J. Xu, J. Zhu, E. H. Sargent and H. Tan, *Nat. Energy*, 2020, **5**, 870–880.
155 K.-W. Yeom, D.-K. Lee and N.-G. Park, *Adv. Energy Mater.*, 2022, **12**, 2202496.
156 D. P. McMeekin, P. Holzhey, S. O. Fürer, S. P. Harvey, L. T. Schelhas, J. M. Ball, S. Mahesh, S. Seo, N. Hawkins, J. Lu, M. B. Johnston, J. J. Berry, U. Bach and H. J. Snaith, *Nat. Mater.*, 2023, **22**, 73–83.
157 Y. Du, Q. Tian, S. Wang, L. Yin, C. Ma, Z. Wang, L. Lang, Y. Yang, K. Zhao and S. Liu, *Adv. Mater.*, 2024, **36**, 2307583.
158 J. Zhou, S. Fu, S. Zhou, L. Huang, C. Wang, H. Guan, D. Pu, H. Cui, C. Wang, T. Wang, W. Meng, G. Fang and W. Ke, *Nat. Commun.*, 2024, **15**, 2324.
159 Y. Wang, P. Lv, J. Pan, J. Chen, X. Liu, M. Hu, L. Wan, K. Cao, B. Liu, Z. Ku, Y.-B. Cheng and J. Lu, *Adv. Mater.*, 2023, **35**, 2304625.
160 N. Sun, S. Fu, Y. Li, L. Chen, J. Chung, M. M. Saeed, K. Dolia, A. Rahimi, C. Li, Z. Song and Y. Yan, *Adv. Funct. Mater.*, 2024, **34**, 2309894.
161 K.-L. Wang, Z.-H. Su, Y.-H. Lou, Q. Lv, J. Chen, Y.-R. Shi, C.-H. Chen, Y.-H. Zhou, X.-Y. Gao, Z.-K. Wang and L.-S. Liao, *Adv. Energy Mater.*, 2022, **12**, 2201274.
162 W. Xu, Y. Gao, W. Ming, F. He, J. Li, X.-H. Zhu, F. Kang, J. Li and G. Wei, *Adv. Mater.*, 2020, **32**, 2003965.
163 D. Zheng, F. Raffin, P. Volovitch and T. Pauporté, *Nat. Commun.*, 2022, **13**, 6655.
164 Z. Wu, S. Sang, J. Zheng, Q. Gao, B. Huang, F. Li, K. Sun and S. Chen, *Angew. Chem., Int. Ed.*, 2024, **63**, e202319170.
165 T. Niu, L. Chao, Y. Xia, K. Wang, X. Ran, X. Huang, C. Chen, J. Wang, D. Li, Z. Su, Z. Hu, X. Gao, J. Zhang and Y. Chen, *Adv. Mater.*, 2024, **36**, 2309171.
166 A. Ng, Z. Ren, H. Hu, P. W. K. Fong, Q. Shen, S. H. Cheung, P. Qin, J.-W. Lee, A. B. Djurišić, S. K. So, G. Li, Y. Yang and C. Surya, *Adv. Mater.*, 2018, **30**, 1804402.
167 M. Li, R. Sun, J. Chang, J. Dong, Q. Tian, H. Wang, Z. Li, P. Yang, H. Shi, C. Yang, Z. Wu, R. Li, Y. Yang, A. Wang, S. Zhang, F. Wang, W. Huang and T. Qin, *Nat. Commun.*, 2023, **14**, 573.
168 W. Xiang, J. Zhang, S. Liu, S. Albrecht, A. Hagfeldt and Z. Wang, *Joule*, 2022, **6**, 315–339.
169 Y. Huang, X. Lei, T. He, Y. Jiang and M. Yuan, *Adv. Energy Mater.*, 2022, **12**, 2100690.
170 J. Hu, J. W. Ahn, Z. Xu, M. J. Jeong, C. Kim, J. H. Noh, H. Min and B. P. Rand, *Adv. Energy Mater.*, 2024, 2400500.
171 F. Li, X. Deng, Z. Shi, S. Wu, Z. Zeng, D. Wang, Y. Li, F. Qi, Z. Zhang, Z. Yang, S.-H. Jang, F. R. Lin, S.-W. Tsang, X.-K. Chen and A. K.-Y. Jen, *Nat. Photonics*, 2023, **17**, 478–484.
172 M. Wang, Z. Shi, C. Fei, Z. J. D. Deng, G. Yang, S. P. Dunfield, D. P. Fenning and J. Huang, *Nat. Energy*, 2023, **8**, 1229–1239.
173 R. Wang, X. Li, J. Qi, C. Su, J. Yang, S. Yang, M. Yuan and T. He, *Adv. Mater.*, 2023, **35**, 2304149.
174 J. Suo, B. Yang, E. Mosconi, D. Bogachuk, T. A. S. Doherty, K. Frohna, D. J. Kubicki, F. Fu, Y. Kim, O. Er-Raji, T. Zhang, L. Baldinelli, L. Wagner, A. N. Tiwari, F. Gao, A. Hinsch, S. D. Stranks, F. De Angelis and A. Hagfeldt, *Nat. Energy*, 2024, **9**, 172–183.

175 H. Meng, K. Mao, F. Cai, K. Zhang, S. Yuan, T. Li, F. Cao, Z. Su, Z. Zhu, X. Feng, W. Peng, J. Xu, Y. Gao, W. Chen, C. Xiao, X. Wu, M. D. McGehee and J. Xu, *Nat. Energy*, 2024, **9**, 536–547.

176 E. A. Alharbi, T. P. Baumeler, A. Krishna, A. Y. Alyamani, F. T. Eickemeyer, O. Ouellette, L. Pan, F. S. Alghamdi, Z. Wang, M. H. Alotaibi, B. Yang, M. Almalki, M. D. Mensi, H. Albrithen, A. Albadri, A. Hagfeldt, S. M. Zakeeruddin and M. Grätzel, *Adv. Energy Mater.*, 2021, **11**, 2003785.

177 S. Wang, L. Tan, J. Zhou, M. Li, X. Zhao, H. Li, W. Tress, L. Ding, M. Grätzel and C. Yi, *Joule*, 2022, **6**, 1344–1356.

178 Y. Liang, F. Li, X. Cui, T. Lv, C. Stampfl, S. P. Ringer, X. Yang, J. Huang and R. Zheng, *Nat. Commun.*, 2024, **15**, 1707.

179 P. Shi, Y. Ding, B. Ding, Q. Xing, T. Kodalle, C. M. Sutter-Fella, I. Yavuz, C. Yao, W. Fan, J. Xu, Y. Tian, D. Gu, K. Zhao, S. Tan, X. Zhang, L. Yao, P. J. Dyson, J. L. Slack, D. Yang, J. Xue, M. K. Nazeeruddin, Y. Yang and R. Wang, *Nature*, 2023, **620**, 323–327.

180 S. Wang, T. Yang, Y. Yang, Y. Du, W. Huang, L. Cheng, H. Li, P. Wang, Y. Wang, Y. Zhang, C. Ma, P. Liu, G. Zhao, Z. Ding, S. Liu and K. Zhao, *Adv. Mater.*, 2023, **35**, 2305314.

181 Q. Tan, Z. Li, G. Luo, X. Zhang, B. Che, G. Chen, H. Gao, D. He, G. Ma, J. Wang, J. Xiu, H. Yi, T. Chen and Z. He, *Nature*, 2023, **620**, 545–551.

182 J. Park, J. Kim, H.-S. Yun, M. J. Paik, E. Noh, H. J. Mun, M. G. Kim, T. J. Shin and S. I. Seok, *Nature*, 2023, **616**, 724–730.

183 X. Jiang, H. Li, Q. Zhou, Q. Wei, M. Wei, L. Jiang, Z. Wang, Z. Peng, F. Wang, Z. Zang, K. Xu, Y. Hou, S. Teale, W. Zhou, R. Si, X. Gao, E. H. Sargent and Z. Ning, *J. Am. Chem. Soc.*, 2021, **143**, 10970–10976.

184 S. Chen, X. Xiao, B. Chen, L. L. Kelly, J. Zhao, Y. Lin, M. F. Toney and J. Huang, *Sci. Adv.*, 2021, **7**, eabb2412.

185 S. Chen, X. Dai, S. Xu, H. Jiao, L. Zhao and J. Huang, *Science*, 2021, **373**, 902–907.

186 C. Wang, Y. Zhao, T. Ma, Y. An, R. He, J. Zhu, C. Chen, S. Ren, F. Fu, D. Zhao and X. Li, *Nat. Energy*, 2022, **7**, 744–753.

187 P. Zhu, D. Wang, Y. Zhang, Z. Liang, J. Li, J. Zeng, J. Zhang, Y. Xu, S. Wu, Z. Liu, X. Zhou, B. Hu, F. He, L. Zhang, X. Pan, X. Wang, N.-G. Park and B. Xu, *Science*, 2024, **383**, 524–531.

188 Y. Gao, H. Raza, Z. Zhang, W. Chen and Z. Liu, *Adv. Funct. Mater.*, 2023, **33**, 2215171.

189 Y. Zhang, L. Xu, Y. Wu, H. Zhang, F. Zeng, J. Xing, B. Liu, Y. Qi, B. Dong, X. Bai and H. Song, *Adv. Funct. Mater.*, 2023, **33**, 2214102.

190 G. Li, Y. Hu, M. Li, Y. Tang, Z. Zhang, A. Musiienko, Q. Cao, F. Akhundova, J. Li, K. Prashanthan, F. Yang, P. Janasik, A. N. S. Appiah, S. Trofimov, N. Livakas, S. Zuo, L. Wu, L. Wang, Y. Yang, B. Agyei-Tuffour, R. W. MacQueen, B. Naydenov, T. Unold, E. Unger, E. Aktas, S. Eigler and A. Abate, *Angew. Chem., Int. Ed.*, 2023, **135**, e202307395.

191 H. Bao, S. Wang, H. Liu and X. Li, *Adv. Energy Mater.*, 2024, **14**, 2303166.

192 J. He, W. Sheng, J. Yang, Y. Zhong, Q. Cai, Y. Liu, Z. Guo, L. Tan and Y. Chen, *Angew. Chem., Int. Ed.*, 2024, **136**, e202315233.

193 Y.-H. Lin, N. Sakai, P. Da, J. Wu, H. C. Sansom, A. J. Ramadan, S. Mahesh, J. Liu, R. D. J. Oliver, J. Lim, L. Aspitarte, K. Sharma, P. K. Madhu, A. B. Morales-Vilches, P. K. Nayak, S. Bai, F. Gao, C. R. M. Grovenor, M. B. Johnston, J. G. Labram, J. R. Durrant, J. M. Ball, B. Wenger, B. Stannowski and H. J. Snaith, *Science*, 2020, **369**, 96–102.

194 Y. Zhao, F. Ma, Z. Qu, S. Yu, T. Shen, H.-X. Deng, X. Chu, X. Peng, Y. Yuan, X. Zhang and J. You, *Science*, 2022, **377**, 531–534.

195 Y. Gao, F. Ren, D. Sun, S. Li, G. Zheng, J. Wang, H. Raza, R. Chen, H. Wang, S. Liu, P. Yu, X. Meng, J. He, J. Zhou, X. Hu, Z. Zhang, L. Qiu, W. Chen and Z. Liu, *Energy Environ. Sci.*, 2023, **16**, 2295–2303.

196 X. Ji, T. Zhou, Q. Fu, W. Wang, Z. Wu, M. Zhang, X. Guo, D. Liu, H. Y. Woo and Y. Liu, *Adv. Energy Mater.*, 2023, **13**, 2203756.

197 M. Wu, Y. Duan, L. Yang, P. You, Z. Li, J. Wang, H. Zhou, S. Yang, D. Xu, H. Zou and Z. Liu, *Adv. Funct. Mater.*, 2023, **33**, 2300128.

198 P. Zhao, D. He, S. Li, H. Cui, Y. Yang, W. Chen, A.-S. Salah, Y. Feng and B. Zhang, *Adv. Funct. Mater.*, 2024, **34**, 2308795.

199 B. Yang, J. Suo, D. Bogachuk, W. Kaiser, C. Baretzky, O. Er-Raji, G. Loukeris, A. A. Alothman, E. Mosconi, M. Kohlstädt, U. Würfel, F. De Angelis and A. Hagfeldt, *Energy Environ. Sci.*, 2024, **17**, 1549–1558.

200 Y. Zheng, Y. Li, R. Zhuang, X. Wu, C. Tian, A. Sun, C. Chen, Y. Guo, Y. Hua, K. Meng, K. Wu and C.-C. Chen, *Energy Environ. Sci.*, 2024, **17**, 1153–1162.

201 S. Hu, P. Zhao, K. Nakano, R. D. J. Oliver, J. Pascual, J. A. Smith, T. Yamada, M. A. Truong, R. Murdey, N. Shioya, T. Hasegawa, M. Ehara, M. B. Johnston, K. Tajima, Y. Kanemitsu, H. J. Snaith and A. Wakamiya, *Adv. Mater.*, 2023, **35**, 2208320.

202 D. B. Khadka, Y. Shirai, M. Yanagida, H. Ota, A. Lyalin, T. Taketsugu and K. Miyano, *Nat. Commun.*, 2024, **15**, 882.

203 A. Maxwell, H. Chen, L. Grater, C. Li, S. Teale, J. Wang, L. Zeng, Z. Wang, S. M. Park, M. Vafaie, S. Sidhik, I. W. Metcalf, Y. Liu, A. D. Mohite, B. Chen and E. H. Sargent, *ACS Energy Lett.*, 2024, **9**, 520–527.

204 X. Gu, W. Xiang, Q. Tian and S. Liu, *Angew. Chem., Int. Ed.*, 2021, **60**, 23164–23170.

205 T. Yang, L. Mao, J. Shi, P. Zeng, F. Li, J. Gong, X. Huang, Z. Wang, W. Cui, D. Huang, H. Zhang, Y. Sun, X. Fang, Z. Liu, M. Liu and X. Cui, *Adv. Energy Mater.*, 2024, **14**, 2303149.

206 W. Zhang, H. Liu, Y. Qu, J. Cui, W. Zhang, T. Shi and H.-L. Wang, *Adv. Mater.*, 2024, **36**, 2309193.

207 Q. Cao, Y. Li, Y. Zhang, J. Zhao, T. Wang, B. Yang, X. Pu, J. Yang, H. Chen, X. Chen, X. Li, S. Ghasemi, H. Salari, A. Hagfeldt and X. Li, *Adv. Energy Mater.*, 2022, **12**, 2201435.

208 S. Wang, C. Yao, L. Li, T. Huang, S. Tan, P. Shi, S. Jin, C. Zhu, Y. Yang, B. Zhu, J. Xue and R. Wang, *Joule*, 2024, **8**, 1105–1119.

209 C. Liu, H. Su, Y. Pu, M. Guo, P. Zhai, L. Liu and H. Fu, *Adv. Funct. Mater.*, 2023, **33**, 2212577.
210 Z. Zhang, Y. Gao, Z. Li, L. Qiao, Q. Xiong, L. Deng, Z. Zhang, R. Long, Q. Zhou, Y. Du, Z. Lan, Y. Zhao, C. Li, K. Müllen and P. Gao, *Adv. Mater.*, 2021, **33**, 2008405.
211 S. M. Park, A. Abtahi, A. M. Boehm and K. R. Graham, *ACS Energy Lett.*, 2020, **5**, 799–806.
212 C. Liu, T. Yang, W. Cai, Y. Wang, X. Chen, S. Wang, W. Huang, Y. Du, N. Wu, Z. Wang, Y. Yang, J. Feng, T. Niu, Z. Ding and K. Zhao, *Adv. Mater.*, 2024, 2311562.
213 H. Gao, K. Xiao, R. Lin, S. Zhao, W. Wang, S. Dayneko, C. Duan, C. Ji, H. Sun, A. D. Bui, C. Liu, J. Wen, W. Kong, H. Luo, X. Zheng, Z. Liu, H. Nguyen, J. Xie, L. Li, M. I. Saidaminov and H. Tan, *Science*, 2024, **383**, 855–859.
214 H. Wang, Y. Zheng, G. Zhang, P. Wang, X. Sui, H. Yuan, Y. Shi, G. Zhang, G. Ding, Y. Li, T. Li, S. Yang and Y. Shao, *Adv. Mater.*, 2024, **36**, 2307855.
215 R. Lin, J. Xu, M. Wei, Y. Wang, Z. Qin, Z. Liu, J. Wu, K. Xiao, B. Chen, S. M. Park, G. Chen, H. R. Atapattu, K. R. Graham, J. Xu, J. Zhu, L. Li, C. Zhang, E. H. Sargent and H. Tan, *Nature*, 2022, **603**, 73–78.
216 S. M. Park, M. Wei, J. Xu, H. R. Atapattu, F. T. Eickemeyer, K. Darabi, L. Grater, Y. Yang, C. Liu, S. Teale, B. Chen, H. Chen, T. Wang, L. Zeng, A. Maxwell, Z. Wang, K. R. Rao, Z. Cai, S. M. Zakeeruddin, J. T. Pham, C. M. Risko, A. Amassian, M. G. Kanatzidis, K. R. Graham, M. Grätzel and E. H. Sargent, *Science*, 2023, **381**, 209–215.
217 W. Shao, H. Wang, S. Fu, Y. Ge, H. Guan, C. Wang, C. Wang, T. Wang, W. Ke and G. Fang, *Adv. Mater.*, 2024, 2310080.
218 D. W. deQuilettes, J. J. Yoo, R. Brenes, F. U. Kosasih, M. Laitz, B. D. Dou, D. J. Graham, K. Ho, Y. Shi, S. S. Shin, C. Ducati, M. G. Bawendi and V. Bulović, *Nat. Energy*, 2024, **9**, 457–466.
219 Y. Hou, E. Aydin, M. De Bastiani, C. Xiao, F. H. Isikgor, D.-J. Xue, B. Chen, H. Chen, B. Bahrami, A. H. Chowdhury, A. Johnston, S.-W. Baek, Z. Huang, M. Wei, Y. Dong, J. Troughton, R. Jalmood, A. J. Mirabelli, T. G. Allen, E. Van Kerschaver, M. I. Saidaminov, D. Baran, Q. Qiao, K. Zhu, S. De Wolf and E. H. Sargent, *Science*, 2020, **367**, 1135–1140.
220 A. Krishna, H. Zhang, Z. Zhou, T. Gallet, M. Dankl, O. Ouellette, F. T. Eickemeyer, F. Fu, S. Sanchez, M. Mensi, S. M. Zakeeruddin, U. Rothlisberger, G. N. M. Reddy, A. Redinger, M. Grätzel and A. Hagfeldt, *Energy Environ. Sci.*, 2021, **14**, 5552–5562.
221 Z. Guo, S. Zhao, N. Shibayama, A. K. Jena, I. Takei and T. Miyasaka, *Adv. Funct. Mater.*, 2022, **32**, 2207554.
222 R. Chen, J. Wang, Z. Liu, F. Ren, S. Liu, J. Zhou, H. Wang, X. Meng, Z. Zhang, X. Guan, W. Liang, P. A. Troshin, Y. Qi, L. Han and W. Chen, *Nat. Energy*, 2023, **8**, 839–849.
223 C. Li, X. Wang, E. Bi, F. Jiang, S. M. Park, Y. Li, L. Chen, Z. Wang, L. Zeng, H. Chen, Y. Liu, C. R. Grice, A. Abudulimu, J. Chung, Y. Xian, T. Zhu, H. Lai, B. Chen, R. J. Ellingson, F. Fu, D. S. Ginger, Z. Song, E. H. Sargent and Y. Yan, *Science*, 2023, **379**, 690–694.
224 H. Zeng, L. Li, F. Liu, M. Li, S. Zhang, X. Zheng, L. Luo, S. You, Y. Zhao, R. Guo, Z. Gong, R. Huang, Z. Li, T. Wang, Y. Cui, Y. Rong and X. Li, *Adv. Energy Mater.*, 2022, **12**, 2102820.
225 S. Yang, J. Dai, Z. Yu, Y. Shao, Y. Zhou, X. Xiao, X. C. Zeng and J. Huang, *J. Am. Chem. Soc.*, 2019, **141**, 5781–5787.
226 Z. Zhang, M. A. Kamarudin, A. K. Baranwal, G. Kapil, S. R. Sahamir, Y. Sanehira, M. Chen, L. Wang, Q. Shen and S. Hayase, *Angew. Chem., Int. Ed.*, 2022, **134**, e202210101.
227 R. Yu, G. Wu, R. Shi, Z. Ma, Q. Dang, Y. Qing, C. Zhang, K. Xu and Z. Tan, *Adv. Energy Mater.*, 2023, **13**, 2203127.
228 H. Zhang, W. Xiang, X. Zuo, X. Gu, S. Zhang, Y. Du, Z. Wang, Y. Liu, H. Wu, P. Wang, Q. Cui, H. Su, Q. Tian and S. Liu, *Angew. Chem., Int. Ed.*, 2023, **135**, e202216634.
229 J. Xu, H. Chen, L. Grater, C. Liu, Y. Yang, S. Teale, A. Maxwell, S. Mahesh, H. Wan, Y. Chang, B. Chen, B. Rehl, S. M. Park, M. G. Kanatzidis and E. H. Sargent, *Nat. Mater.*, 2023, **22**, 1507–1514.
230 C. Liu, Y. Yang, H. Chen, J. Xu, A. Liu, A. S. R. Bati, H. Zhu, L. Grater, S. S. Hadke, C. Huang, V. K. Sangwan, T. Cai, D. Shin, L. X. Chen, M. C. Hersam, C. A. Mirkin, B. Chen, M. G. Kanatzidis and E. H. Sargent, *Science*, 2023, **382**, 810–815.
231 D. Li, Y. Huang, R. Ma, H. Liu, Q. Liang, Y. Han, Z. Ren, K. Liu, P. Wai-Keung Fong, Z. Zhang, Q. Lian, X. Lu, C. Cheng and G. Li, *Adv. Energy Mater.*, 2023, **13**, 2204247.
232 E. Ochoa-Martinez, M. Ochoa, R. D. Ortuso, P. Ferdowsi, R. Carron, A. N. Tiwari, U. Steiner and M. Saliba, *ACS Energy Lett.*, 2021, **6**, 2626–2634.
233 Y. Xu, X. Guo, Z. Lin, Q. Wang, J. Su, J. Zhang, Y. Hao, K. Yang and J. Chang, *Angew. Chem., Int. Ed.*, 2023, **62**, e202306229.
234 R. Sun, Q. Tian, M. Li, H. Wang, J. Chang, W. Xu, Z. Li, Y. Pan, F. Wang and T. Qin, *Adv. Funct. Mater.*, 2023, **33**, 2210071.
235 X. Zhao, R. Luo, C. Yu, X. Xu, W. Zhu, Y. Min and N. Cai, *Adv. Funct. Mater.*, 2024, 2307568.
236 L. Luo, H. Zeng, Z. Wang, M. Li, S. You, B. Chen, A. Maxwell, Q. An, L. Cui, D. Luo, J. Hu, S. Li, X. Cai, W. Li, L. Li, R. Guo, R. Huang, W. Liang, Z.-H. Lu, L. Mai, Y. Rong, E. H. Sargent and X. Li, *Nat. Energy*, 2023, **8**, 294–303.
237 Y. Wu, G. Xu, J. Xi, Y. Shen, X. Wu, X. Tang, J. Ding, H. Yang, Q. Cheng, Z. Chen, Y. Li and Y. Li, *Joule*, 2023, **7**, 398–415.
238 H. Guo, G. W. Yoon, Z. J. Li, Y. Yun, S. Lee, Y.-H. Seo, N. J. Jeon, G. S. Han and H. S. Jung, *Adv. Energy Mater.*, 2024, **14**, 2302743.
239 T.-H. Han, J.-W. Lee, C. Choi, S. Tan, C. Lee, Y. Zhao, Z. Dai, N. De Marco, S.-J. Lee, S.-H. Bae, Y. Yuan, H. M. Lee, Y. Huang and Y. Yang, *Nat. Commun.*, 2019, **10**, 520.
240 Q. Cao, Y. Li, H. Zhang, J. Yang, J. Han, T. Xu, S. Wang, Z. Wang, B. Gao, J. Zhao, X. Li, X. Ma, S. M. Zakeeruddin, W. E. I. Sha, X. Li and M. Grätzel, *Sci. Adv.*, 2021, **7**, eabg0633.
241 T. Wang, Y. Li, Q. Cao, J. Yang, B. Yang, X. Pu, Y. Zhang, J. Zhao, Y. Zhang, H. Chen, A. Hagfeldt and X. Li, *Energy Environ. Sci.*, 2022, **15**, 4414–4424.

242 C. Zhao, H. Zhang, M. Almalki, J. Xu, A. Krishna, F. T. Eickemeyer, J. Gao, Y. M. Wu, S. M. Zakeeruddin, J. Chu, J. Yao and M. Grätzel, *Adv. Mater.*, 2023, **35**, 2211619.
243 K. Zhang, Y. Wang, M. Tao, L. Guo, Y. Yang, J. Shao, Y. Zhang, F. Wang and Y. Song, *Adv. Mater.*, 2023, **35**, 2211593.
244 N. Ren, P. Wang, J. Jiang, R. Li, W. Han, J. Liu, Z. Zhu, B. Chen, Q. Xu, T. Li, B. Shi, Q. Huang, D. Zhang, S. Apergi, G. Brocks, C. Zhu, S. Tao, Y. Zhao and X. Zhang, *Adv. Mater.*, 2023, **35**, 2211806.
245 Y. Liang, F. Li, X. Cui, T. Lv, C. Stampfl, S. P. Ringer, X. Yang, J. Huang and R. Zheng, *Nat. Commun.*, 2024, **15**, 1707.
246 T. P. Baumeler, E. A. Alharbi, G. Kakavelakis, G. C. Fish, M. T. Aldosari, M. S. Albishi, L. Pfeifer, B. I. Carlsen, J.-H. Yum, A. S. Alharbi, M. D. Mensi, J. Gao, F. T. Eickemeyer, K. Sivula, J.-E. Moser, S. M. Zakeeruddin and M. Grätzel, *ACS Energy Lett.*, 2023, **8**, 2456–2462.
247 D. Sun, Y. Gao, H. Raza, S. Liu, F. Ren, X. Hu, H. Wang, X. Meng, J. Wang, R. Chen, H. Sun, J. He, J. Zhou, Y. Pan, Z. Sun, W. Chen and Z. Liu, *Adv. Funct. Mater.*, 2023, **33**, 2303225.
248 Y. Zhao, I. Yavuz, M. Wang, M. H. Weber, M. Xu, J.-H. Lee, S. Tan, T. Huang, D. Meng, R. Wang, J. Xue, S.-J. Lee, S.-H. Bae, A. Zhang, S.-G. Choi, Y. Yin, J. Liu, T.-H. Han, Y. Shi, H. Ma, W. Yang, Q. Xing, Y. Zhou, P. Shi, S. Wang, E. Zhang, J. Bian, X. Pan, N.-G. Park, J.-W. Lee and Y. Yang, *Nat. Mater.*, 2022, **21**, 1396–1402.
249 X. Li, W. Zhang, X. Guo, C. Lu, J. Wei and J. Fang, *Science*, 2022, **375**, 434–437.
250 Q. Fu, M. Chen, Q. Li, H. Liu, R. Wang and Y. Liu, *J. Am. Chem. Soc.*, 2023, **145**, 21687–21695.
251 Z. Shi, R. Guo, R. Luo, X. Wang, J. Ma, J. Feng, X. Niu, E. Alvianto, Z. Jia, X. Guo, H. Liang, J. Chen, Z. Li, K. Sun, X. Jiang, Y. Wu, P. Müller-Buschbaum, W. Hu and Y. Hou, *ACS Energy Lett.*, 2024, **9**, 419–427.
252 Y.-C. Chin, M. Daboczi, C. Henderson, J. Luke and J.-S. Kim, *ACS Energy Lett.*, 2022, **7**, 560–568.
253 L. Shen, P. Song, L. Zheng, L. Wang, X. Zhang, K. Liu, Y. Liang, W. Tian, Y. Luo, J. Qiu, C. Tian, L. Xie and Z. Wei, *Adv. Mater.*, 2023, **35**, 2301624.
254 J. He, G. Hu, Y. Jiang, S. Zeng, G. Niu, G. Feng, Z. Liu, K. Yang, C. Shao, Y. Zhao, F. Wang, Y. Li and J. Wang, *Angew. Chem., Int. Ed.*, 2023, **62**, e202311865.
255 Y. Zhou, Z. Wang, J. Jin, X. Zhang, J. Zou, F. Yao, Z. Zhu, X. Cui, D. Zhang, Y. Yu, C. Chen, D. Zhao, Q. Cao, Q. Lin and Q. Tai, *Angew. Chem., Int. Ed.*, 2023, **135**, e202300759.
256 Y. Li, Y. Zhang, P. Zhu, J. Li, J. Wu, J. Zhang, X. Zhou, Z. Jiang, X. Wang and B. Xu, *Adv. Funct. Mater.*, 2023, **33**, 2309010.
257 J. Cao, Q. Chen, W. Wu, J. Fu, Z. Zhang, L. Chen, R. Wang, W. Yu, L. Wang, X. Nie, J. Zhang, Y. Zhou, B. Song and Y. Li, *Energy Environ. Sci.*, 2024, **17**, 3454–3469.
258 Y. Cao, J. Feng, M. Wang, N. Yan, J. Lou, X. Feng, F. Xiao, Y. Liu, D. Qi, Y. Yuan, X. Zhu and S. Liu, *Adv. Energy Mater.*, 2023, **13**, 2302103.
259 X. Liu, B. Zheng, L. Shi, S. Zhou, J. Xu, Z. Liu, J. S. Yun, E. Choi, M. Zhang, Y. Lv, W.-H. Zhang, J. Huang, C. Li, K. Sun, J. Seidel, M. He, J. Peng, X. Hao and M. Green, *Nat. Photonics*, 2023, **17**, 96–105.
260 J. Deng, H. Ahangar, Y. Xiao, Y. Luo, X. Cai, Y. Li, D. Wu, L. Yang, E. Sheibani and J. Zhang, *Adv. Funct. Mater.*, 2024, **34**, 2309484.
261 S. Wang, Y. Li, J. Yang, T. Wang, B. Yang, Q. Cao, X. Pu, L. Etgar, J. Han, J. Zhao, X. Li and A. Hagfeldt, *Angew. Chem., Int. Ed.*, 2022, **134**, e202116534.
262 C. Fei, N. Li, M. Wang, X. Wang, H. Gu, B. Chen, Z. Zhang, Z. Ni, H. Jiao, W. Xu, Z. Shi, Y. Yan and J. Huang, *Science*, 2023, **380**, 823–829.
263 F. Ye, S. Zhang, J. Warby, J. Wu, E. Gutierrez-Partida, F. Lang, S. Shah, E. Saglamkaya, B. Sun, F. Zu, S. Shoaee, H. Wang, B. Stiller, D. Neher, W.-H. Zhu, M. Stolterfoht and Y. Wu, *Nat. Commun.*, 2022, **13**, 7454.
264 W. Peng, K. Mao, F. Cai, H. Meng, Z. Zhu, T. Li, S. Yuan, Z. Xu, X. Feng, J. Xu, M. D. McGehee and J. Xu, *Science*, 2023, **379**, 683–690.
265 X. Zhang, W. Qiu, S. Apergi, S. Singh, P. Marchezi, W. Song, C. Sternemann, K. Elkhouly, D. Zhang, A. Aguirre, T. Merckx, A. Krishna, Y. Shi, A. Bracesco, C. Helvoirt, F. Bens, V. Zardetto, J. D'Haen, A. Yu, G. Brocks, T. Aernouts, E. Moons, S. Tao, Y. Zhan, Y. Kuang and J. Poortmans, *ACS Energy Lett.*, 2023, **8**, 2532–2542.
266 L. Duan, D. Zheng, B. Farhadi, S. Wu, H. Wang, L. Peng, L. Liu, M. Du, Y. Zhang, K. Wang and S. Liu, *Adv. Mater.*, 2024, 2314098.
267 K. Artuk, D. Turkay, M. D. Mensi, J. A. Steele, D. A. Jacobs, M. Othman, X. Y. Chin, S.-J. Moon, A. N. Tiwari, A. Hessler-Wyser, Q. Jeangros, C. Ballif and C. M. Wolff, *Adv. Mater.*, 2024, **36**, 2311745.
268 N. S. Hill, M. V. Cowley, N. Gluck, M. H. Fsadni, W. Clarke, Y. Hu, M. J. Wolf, N. Healy, M. Freitag, T. J. Penfold, G. Richardson, A. B. Walker, P. J. Cameron and P. Docampo, *Adv. Mater.*, 2023, **35**, 2302146.
269 Z. Chen, Y. Li, Z. Liu, J. Shi, B. Yu, S. Tan, Y. Cui, C. Tan, F. Tian, H. Wu, Y. Luo, D. Li and Q. Meng, *Adv. Energy Mater.*, 2023, **13**, 2202799.
270 T. Song, H. Jang, J. Seo, J. Roe, S. Song, J. W. Kim, J. Yeop, Y. Lee, H. Lee, S. Cho and J. Y. Kim, *ACS Nano*, 2024, **18**, 2992–3001.
271 L. Liu, Y. Yang, M. Du, Y. Cao, X. Ren, L. Zhang, H. Wang, S. Zhao, K. Wang and S. Liu, *Adv. Energy Mater.*, 2023, **13**, 2202802.
272 D. S. Utomo, L. M. Svirskaite, A. Prasetio, V. Malinauskiene, P. Dally, E. Aydin, A. Musiienko, V. Getautis, T. Malinauskas, R. Azmi and S. De Wolf, *ACS Energy Lett.*, 2024, **9**, 1682–1692.
273 X. Wang, Y. Zhong, X. Luo, W. Sheng, J. Yang, L. Tan and Y. Chen, *Energy Environ. Sci.*, 2024, **17**, 569–579.
274 F. H. Isikgor, S. Zhumagali, L. V. T. Merino, M. De Bastiani, I. McCulloch and S. De Wolf, *Nat. Rev. Mater.*, 2023, **8**, 89–108.
275 Z. Dai, S. K. Yadavalli, M. Chen, A. Abbaspourtamijani, Y. Qi and N. P. Padture, *Science*, 2021, **372**, 618–622.
276 A. Ullah, K. H. Park, H. D. Nguyen, Y. Siddique, S. F. A. Shah, H. Tran, S. Park, S. I. Lee, K.-K. Lee, C.-H. Han,

K. Kim, S. Ahn, I. Jeong, Y. S. Park and S. Hong, *Adv. Energy Mater.*, 2022, **12**, 2103175.

277 C.-M. Hung, C.-L. Mai, C.-C. Wu, B.-H. Chen, C.-H. Lu, C.-C. Chu, M.-C. Wang, S.-D. Yang, H.-C. Chen, C.-Y. Yeh and P.-T. Chou, *Angew. Chem., Int. Ed.*, 2023, **135**, e202309831.

278 S. N. Afraj, C.-H. Kuan, J.-S. Lin, J.-S. Ni, A. Velusamy, M.-C. Chen and E. W.-G. Diau, *Adv. Funct. Mater.*, 2023, **33**, 2213939.

279 M. Liu, M. Li, Y. Li, Y. An, Z. Yao, B. Fan, F. Qi, K. Liu, H.-L. Yip, F. R. Lin and A. K.-Y. Jen, *Adv. Energy Mater.*, 2024, **14**, 2303742.

280 W. Jiang, F. Li, M. Li, F. Qi, F. R. Lin and A. K.-Y. Jen, *Angew. Chem., Int. Ed.*, 2022, **61**, e202213560.

281 X. Zheng, Z. Li, Y. Zhang, M. Chen, T. Liu, C. Xiao, D. Gao, J. B. Patel, D. Kuciauskas, A. Magomedov, R. A. Scheidt, X. Wang, S. P. Harvey, Z. Dai, C. Zhang, D. Morales, H. Pruett, B. M. Wieliczka, A. R. Kirmani, N. P. Padture, K. R. Graham, Y. Yan, M. K. Nazeeruddin, M. D. McGehee, Z. Zhu and J. M. Luther, *Nat. Energy*, 2023, **8**, 462–472.

282 M. Liu, L. Bi, W. Jiang, Z. Zeng, S.-W. Tsang, F. R. Lin and A. K.-Y. Jen, *Adv. Mater.*, 2023, **35**, 2304415.

283 A. Farag, T. Feeney, I. M. Hossain, F. Schackmar, P. Fassl, K. Küster, R. Bäuerle, M. A. Ruiz-Preciado, M. Hentschel, D. B. Ritzer, A. Diercks, Y. Li, B. A. Nejand, F. Laufer, R. Singh, U. Starke and U. W. Paetzold, *Adv. Energy Mater.*, 2023, **13**, 2203982.

284 K. Almasabi, X. Zheng, B. Turedi, A. Y. Alsalloum, M. N. Lintangpradipto, J. Yin, L. Gutiérrez-Arzaluz, K. Kotsovos, A. Jamal, I. Gereige, O. F. Mohammed and O. M. Bakr, *ACS Energy Lett.*, 2023, **8**, 950–956.

285 Z. Zhang, R. Zhu, Y. Tang, Z. Su, S. Hu, X. Zhang, J. Zhang, J. Zhao, Y. Xue, X. Gao, G. Li, J. Pascual, A. Abate and M. Li, *Adv. Mater.*, 2024, **36**, 2312264.

286 Z. Yi, W. Wang, R. He, J. Zhu, W. Jiao, Y. Luo, Y. Xu, Y. Wang, Z. Zeng, K. Wei, J. Zhang, S.-W. Tsang, C. Chen, W. Tang and D. Zhao, *Energy Environ. Sci.*, 2024, **17**, 202–209.

287 C. Li, Z. Zhang, H. Zhang, W. Yan, Y. Li, L. Liang, W. Yu, X. Yu, Y. Wang, Y. Yang, M. K. Nazeeruddin and P. Gao, *Angew. Chem., Int. Ed.*, 2024, **136**, e202315281.

288 T. Feeney, J. Petry, A. Torche, D. Hauschild, B. Hacene, C. Wansorra, A. Diercks, M. Ernst, L. Weinhardt, C. Heske, G. Gryn'ova, U. W. Paetzold and P. Fassl, *Matter*, 2024, **7**, 1–25.

289 R. He, W. Wang, Z. Yi, F. Lang, C. Chen, J. Luo, J. Zhu, J. Thiesbrummel, S. Shah, K. Wei, Y. Luo, C. Wang, H. Lai, H. Huang, J. Zhou, B. Zou, X. Yin, S. Ren, X. Hao, L. Wu, J. Zhang, J. Zhang, M. Stolterfoht, F. Fu, W. Tang and D. Zhao, *Nature*, 2023, **618**, 80–86.

290 R. Lin, Y. Wang, Q. Lu, B. Tang, J. Li, H. Gao, Y. Gao, H. Li, C. Ding, J. Wen, P. Wu, C. Liu, S. Zhao, K. Xiao, Z. Liu, C. Ma, Y. Deng, L. Li, F. Fan and H. Tan, *Nature*, 2023, **620**, 994–1000.

291 S. Mariotti, E. Köhnen, F. Scheler, K. Sveinbjörnsson, L. Zimmermann, M. Piot, F. Yang, B. Li, J. Warby, A. Musiienko, D. Menzel, F. Lang, S. Keßler, I. Levine, D. Mantione, A. Al-Ashouri, M. S. Härtel, K. Xu, A. Cruz, J. Kurpiers, P. Wagner, H. Köbler, J. Li, A. Magomedov, D. Mecerreyes, E. Unger, A. Abate, M. Stolterfoht, B. Stannowski, R. Schlatmann, L. Korte and S. Albrecht, *Science*, 2023, **381**, 63–69.

292 H. Cui, L. Huang, S. Zhou, C. Wang, X. Hu, H. Guan, S. Wang, W. Shao, D. Pu, K. Dong, J. Zhou, P. Jia, W. Wang, C. Tao, W. Ke and G. Fang, *Energy Environ. Sci.*, 2023, **16**, 5992–6002.

293 W. Wang, X. Liu, J. Wang, C. Chen, J. Yu, D. Zhao and W. Tang, *Adv. Energy Mater.*, 2023, **13**, 2300694.

294 X. Deng, F. Qi, F. Li, S. Wu, F. R. Lin, Z. Zhang, Z. Guan, Z. Yang, C.-S. Lee and A. K.-Y. Jen, *Angew. Chem., Int. Ed.*, 2022, **134**, e202203088.

295 K. Hossain, A. Kulkarni, U. Bothra, B. Klingebiel, T. Kirchartz, M. Saliba and D. Kabra, *ACS Energy Lett.*, 2023, **8**, 3860–3867.

296 R. Guo, X. Zhang, X. Zheng, L. Li, M. Li, Y. Zhao, S. Zhang, L. Luo, S. You, W. Li, Z. Gong, R. Huang, Y. Cui, Y. Rong, H. Zeng and X. Li, *Adv. Funct. Mater.*, 2023, **33**, 2211955.

297 H. Tang, Z. Shen, Y. Shen, G. Yan, Y. Wang, Q. Han and L. Han, *Science*, 2024, **383**, 1236–1240.

298 D. Song, S. Ramakrishnan, Y. Zhang and Q. Yu, *ACS Energy Lett.*, 2024, **9**, 1466–1472.

299 Z. Li, X. Sun, X. Zheng, B. Li, D. Gao, S. Zhang, X. Wu, S. Li, J. Gong, J. M. Luther, Z. Li and Z. Zhu, *Science*, 2023, **382**, 284–289.

300 S. Wang, D. Khan, W. Zhou, Y. Sui, T. Zhang, G. Yu, Y. Huang, X. Yang, X. Chen, H. Yan, J. Tang, F. Yang, P. Han, Z. Zheng, Y. Zhang and Z. Tang, *Adv. Funct. Mater.*, 2024, 2316202.

301 G. Yang, Z. Ren, K. Liu, M. Qin, W. Deng, H. Zhang, H. Wang, J. Liang, F. Ye, Q. Liang, H. Yin, Y. Chen, Y. Zhuang, S. Li, B. Gao, J. Wang, T. Shi, X. Wang, X. Lu, H. Wu, J. Hou, D. Lei, S. K. So, Y. Yang, G. Fang and G. Li, *Nat. Photonics*, 2021, **15**, 681–689.

302 F. Zhang, S. Y. Park, C. Yao, H. Lu, S. P. Dunfield, C. Xiao, S. Uličná, X. Zhao, L. Du Hill, X. Chen, X. Wang, L. E. Mundt, K. H. Stone, L. T. Schelhas, G. Teeter, S. Parkin, E. L. Ratcliff, Y.-L. Loo, J. J. Berry, M. C. Beard, Y. Yan, B. W. Larson and K. Zhu, *Science*, 2022, **375**, 71–76.

303 G. Wu, R. Liang, M. Ge, G. Sun, Y. Zhang and G. Xing, *Adv. Mater.*, 2022, **34**, 2105635.

304 Y.-W. Jang, S. Lee, K. M. Yeom, K. Jeong, K. Choi, M. Choi and J. H. Noh, *Nat. Energy*, 2021, **6**, 63–71.

305 S. Sidhik, Y. Wang, M. De Siena, R. Asadpour, A. J. Torma, T. Terlier, K. Ho, W. Li, A. B. Puthirath, X. Shuai, A. Agrawal, B. Traore, M. Jones, R. Giridharagopal, P. M. Ajayan, J. Strzalka, D. S. Ginger, C. Katan, M. A. Alam, J. Even, M. G. Kanatzidis and A. D. Mohite, *Science*, 2022, **377**, 1425–1430.

306 C. Zhao, J. Guo, J. Tao, J. Chu, S. Chen and G. Xing, *Light:Sci. Appl.*, 2024, **13**, 170.

307 F. Ye, T. Tian, J. Su, R. Jiang, J. Li, C. Jin, J. Tong, S. Bai, F. Huang, P. Müller-Buschbaum, Y.-B. Cheng and T. Bu, *Adv. Energy Mater.*, 2024, **14**, 2302775.

308 F. Wang, K. Zhou, C. Zhou, X. Liang, T. Wang, Y. Sun, Y. Li, Q. Li, X. Zhou, G. Yang, D. Duan, J. Zhu, Q. Zhu, H. Lin, Y. Shi, C. Yang, G. Xing and H. Hu, *Adv. Energy Mater.*, 2024, 2400021.

309 S. Ye, H. Rao, M. Feng, L. Xi, Z. Yen, D. H. L. Seng, Q. Xu, C. Boothroyd, B. Chen, Y. Guo, B. Wang, T. Salim, Q. Zhang, H. He, Y. Wang, X. Xiao, Y. M. Lam and T. C. Sum, *Nat. Energy*, 2023, **8**, 284–293.

310 H. Chen, S. Teale, B. Chen, Y. Hou, L. Grater, T. Zhu, K. Bertens, S. M. Park, H. R. Atapattu, Y. Gao, M. Wei, A. K. Johnston, Q. Zhou, K. Xu, D. Yu, C. Han, T. Cui, E. H. Jung, C. Zhou, W. Zhou, A. H. Proppe, S. Hoogland, F. Laquai, T. Filleter, K. R. Graham, Z. Ning and E. H. Sargent, *Nat. Photonics*, 2022, **16**, 352–358.

311 J. Wen, Y. Zhao, P. Wu, Y. Liu, X. Zheng, R. Lin, S. Wan, K. Li, H. Luo, Y. Tian, L. Li and H. Tan, *Nat. Commun.*, 2023, **14**, 7118.

312 B. Li, Q. Liu, J. Gong, S. Li, C. Zhang, D. Gao, Z. Chen, Z. Li, X. Wu, D. Zhao, Z. Yu, X. Li, Y. Wang, H. Lu, X. C. Zeng and Z. Zhu, *Nat. Commun.*, 2024, **15**, 2753.

313 T. Wang, L. Bi, L. Yang, Z. Zeng, X. Ji, Z. Hu, S.-W. Tsang, H.-L. Yip, Q. Fu, A. K.-Y. Jen and Y. Liu, *J. Am. Chem. Soc.*, 2024, **146**, 7555–7564.

314 Y. Luo, K. Liu, L. Yang, W. Feng, L. Zheng, L. Shen, Y. Jin, Z. Fang, P. Song, W. Tian, P. Xu, Y. Li, C. Tian, L. Xie and Z. Wei, *Nat. Commun.*, 2023, **14**, 3738.

315 H. Li, C. Zhang, C. Gong, D. Zhang, H. Zhang, Q. Zhuang, X. Yu, S. Gong, X. Chen, J. Yang, X. Li, R. Li, J. Li, J. Zhou, H. Yang, Q. Lin, J. Chu, M. Grätzel, J. Chen and Z. Zang, *Nat. Energy*, 2023, **8**, 946–955.

316 R. Azmi, D. S. Utomo, B. Vishal, S. Zhumagali, P. Dally, A. M. Risqi, A. Prasetio, E. Ugur, F. Cao, I. F. Imran, A. A. Said, A. R. Pininti, A. S. Subbiah, E. Aydin, C. Xiao, S. I. Seok and S. De Wolf, *Nature*, 2024, **628**, 93–98.

317 M. Abdi-Jalebi, M. Ibrahim Dar, S. P. Senanayak, A. Sadhanala, Z. Andaji-Garmaroudi, L. M. Pazos-Outón, J. M. Richter, A. J. Pearson, H. Sirringhaus, M. Grätzel and R. H. Friend, *Sci. Adv.*, 2019, **5**, eaav2012.

318 J. Xue, R. Wang, X. Chen, C. Yao, X. Jin, K.-L. Wang, W. Huang, T. Huang, Y. Zhao, Y. Zhai, D. Meng, S. Tan, R. Liu, Z.-K. Wang, C. Zhu, K. Zhu, M. C. Beard, Y. Yan and Y. Yang, *Science*, 2021, **371**, 636–640.

319 S. You, F. T. Eickemeyer, J. Gao, J.-H. Yum, X. Zheng, D. Ren, M. Xia, R. Guo, Y. Rong, S. M. Zakeeruddin, K. Sivula, J. Tang, Z. Shen, X. Li and M. Grätzel, *Nat. Energy*, 2023, **8**, 515–525.

320 A. Al-Ashouri, E. Köhnen, B. Li, A. Magomedov, H. Hempel, P. Caprioglio, J. A. Márquez, A. B. M. Vilches, E. Kasparavičius, J. A. Smith, N. Phung, D. Menzel, M. Grischek, L. Kegelmann, D. Skroblin, C. Gollwitzer, T. Malinauskas, M. Jošt, G. Matič, B. Rech, R. Schlatmann, M. Topič, L. Korte, A. Abate, B. Stannowski, D. Neher, M. Stolterfoht, T. Unold, V. Getautis and S. Albrecht, *Science*, 2020, **370**, 1300–1309.

321 S. Zhang, F. Ye, X. Wang, R. Chen, H. Zhang, L. Zhan, X. Jiang, Y. Li, X. Ji, S. Liu, M. Yu, F. Yu, Y. Zhang, R. Wu, Z. Liu, Z. Ning, D. Neher, L. Han, Y. Lin, H. Tian, W. Chen, M. Stolterfoht, L. Zhang, W.-H. Zhu and Y. Wu, *Science*, 2023, **380**, 404–409.

322 J. Zhu, Y. Luo, R. He, C. Chen, Y. Wang, J. Luo, Z. Yi, J. Thiesbrummel, C. Wang, F. Lang, H. Lai, Y. Xu, J. Wang, Z. Zhang, W. Liang, G. Cui, S. Ren, X. Hao, H. Huang, Y. Wang, F. Yao, Q. Lin, L. Wu, J. Zhang, M. Stolterfoht, F. Fu and D. Zhao, *Nat. Energy*, 2023, **8**, 714–724.

323 J. Zhou, L. Tan, Y. Liu, H. Li, X. Liu, M. Li, S. Wang, Y. Zhang, C. Jiang, R. Hua, W. Tress, S. Meloni and C. Yi, *Joule*, 2024, **8**, 1–16.

324 H. Zhang, S. Zhang, X. Ji, J. He, H. Guo, S. Wang, W. Wu, W.-H. Zhu and Y. Wu, *Angew. Chem., Int. Ed.*, 2024, **136**, e202401260.

325 Q. Chen, C. Wang, Y. Li and L. Chen, *J. Am. Chem. Soc.*, 2020, **142**, 18281–18292.

326 J. Qiu, X. Mei, M. Zhang, G. Wang, S. Zou, L. Wen, J. Huang, Y. Hua and X. Zhang, *Angew. Chem., Int. Ed.*, 2024, **63**, e202401751.

327 X. Yue, X. Zhao, B. Fan, Y. Yang, L. Yan, S. Qu, H. Huang, Q. Zhang, H. Yan, P. Cui, J. Ji, J. Ma and M. Li, *Adv. Funct. Mater.*, 2023, **33**, 2209921.

328 J. Duan, M. Wang, Y. Wang, J. Zhang, Q. Guo, Q. Zhang, Y. Duan and Q. Tang, *ACS Energy Lett.*, 2021, **6**, 2336–2342.

329 X. Jiang, B. Zhang, G. Yang, Z. Zhou, X. Guo, F. Zhang, S. Yu, S. Liu and S. Pang, *Angew. Chem., Int. Ed.*, 2023, **62**, e202302462.

330 Z. Iqbal, F. Zu, A. Musiienko, E. Gutierrez-Partida, H. Köbler, T. W. Gries, G. V. Sannino, L. Canil, N. Koch, M. Stolterfoht, D. Neher, M. Pavone, A. B. Muñoz-García, A. Abate and Q. Wang, *ACS Energy Lett.*, 2023, **8**, 4304–4314.

331 T. Li, J. Xu, R. Lin, S. Teale, H. Li, Z. Liu, C. Duan, Q. Zhao, K. Xiao, P. Wu, B. Chen, S. Jiang, S. Xiong, H. Luo, S. Wan, L. Li, Q. Bao, Y. Tian, X. Gao, J. Xie, E. H. Sargent and H. Tan, *Nat. Energy*, 2023, **8**, 610–620.

332 C. Zhang, Y. Son, H. Kim, S.-H. Lee, X. Liang, G. Fu, S.-U. Lee, D.-A. Park, Q. Jiang, K. Zhu and N.-G. Park, *Joule*, 2024, **8**, 1394–1411.

333 C. Qin, X. Wu, L. Tang, X. Chen, M. Li, Y. Mou, B. Su, S. Wang, C. Feng, J. Liu, X. Yuan, Y. Zhao and H. Wang, *Nat. Commun.*, 2023, **14**, 5238.

334 T. Yang, W. Zhao, X. Liu and S. Liu, *Adv. Energy Mater.*, 2023, **13**, 2204192.

